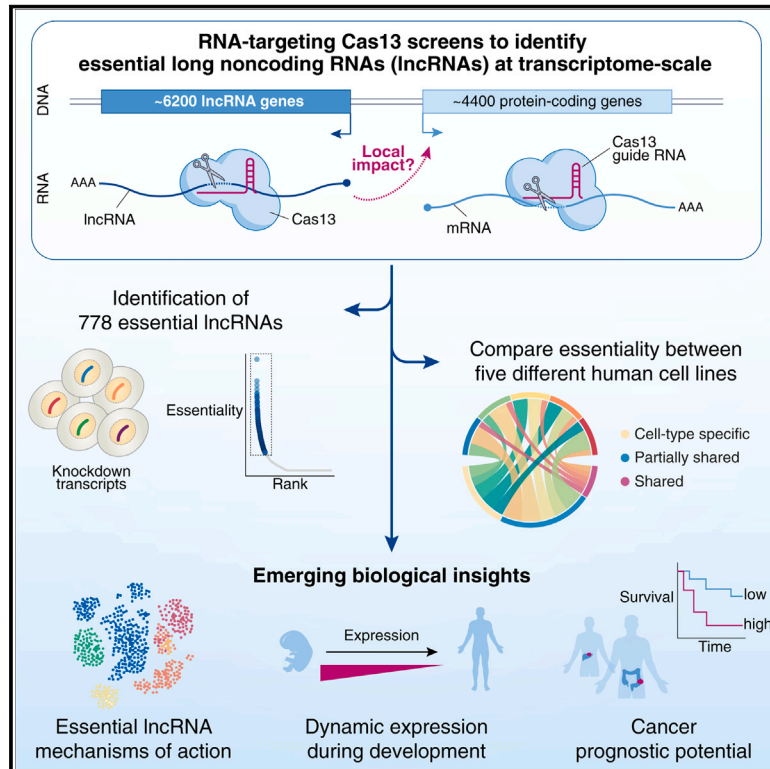


# Transcriptome-scale RNA-targeting CRISPR screens reveal essential lncRNAs in human cells

## Graphical abstract



## Authors

Wen-Wei Liang (梁雯薇), Simon Müller, Sydney K. Hart, ..., Olena Kolumba, Breanna Williams, Neville E. Sanjana

## Correspondence

neville@sanjanalab.org

## In brief

Massively parallel CRISPR-Cas13 screens in multiple human cell lines uncover universally essential and context-specific essential lncRNAs that exhibit dynamic expression during development and in specific tumor types, and these lncRNAs function independently from neighboring protein-coding genes.

## Highlights

- Transcriptome-wide CRISPR-Cas13 screens to identify essential human lncRNAs
- Discovery of 46 universally essential and >700 context-specific essential lncRNAs
- Most essential lncRNAs operate independently of their nearest protein-coding genes
- Dynamic expression of essential lncRNAs during development and in specific tumors

Article

# Transcriptome-scale RNA-targeting CRISPR screens reveal essential lncRNAs in human cells

Wen-Wei Liang (梁雯薇),<sup>1,2,3</sup> Simon Müller,<sup>1,2,3</sup> Sydney K. Hart,<sup>1,2</sup> Hans-Hermann Wessels,<sup>1,2</sup> Alejandro Méndez-Mancilla,<sup>1,2</sup> Akash Sookdeo,<sup>1,2</sup> Olivia Choi,<sup>1,2</sup> Christina M. Caragine,<sup>1,2</sup> Alba Corman,<sup>1,2</sup> Lu Lu (芦璐),<sup>1,2</sup> Olena Kolumba,<sup>1,2</sup> Breanna Williams,<sup>1,2</sup> and Neville E. Sanjana<sup>1,2,4,\*</sup>

<sup>1</sup>New York Genome Center, New York, NY 10013, USA

<sup>2</sup>Department of Biology, New York University, New York, NY 10013, USA

<sup>3</sup>These authors contributed equally

<sup>4</sup>Lead contact

\*Correspondence: [neville@sanjanalab.org](mailto:neville@sanjanalab.org)

<https://doi.org/10.1016/j.cell.2024.10.021>

## SUMMARY

Mammalian genomes host a diverse array of RNA that includes protein-coding and noncoding transcripts. However, the functional roles of most long noncoding RNAs (lncRNAs) remain elusive. Using RNA-targeting CRISPR-Cas13 screens, we probed how the loss of ~6,200 lncRNAs impacts cell fitness across five human cell lines and identified 778 lncRNAs with context-specific or broad essentiality. We confirm their essentiality with individual perturbations and find that the majority of essential lncRNAs operate independently of their nearest protein-coding genes. Using transcriptome profiling in single cells, we discover that the loss of essential lncRNAs impairs cell-cycle progression and drives apoptosis. Many essential lncRNAs demonstrate dynamic expression across tissues during development. Using ~9,000 primary tumors, we pinpoint those lncRNAs whose expression in tumors correlates with survival, yielding new biomarkers and potential therapeutic targets. This transcriptome-wide survey of functional lncRNAs advances our understanding of noncoding transcripts and demonstrates the potential of transcriptome-scale noncoding screens with Cas13.

## INTRODUCTION

The human genome is pervasively transcribed into RNA and encodes thousands of long noncoding RNAs (lncRNAs) that are often spliced and polyadenylated but not translated into proteins.<sup>1–3</sup> Of annotated lncRNAs, very few (<1%) have been linked with a clear functional role.<sup>4</sup> In those rare cases, lncRNAs have been found to sequester microRNAs (miRNAs),<sup>5</sup> block translation,<sup>6</sup> form biomolecular condensates,<sup>7</sup> encode micropeptides,<sup>8,9</sup> and regulate proteins or RNA.<sup>10,11</sup> Their low sequence conservation,<sup>12,13</sup> low abundance,<sup>14,15</sup> and cell-type-specific expression<sup>16</sup> make it challenging to distinguish them from unstable transcriptional noise.<sup>17</sup> Even though genome-wide bioinformatic analyses and comparative sequencing studies have identified conserved lncRNAs,<sup>18,19</sup> suggesting possible functional roles, follow-up experimental validation has been limited to low-throughput studies, focusing on one lncRNA at a time.<sup>4</sup>

Recently, CRISPR-Cas9 pooled screens using CRISPR interference (CRISPRi) and CRISPR activation (CRISPRa) have been applied to identify functional lncRNAs.<sup>20,21</sup> While valuable, Cas9-based approaches often suffer from unintended on-target activity—that is, binding at the intended genomic locus but perturbing additional nearby genes. Moreover, DNA-based

perturbation of a lncRNA locus might also suppress functional DNA elements unrelated to the lncRNA transcript.<sup>22</sup>

To overcome these limitations, we have developed RNA-targeting CRISPR screens to systematically perturb lncRNAs on a transcriptome scale with transcript- and strand-specificity, ensuring no unintended modulation of nearby genes or functional DNA elements in the locus.<sup>23–25</sup> Here, we perturb 6,199 lncRNAs in five distinct human cell lines using massively parallel CRISPR-Cas13 forward transcriptomic screens and identify a core set of shared essential lncRNAs, compare their essentiality to nearby protein-coding genes (PCGs), profile transcriptomic changes after perturbation in single cells, and describe key roles in development and cancer progression.

## RESULTS

### Transcriptome-scale Cas13 screens for essential lncRNAs

Using the RNA-targeting CRISPR-Cas13 nuclease,<sup>26</sup> we systematically identified essential lncRNAs and, via targeting of nearby PCGs, also discerned whether these PCGs were similarly essential. Using an atlas of lncRNA expression across 7 organs and 26 developmental stages (4 weeks post-conception to old age),<sup>19</sup> we designed the Cas13 library to target all lncRNAs

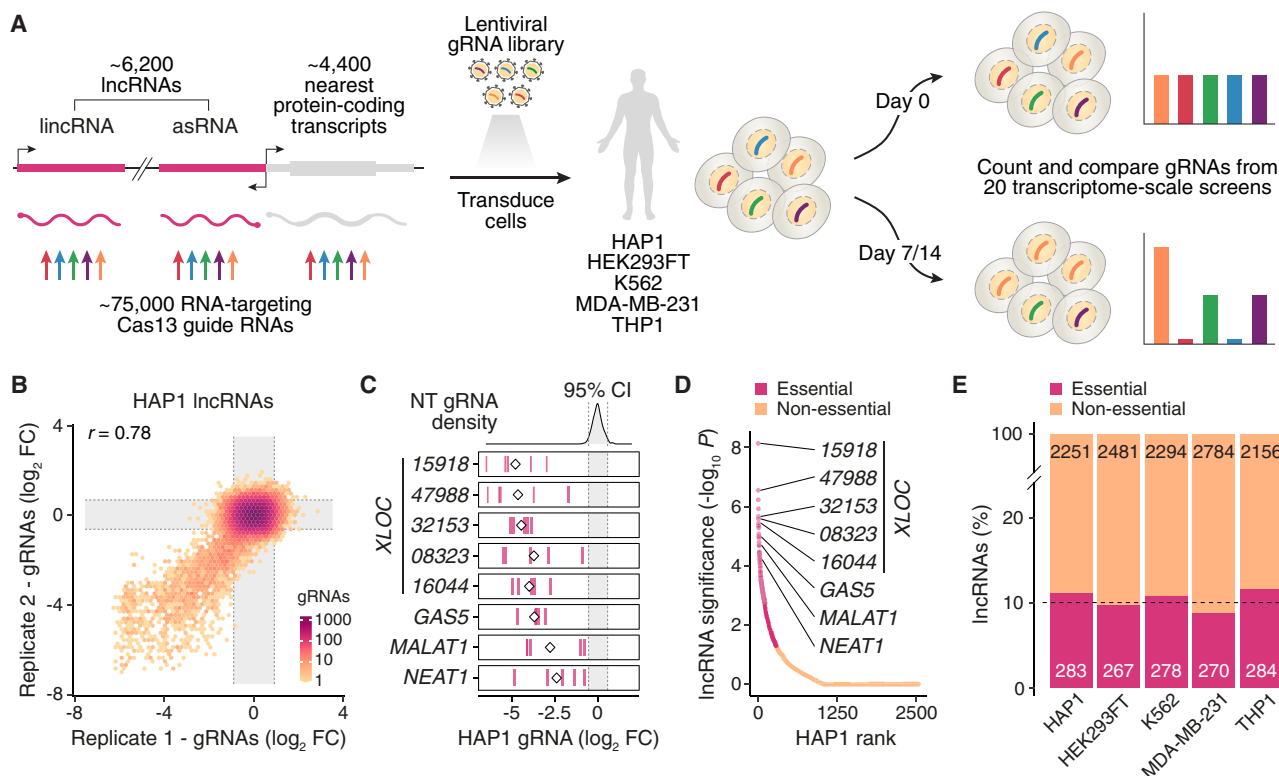


**Figure 1. Transcriptome-scale RNA-targeting CRISPR screens to identify essential lncRNAs in human cells**

(A) Overview of the Cas13-based loss-of-function screens to identify essential long noncoding RNAs (lncRNAs). lincRNA, long intergenic noncoding RNA; asRNA, antisense RNA; gRNA, guide RNA.

(B) Fold-change (FC) of gRNAs targeting lncRNAs in two independent biological replicates pooled screens in HAP1 cells at 14 days after Cas13 induction. Color denotes the number of Cas13 gRNAs.

(C) FC (day 14 vs. day 0) of five individual gRNAs (pink lines) targeting the indicated genes. The shaded region indicates the 95% confidence interval computed using the distribution of non-targeting (NT) gRNAs. The diamond denotes the mean FC of the five gRNAs in HAP1 cells.

(D) Ranking of lncRNAs via robust-rank aggregation (RRA) in HAP1 screens, based on consistent depletion of five individual guide RNA (gRNA) targeting the same gene.

(E) Essential (RRA  $p < 0.05$ ) and non-essential lncRNAs from the Cas13 screens in the five cell lines.

In (B) and (C), the dashed lines indicate the 95% confidence interval for NT gRNAs.

See also [Figures S1, S2, and S3](#).

expressed at 5 reads per kilobase of transcript per million mapped reads (RPKM) or more in at least one organ or donor across all stages ( $n = 297$  human tissue samples). We also targeted an additional ~2,500 lncRNAs from a recent pooled genetic screen using a DNA-targeting CRISPR and those present in a manually curated database of lncRNAs (lncRNAdb).<sup>20,27</sup> In total, we designed a library of ~75,000 guide RNAs (gRNAs) to target 6,199 lncRNAs and 4,390 PCGs with ~8 gRNAs each (Figures 1A and S1A–S1C; Tables S1A and S1B).

We engineered five human cell lines, HAP1, HEK293FT, K562, MDA-MB-231, and THP1, to express the nuclear-localized *RfxCas13d* effector under doxycycline-inducible control (Figure S1D). RNA sequencing (RNA-seq) of the parental and Cas13-engineered cell lines indicated no significant differences in gene expression post-induction (Figure S1E; Tables S1C and S1D). Next, we transduced each cell line with the lentiviral gRNA library at a low multiplicity of infection to ensure each cell received only a single perturbation and induced Cas13

expression via doxycycline addition. We harvested genomic DNA from these cells at 0, 7, and 14 days post-Cas13 induction and computed changes in gRNA abundance via amplicon sequencing ( $n = 20$  transcriptome-scale datasets with two biological replicates for each cell line/time point) (Figure 1A). We found strong agreement between the two independent transduction replicates for each cell line (Figures 1B, S1F, and S1G; Tables S1A–S1E).

We computed changes in gRNA abundance between an early time point (the day of Cas13 induction, which we term day 0) and 14 days after Cas13 induction. We detected consistent depletion among gRNAs targeting lncRNAs with established roles in cell survival, proliferation, and differentiation, such as *MALAT1*<sup>28</sup> and *NEAT1*,<sup>29</sup> as well as essential lncRNAs not described in prior literature (Figures 1C and S1H). In all cell lines, we also observed consistent depletion of gRNAs that target known essential PCGs, as identified by Cas9-based knockout screens performed in more than 1,000 cancer cell lines by the DepMap Consortium

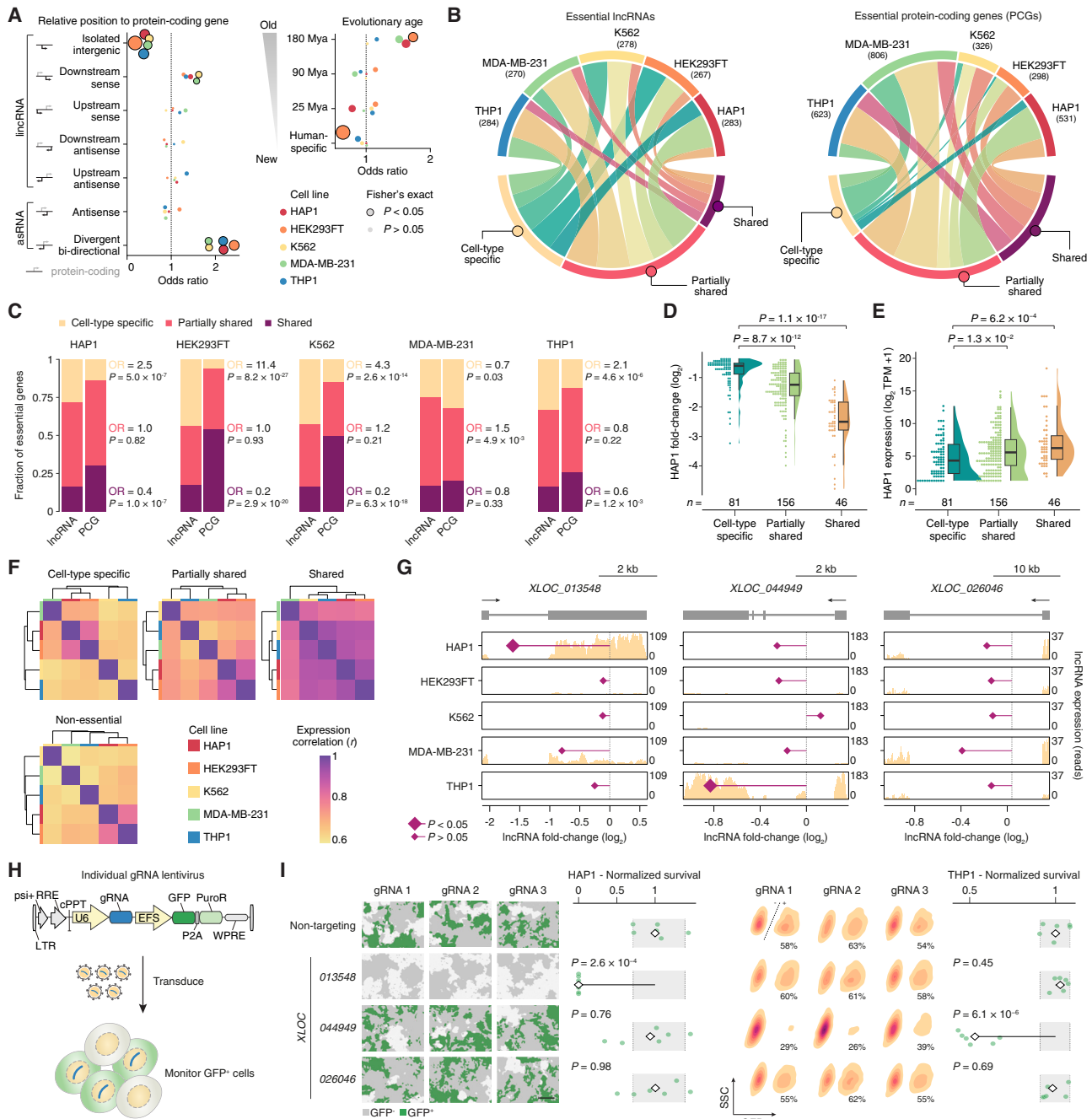


**Figure 2. Distinct and common essential lncRNAs across five cell lines**

(A) Enrichment of essential lncRNAs over non-essential lncRNAs for genomic position to nearest protein-coding gene (PCG) (left) and evolutionary age (right). For evolutionary age, mya denotes million years ago. The odds ratio is determined by a Fisher's exact test with the significance given by the dot size (dark outline indicates  $p < 0.05$ ).

(B) Distribution of shared, partially shared, and cell-type-specific essential lncRNAs (left) and PCGs (right) across all five cell lines. Shared genes are essential in all cell lines, and partially shared genes are essential in two to four cell lines. Numbers in parentheses indicate the number of essential genes in each cell line.

(C) The proportion of essential lncRNAs and PCGs in each cell line. Fisher's exact test for essential lncRNAs compared with essential PCGs for each essentiality category (see categories in B).

(D) Fold-change (FC, day 14 vs. day 0) of cell-type-specific, partially shared, and shared essential lncRNAs in HAP1 cells after Cas13 induction.

(E) Expression of cell-type-specific, partially shared, and shared essential lncRNAs in HAP1 cells.

(F) Pearson correlation of essential (upper) and non-essential lncRNAs (lower) expression across five cell lines.

(G) FC (day 14 vs. day 0, x axis) and RNA-seq reads/expression (y axis) for two cell-specific essential and one non-essential lncRNAs.

(legend continued on next page)

(Figure S1I). Given that we designed multiple gRNAs to target each gene (lncRNA or protein-coding), we assessed the depletion of distinct gRNAs targeting the same gene (Figure S1J) and computed a gene-level ranking using robust-rank aggregation (RRA) (Figures 1D and S2A; Tables S2F–S2J). Many of the highly depleted (essential) lncRNAs were already identified as essential at day 7 after Cas13 induction (Figure S2B).

As a quality control measure, we compared the change in abundance of Cas13 gRNAs designed to target 4,390 PCGs targeted in the library with Cas9-based knockout screens from the DepMap Consortium.<sup>30</sup> The enrichment/depletion of these gRNAs demonstrated a high correlation with DepMap datasets utilizing DNA-targeting perturbations ( $0.59 < r < 0.72$ , Figure S2C), suggesting that Cas13 and Cas9 can both identify essential PCGs and do so in a comparable manner. The PCGs commonly classified as essential by DepMap were also depleted in the RNA-targeting CRISPR screens (Figure S2D).

For each cell line, we performed stranded total RNA-seq after ribosomal RNA depletion to quantify the expression of lncRNAs and PCGs (Tables S1C and S1D). Approximately 10% of the expressed lncRNAs exhibited significant depletion in each cell line (Figure 1E), a proportion similar to essential PCGs in the human genome found using genome-scale Cas9 knockout screens.<sup>31–34</sup> As others have found,<sup>13,35</sup> the correlation of transcript expression among lncRNAs is generally lower than that among PCGs across cell lines (Figure S2E). In each cell line, we also found a lower correlation between expression and essentiality—using both our Cas13 screens (for lncRNAs and PCGs) and Cas9-based DepMap screens (for PCGs) (Figure S2F–G). After stratifying lncRNAs and PCGs into expression quartiles, we compared the enrichment of essential genes in each quartile (Figures S3A–S3D). For both lncRNAs and PCGs, we found that highly expressed genes (Q4) are more likely to be essential compared with lowly expressed (Q1) genes, although the majority of highly expressed genes (~86% lncRNAs, ~60% PCGs) are not essential. However, we also observed a key difference between lncRNAs and PCGs: we identified a higher fraction of essential lncRNAs in the lower expression quartiles (Q1) compared with PCGs (Figure S3E). This suggests that lncRNAs not only exhibit lower expression correlation between cell lines but also function effectively at lower expression levels.

### Distinct and common essential lncRNAs for proliferation

Using large-scale pooled transcriptome screens, we compared lncRNAs across the five cell lines to identify shared and cell-specific essential lncRNAs. We identified a total of 778 lncRNAs that were essential in one or more cell lines. As a group, we found that

essential lncRNAs were enriched for divergent bi-directional transcripts and tended to have fewer isolated intergenic transcripts (Figure 2A). Additionally, there were fewer human-specific transcripts than expected and a larger fraction of older (180 Mya) transcripts, indicating the essential lncRNAs are more likely to be evolutionarily conserved (Figure 2A).

Among the 778 essential lncRNAs, we found that 61% (477 essential lncRNAs) were cell-type-specific (essential in only one cell line), 33% (255) were partially shared (essential in two to four cell lines), and 6% (46) were shared essentials (essential in all five cell lines) (Figures S4A and S4B). Compared with PCGs, essential lncRNAs were more cell-type-specific with less overlap between cell lines (Fisher's exact test,  $p < 0.05$ , Figures 2B and 2C). The shared essential lncRNAs—those essential in all 5 cell lines—exhibited higher depletion in the pooled screens than partially shared or cell-type-specific essential lncRNAs (Figures 2D and S4C). They also had higher transcript abundance compared with cell-type-specific essential lncRNAs, which was consistently observed across multiple cell lines (Figures 2E and S4D).

In general, cell-type-specific—but essential—lncRNAs have a lower correlation in expression across cell lines compared with shared essential lncRNAs (Figure 2F). For instance, the lncRNAs *XLOC\_013548* and *XLOC\_044949* showed variable expression levels across cell lines and were specifically depleted in HAP1 and THP1, respectively (Figure 2G). To rigorously test cell-type-specific functions, we designed an orthogonal assay using individual (arrayed) knockdown and time-lapse imaging (Figure 2H; Table S3A). We targeted each lncRNA with three independent gRNAs. These results indicate clear cell-type-specific depletion: *XLOC\_013548* showed essentiality exclusively in HAP1 cells and *XLOC\_044949* solely in THP1 cells. Importantly, *XLOC\_026046*—a non-essential lncRNA—did not show any depletion in HAP1 or THP1 cells (Figures 2I and S4E). This is in agreement with a previous (CRISPRi-based) study of essential lncRNAs that found similar cell-type-dependent effects.<sup>20</sup>

To directly demonstrate that lncRNA expression alone does not determine essentiality, we targeted two essential (*XLOC\_037681* and *XLOC\_005888*) and two non-essential lncRNAs (*XLOC\_044281* and *XLOC\_000008*) with similarly high expression using three Cas13 gRNAs in HAP1 cells (Figure S4F; Tables S3A and S3B). After confirming transcript knockdown, we found that only cells with perturbations targeting essential lncRNAs deplete after 4 days in a competitive growth assay compared with cells transduced with control (non-targeting) gRNAs (Figures S4G–S4I). This reinforces our prior findings that differences in growth and gRNA depletion are not due to higher levels of off-target, *trans* cleavage resulting from targeting

(H) A GFP-labeled competition assay to quantify the impact of knockdown of essential lncRNAs.

(I) Representative images of HAP1 (left) and flow cytometry of THP1 (right) cells transduced with individual gRNAs targeting highly expressed lncRNAs indicated in (G) 6 days after Cas13 induction. Survival of GFP<sup>+</sup> cells transduced with three non-overlapping gRNAs per gene normalized to non-targeting (NT) gRNAs (right). Each green circle denotes a single gRNA and single transduction replicate. The diamonds denote the mean survival ( $n = 6$  experiments with three gRNAs from two independent transductions). The dashed lines indicate the 95% confidence interval for NT gRNAs. Statistical significance was determined by a Student's *t* test. Scale bar for HAP1 images: 200  $\mu$ m.

In (D) and (E), boxplots indicate the median, 25th, and 75th percentiles, while whiskers are 1.5 times the interquartile range, and statistical significance was determined by a two-sided Mann-Whitney U test.

See also Figure S4.

of highly expressed lncRNAs but instead reflect differential essentiality.<sup>36</sup>

### Shared essential lncRNAs are required for cell proliferation

Next, we proceeded to examine the 46 shared essential lncRNAs in greater detail (Figure 3A). This core set includes *MALAT1*, an abundant lncRNA that has previously been shown to regulate cell motility and cancer metastasis,<sup>37–40</sup> and *MIR17HG*, a miRNA host gene lncRNA that promotes cancer progression.<sup>41,42</sup> In addition, the shared essential lncRNAs include several lncRNAs that have not been previously described in the literature or identified in prior functional genomic studies. Only six of the 46 shared essential lncRNAs were found in a previous study of essential lncRNAs, and for those lncRNAs, they were typically found in only one of the cell lines profiled.<sup>20</sup> Among the shared essential lncRNAs, the majority are antisense RNAs—either antisense to a PCG or divergent bi-directional transcripts (Figures S5A and S5B).

For seven of the shared essential lncRNAs, we cloned three distinct gRNAs to perturb them and confirmed on-target knockdown of all transcripts in HAP1, HEK293FT, and MDA-MB-231 cells (Figure S5C; Tables S3A and S3B). Next, we measured cell growth via the same competitive growth assay. Individual knockdowns resulted in a significant reduction in cells carrying essential lncRNA perturbations compared with cells transduced with control (non-targeting) gRNAs, including for well-known essential lncRNAs like *MALAT1*<sup>28</sup> and *MIR17HG*<sup>43</sup> (Figures 3B and S5D).

To better understand mechanisms underlying essential lncRNAs, we measured how lncRNA perturbations impact cell-cycle progression and apoptosis. To monitor cell-cycle changes, we used a fluorescence ubiquitination cell-cycle indicator (FUCCI) in MDA-MB-231 cells (Figures 3C and S5E–S5G).<sup>44,45</sup> We found that five of the seven shared essential lncRNAs, including *MALAT1*, induced a significant accumulation of cells in the G2-M phase, while two, *XLOC\_047988* and *XLOC\_015918*, led to cell accumulation in the G1 phase (Figures 3D and S5H; Table S3C), in agreement with the findings from competitive growth assays (Figure S5I). We also analyzed the rate of apoptosis using annexin V staining and noted that knockdown of essential lncRNAs consistently increased apoptosis but to differing degrees for each lncRNA (Figures 3E and 3F). Specifically, the knockdown of *XLOC\_032153*, *XLOC\_016044*, and *XLOC\_008323* resulted in a higher level of apoptosis than knockdown of *MALAT1* (Figure 3F). For these seven shared essential lncRNAs, we also performed an orthogonal, non-CRISPR knockdown by targeting each lncRNA with pools of three small interfering RNAs (siRNAs) (Figure S5J; Table S3D). After confirming efficient transcript knockdown by RNAi, we found similar reductions in cell proliferation and increases in apoptosis (Figures S5K and S5L). These individual perturbations of shared or cell-type-specific essential as well as non-essential lncRNAs confirm the pooled screen findings, recapitulating the varying degrees of depletion observed in different cell lines in the initial pooled screens.

### Essential lncRNAs act independently of nearest PCGs

A long-standing mechanistic question is whether lncRNAs act locally (e.g., *ANRIL* suppresses transcription of nearby PCGs

and *XIST* silences genes on the X chromosome)<sup>46,47</sup> or have more global effects. To reveal whether the essentiality of lncRNAs and PCGs depends on their genomic proximity to each other, we examined 5,452 pairs of lncRNA and their nearest PCGs. Through our massively parallel screens, each gene in the pair (lncRNA and PCG) was knocked down via Cas13 in five cell lines. By perturbing lncRNAs and PCGs at the RNA level, our approach has the advantage of being able to target genes with greater specificity (e.g., transcript-specific and strand-specific) than DNA-targeting approaches, which can modulate multiples genes if they are in close proximity.<sup>20,21</sup>

In this manner, we were able to identify hundreds of essential genes within these pairs across all cell lines (Figure 4A). The asymmetric distribution between essential lncRNAs and PCGs suggests that most often one—but not both—genes are crucial for cell proliferation. Interestingly, we found that across all cell lines there is only a small fraction of lncRNA-PCG pairs in which both genes are essential (Figures 4B, S6A, and S6B). For example, in HAP1 cells, we identified many more lncRNA-PCG pairs where either the lncRNA or PCG was essential (590 pairs) and substantially fewer where both the lncRNA and its nearest PCG were essential (54 pairs) (Figures 4C and S6C–S6F).

To validate this observation, we selected three lncRNAs with an antisense orientation to nearby PCGs with either one essential gene (lncRNA or PCG) or both classified as essential (Figure 4D). In all three cases, we targeted each gene in the pair using three independent gRNAs, confirmed strand-specific on-target knockdown, and monitored cell growth via the same imaging-based assay as before (Figures 4E and S7G). For all 3 pairs (6 genes), we confirmed the depletion/essentiality as observed in the pooled screen. For example, we found that the PCG *WARS2*—located in an antisense orientation adjacent to the essential lncRNA *XLOC\_001366*—was dispensable and its depletion had no impact on growth compared with cells receiving control (non-targeting) perturbations. For this pair, only the lncRNA was essential, and when the lncRNA *XLOC\_001366* was targeted by Cas13, it led to a significant reduction in proliferation. By contrast, we found that the lncRNA *XLOC\_020797*—located in an antisense orientation adjacent to the essential PCG *SRSF1*—was dispensable. Interestingly, *XLOC\_020797* was identified as essential in a prior CRISPRi screen,<sup>20</sup> which may be a misclassification given the close proximity between the transcription start sites of *XLOC\_020797* and *SRSF1* (<1 kb), the overlapping transcripts, and the essentiality of *SRSF1*. This nuanced interplay highlights the relative autonomy of essential lncRNAs, and their nearby PCGs.

For the third lncRNA-PCG pair (*SLC16A1-AS1* and *SLC16A1*), both the lncRNA and the nearby PCG were essential in the HAP1 pooled screens. We confirmed these results in the competition assay, showing that knockdown of the lncRNA (*SLC16A1-AS1*) and the PCG (*SLC16A1*) reduces cell proliferation when compared with non-targeting controls, although *SLC16A1-AS1* knockdown results in a more profound phenotypic effect (Figures 4E and S7G). This is consistent with DepMap classification,<sup>30</sup> which designates *SLC16A1* as strongly selective (essential in multiple cell lines). Among the 43 shared essential lncRNAs with a paired PCG perturbation in the library, the nearest PCG is essential for 21 of them in at least one cell line and only for four of

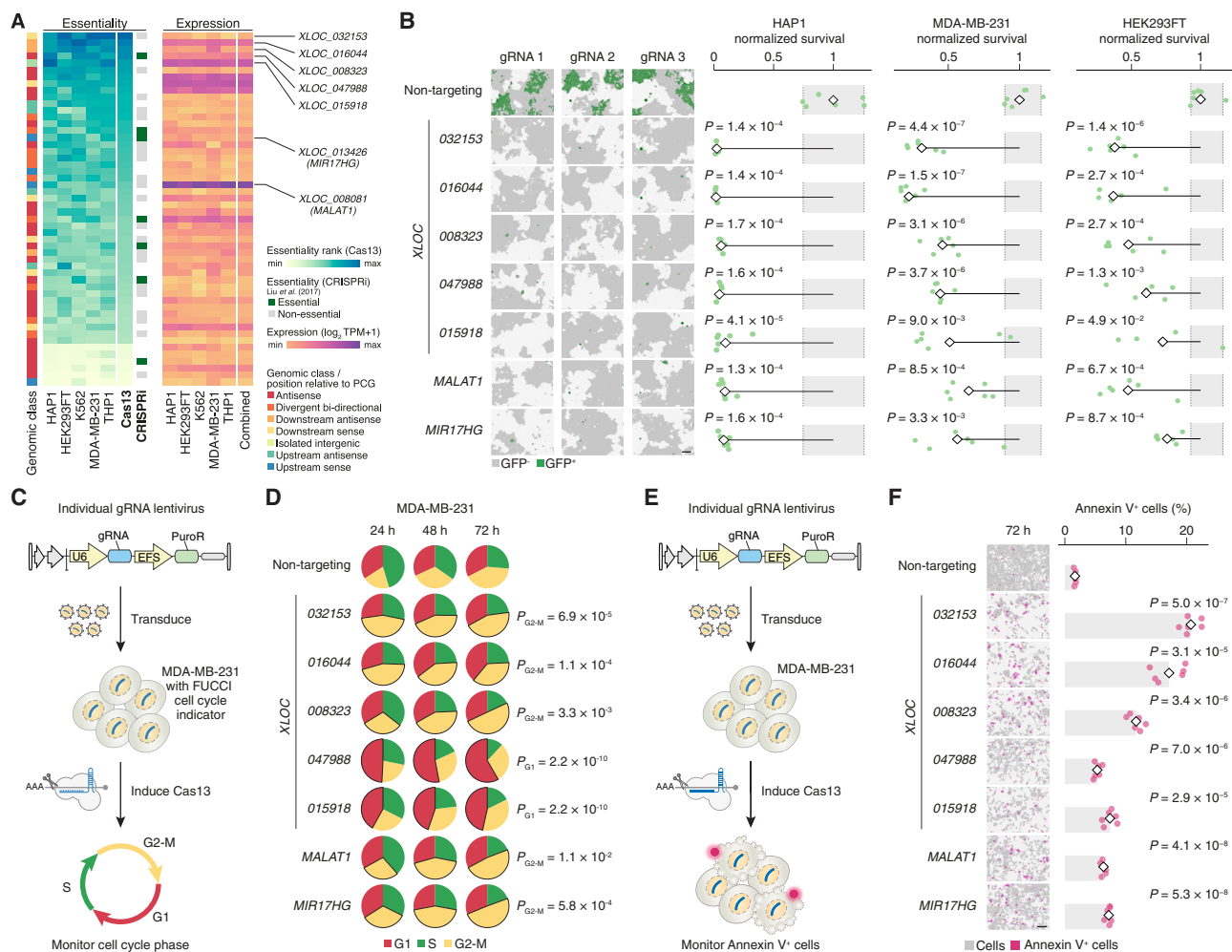


**Figure 3. Knockdown of shared essential lncRNAs reduces cell survival**

(A) Essentiality, expression levels, and genomic classification of shared essential lncRNAs ordered by their median essentiality ( $n = 5$  cell lines). For comparison, six non-essential lncRNAs are included at the bottom of the heatmap. For some lncRNAs, a prior CRISPRi screen examined essentiality, and we have indicated those lncRNAs found to be essential in any cell line screened ( $n = 7$  cell lines screened with CRISPRi)<sup>20</sup>.

(B) Representative images of HAP1 cells transduced with individual gRNAs targeting shared essential lncRNAs indicated in (A) 4 days after Cas13 induction (left). Survival of GFP<sup>+</sup> cells transduced with three non-overlapping gRNAs per gene normalized to non-targeting (NT) gRNAs in HAP1, MDA-MB-231, and HEK293FT (right). Each green circle denotes a single gRNA and single transduction replicate. The diamonds denote the mean survival ( $n = 6$  experiments with three gRNAs from two independent transductions). The gray shaded area indicates the 95% confidence interval for NT gRNAs.

(C) Fluorescence ubiquitination cell-cycle indicator (FUCCI) assay to measure cell fraction in different cell-cycle phases.

(D) Median distribution of MDA-MB-231 cells transduced with indicated gRNAs in cell-cycle phases G1 (red), S (green), and G2-M (yellow) 24, 48, and 72 h after Cas13 induction ( $n = 54$  images per perturbation and time point with 9 images per biological replicate and 6 biological replicates per perturbation).  $P$  values from the predominantly enriched cell-cycle phase (determined for each lncRNA individually) were computed by a Mann-Whitney U test to test for differences from cells transduced with NT gRNAs.

(E) Apoptosis assay using annexin V staining.

(F) Representative images of MDA-MB-231 cells transduced with gRNAs targeting shared essential lncRNAs at 72 h after Cas13 induction (left). Annexin V<sup>+</sup> cells were quantified and normalized to the total cell area (right). Each pink circle denotes a single gRNA and single transduction replicate. The diamonds denote the mean survival ( $n = 54$  images per perturbation with 9 images per biological replicate and 6 biological replicates per perturbation).

In (B) and (F), statistical significance was determined by a Student's  $t$  test. Scale bar: 200  $\mu$ m.

See also Figure S5.

them in all cell lines (Figure 4F). In 15 out of 21 instances where the nearest PCG is essential, the lncRNA is located very close ( $<1$  kb) to the nearest PCG.

Given this minimal overlap between essential lncRNAs and neighboring PCGs, we wondered whether lncRNA loci may instead contact other (essential) PCGs in the native,

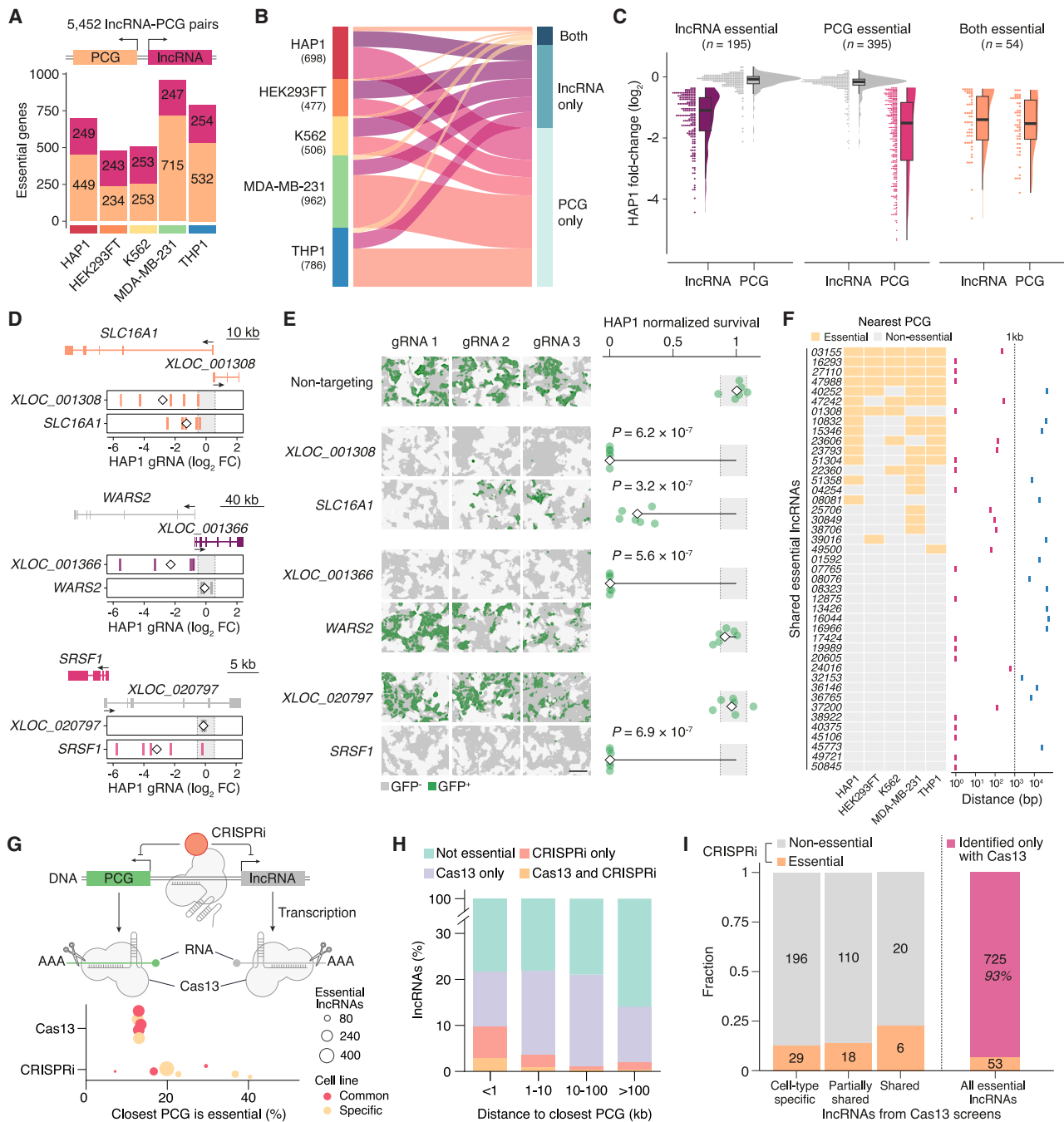


**Figure 4. Nearest protein-coding genes of essential lncRNAs are often not essential**

(A) Number of essential lncRNAs and PCGs across five cell lines.

(B) Alluvial diagram of lncRNA-PCG pairs, depicting pairs where only the lncRNA is essential, where only the PCG is essential, and where both the lncRNA and nearest PCG are essential. Numbers in parentheses indicate lncRNA-PCG pairs with at least one essential gene in each cell line.

(C) Fold-change (FC, day 14 vs. day 0) of lncRNAs and PCGs in each lncRNA-PCG pair in HAP1 cells after Cas13 induction. The pairs are separated by those pairs where only the lncRNA is essential (left), where only the PCG is essential (middle), and where both the lncRNA and nearest PCG are essential (right). Boxplots indicate the median and interquartile range (IQR) with whiskers indicating 1.5x IQR.

(D) Examples of lncRNA-PCG pairs where one or both genes are essential. FC of five individual gRNAs targeting the indicated genes with the 95% confidence interval (CI) of non-targeting (NT) gRNAs (gray). The diamond denotes the mean of the five gRNAs.

(E) Representative images of HAP1 cells transduced with individual gRNAs targeting indicated genes 5 days after Cas13 induction (left). Survival of GFP<sup>+</sup> cells transduced with three non-overlapping gRNAs per gene normalized to the median of NT gRNAs (right). Each green circle denotes a single gRNA and single

(legend continued on next page)

three-dimensional genome. Using chromosome conformation capture (Hi-C) datasets,<sup>48</sup> we found that 53%–62% of essential lncRNAs are found in the same topologically associating domains (TADs) that contain essential PCGs from DepMap screens (Figures S7A and S7B). To quantify direct contacts, we performed H3K27ac HiChIP, a sequencing-based proximity assay to detect genome elements in close contact with PCG promoters, in HAP1 cells. We found that only a minority of essential lncRNAs (4%–11%) directly contact essential PCGs (Figures S7C–S7F). These results suggest that most essential lncRNAs do not exert their influence on cell fitness through the modulation of nearby essential PCGs. Essential lncRNAs (when defined by the essentiality of the transcript itself) are not transcriptional bystanders but rather co-evolved genes, required for proliferation of human cells.

Next, we assessed the ability of CRISPR-Cas13 to identify lncRNAs where the transcript itself is essential—and not neighboring PCGs—by comparing our set of essential lncRNAs with those from a set of CRISPRi-based lncRNA screens.<sup>20</sup> Compared with the CRISPRi screens, the RNA-targeting (Cas13) screens identify a smaller fraction of essential lncRNAs that are close to essential PCGs (Figure 4G; Table S1A). When comparing essential lncRNAs, the ones identified solely in the prior CRISPRi screens are enriched for lncRNAs located in close proximity (<1 kb) to a nearby PCG (Figure 4H). Given that CRISPRi cannot selectively target specific transcripts when transcription start sites are in close proximity,<sup>49</sup> these results suggest that RNA-targeting CRISPRs avoid confounding effects of neighboring essential PCGs (false positives). For instance, we identified lncRNA-PCG pairs in close proximity, where either both genes were essential, with the PCG also identified by Cas9-based knockout screens (Figure S7H), or only the lncRNA was essential (Figure S7I). We further investigated putative false positive hits from the CRISPRi screen—cases where the lncRNA is close to an essential PCG—and were able to resolve several complex loci at the transcript level (Figure S7J). In total, we identified 725 essential lncRNAs that were not reported in the previous genome-scale CRISPRi study (Figure 4I). In this manner, Cas13 targeting can reveal the functional autonomy of essential lncRNAs from nearby PCGs and reduce false positives in complex loci containing essential PCGs.

### Single-cell sequencing identifies proliferation-associated pathways

Next, we sought to understand the mechanisms underlying how individual essential lncRNAs contribute to cell proliferation. To

this end, we used Cas13 RNA Perturb-seq (CaRPool-seq) to couple pooled CRISPR-Cas13 perturbations with a transcriptomic readout in single cells.<sup>50</sup> This method incorporates the direct capture of barcode gRNAs (bcgRNAs) within gRNA arrays, facilitating the identification of specific perturbations in single cells. We designed a new pooled Cas13 library targeting 50 essential lncRNAs and 21 PCGs with three individual gRNA arrays for each target. Each array included two distinct gRNAs that target the same gene (lncRNA or PCG) and a corresponding bcgRNA to identify the array (Figure 5A; Table S4A). After transducing the pooled library into MDA-MB-231, we analyzed the gRNA array representation and found strong correlation with the prior transcriptome-wide screen (Figures 5B and S8A; Table S4B).

We then transduced both MDA-MB-231 and HAP1 cells with this focused library and performed single-cell RNA-seq. After sequencing and analysis, we obtained 5,933 single MDA-MB-231 and 6,606 single HAP1 cells. For a subset of the lncRNAs, we also targeted their closest PCGs. We found minimal impact on the expression of closest PCGs when the corresponding essential lncRNAs were perturbed (14 out of 16 cases showed no differential expression, Figure S8B). However, we identified distinct expression patterns triggered by essential lncRNA perturbations in both MDA-MB-231 and HAP1 cells (Figures 5C and S8C–S8F; Table S4C). For example, in MDA-MB-231 cells, we found downregulation of known essential genes, such as the translation initiation factor *EIF2B3*, inhibitor of apoptosis family member survivin (encoded by *BIRC5*), and mitotic spindle regulator *AURKB* (Figure 5C). Concurrently, we observed upregulation in genes associated with reduced proliferation, as identified in a recent overexpression screen (Figures S8C and S8E).<sup>52</sup>

Gene set enrichment analysis (GSEA) revealed unique pathways modulated by different perturbations (Figure 5D; Tables S4D and S4E). Reassuringly, we noted a pronounced downregulation of the MYC (normalized enrichment score [NES] = –6.00) and mTOR (NES = –2.96) pathways following perturbations of *MYC* and *MTOR*, respectively. Additionally, perturbations of essential genes, whether lncRNAs or PCGs, consistently upregulated the tumor-suppressive p53 pathway, while downregulating pathways associated with proliferation such as mitotic spindle organization and cell-cycle checkpoints (e.g., E2F targets and G2M checkpoint). Overall, changes in pathways were consistent across both cell lines—MDA-MB-231 and HAP1—that were used in the CaRPool-seq (Figures 5D and S9A). We also performed bulk stranded mRNA-seq after

transduction replicate. The diamonds denote the mean survival ( $n = 6$  experiments with three gRNAs from two independent transductions). The dashed lines indicate the 95% CI for NT gRNAs. Statistical significance was determined by a Student's *t* test. Scale bar: 200  $\mu$ m.

(F) Essentiality of the closest PCGs (left) and the distance between lncRNAs and closest PCGs (right) for the shared essential lncRNAs. Orange boxes indicate that the closest PCG is essential. For distances, pink lines denote a distance of less than 1 kb between the lncRNA and PCG, and blue lines denote a distance greater than 1 kb. (G) Key mechanistic differences in knockdown of lncRNAs and nearby genes with DNA-targeting CRISPRi or RNA-targeting Cas13 (upper). The proportion of essential closest PCGs for lncRNAs identified in this study and a prior lncRNA pooled CRISPRi screen (lower).<sup>20</sup> Dot size corresponds to the number of essential lncRNAs identified. Common cell lines used in both studies (HEK293FT, K562, and MDA-MB-231) are labeled in pink, and the study-specific cell lines are labeled in yellow.

(H) The fraction of essential lncRNAs identified in the CRISPRi study and this study, categorized by the distance to their nearest PCG and whether they were identified as essential in the DNA-targeting (CRISPRi) study, this RNA-targeting (Cas13) study, or both studies.

(I) The fraction of essential lncRNAs identified in both DNA- and RNA-targeting studies, categorized by essentiality level (left) and all essential lncRNAs (right) from this (RNA-targeting) study.

See also Figures S6 and S7.

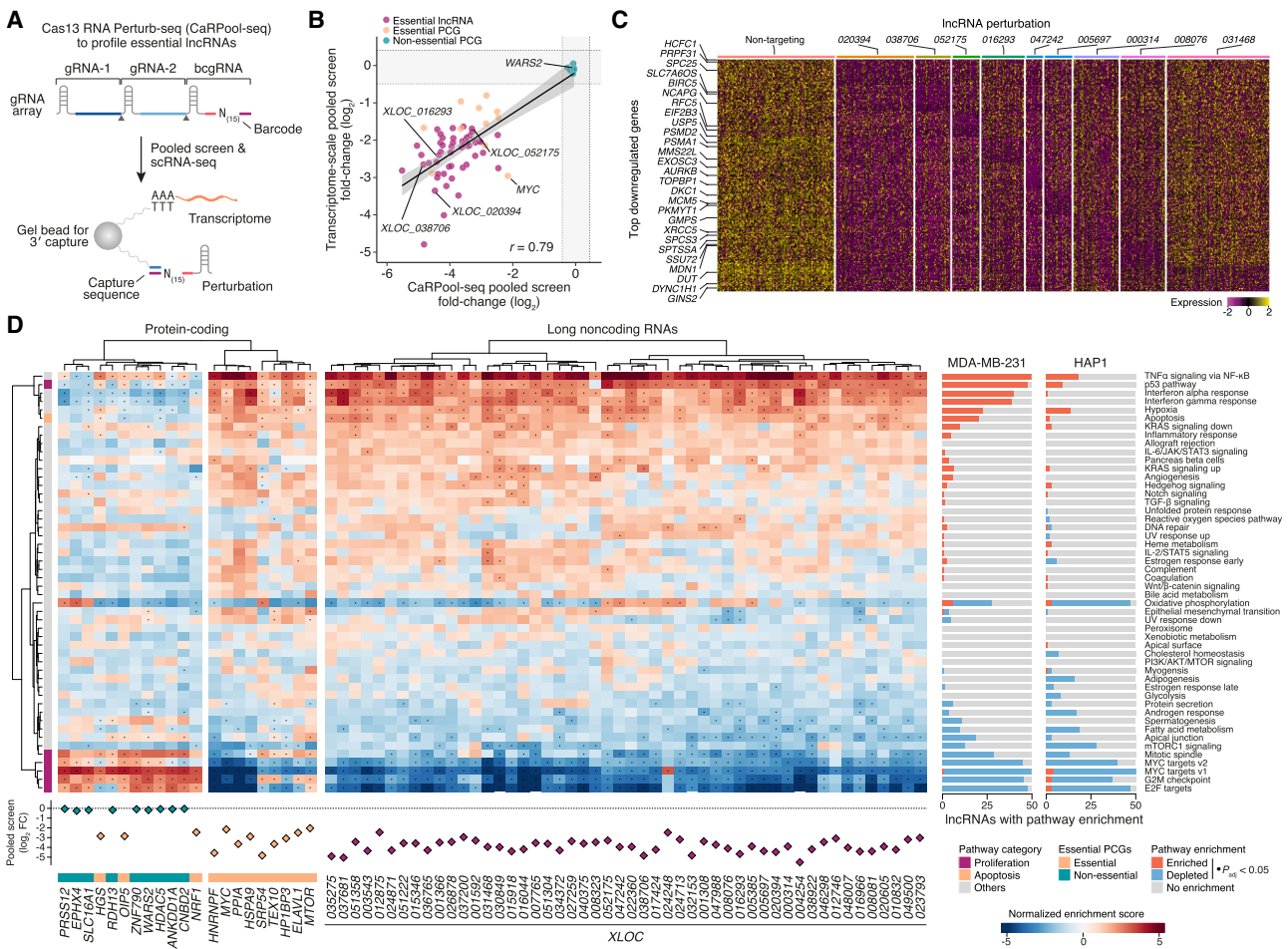


**Figure 5. Single-cell transcriptomics after Cas13 perturbation (CaRPool-seq) of essential lncRNAs identifies shared cellular pathways for proliferation**

(A) Schematic of Cas13 RNA Perturb-seq (CaRPool-seq) using guide RNA (gRNA) arrays that encode two gRNAs that target the same gene (lncRNA or protein-coding). Each array also contains a barcode gRNA (bcgRNA) to enable identification of the gRNA array using single-cell sequencing.

(B) Correlation between fold-change (FC) from the transcriptome-scale pooled screen (day 14 vs. day 0) and the CaRPool-seq pooled screen (day 12 vs. day 0) for 50 essential lncRNAs (purple) and 21 protein-coding genes (orange and green) in MDA-MB-231 cells. The dashed lines indicate the 95% confidence interval for non-targeting gRNAs.

(C) Single-cell mRNA expression heatmap with the 25 most differentially downregulated genes for each lncRNA perturbation in MDA-MB-231 cells ( $p_{adj} < 0.05$ ). For each lncRNA, transcripts with the lowest median DepMap scores are labeled ( $n = 3$  most essential transcripts per lncRNA and median over 1,095 DepMap cell lines). Statistical significance was determined by a two-sided Mann-Whitney U test with Bonferroni correction.

(D) Normalized enrichment scores (NESS) from gene set enrichment analysis (GSEA) for 21 perturbed PCGs (left) and 50 perturbed essential lncRNAs (middle) in MDA-MB-231 cells. The number of lncRNAs with the indicated pathway (MSigDB Hallmark pathways<sup>51</sup>) enriched or depleted ( $p_{adj} < 0.05$ , black dots) in CaRPool-seq from MDA-MB-231 and HAP1 cells (right). Statistical significance was determined by a Kolmogorov-Smirnov test with Benjamini-Hochberg correction. Pathways categorized as proliferation or apoptosis are labeled (far left column).<sup>51</sup> The FC in gRNA array abundance from the pooled readout of the MDA-MB-231 CaRPool-seq is shown at the bottom.

See also [Figures S8](#) and [S9](#).

perturbing five essential lncRNAs also targeted in the CaRPool-seq library and found that pathway enrichment in the bulk RNA-seq was correlated with the single-cell data ([Figures S9B](#) and [S9C](#); [Tables S4F](#) and [S4G](#)).

Despite the global similarities in gene expression and proliferation pathway changes upon knockdown of essential lncRNAs, we found that most pathways remain unaffected by respective lncRNA perturbations ([Figures 5D](#) and [S9A](#)). We also identified that specific subsets of lncRNAs have distinct effects on certain

pathways, such as the oxidative phosphorylation. Interestingly, the two essential lncRNAs that induced G1 phase accumulation in the cell-cycle analyses—*XLOC\_047988* and *XLOC\_015918*—also led to increased enrichment of genes associated with hypoxia ([Figure S9D](#)). In line with these findings, prior work has shown that hypoxia induces G1 arrest.<sup>53</sup> Furthermore, while nearly all lncRNA perturbations upregulated the p53 pathway, we observed direct *TP53* transcript upregulation only in a subset of these cases ([Figure S9E](#)). In others, we noted a downregulation

of *MDM2*, a post-translational repressor of p53, which can lead to altered p53 protein expression.<sup>54</sup> Despite the consistent upregulation of *TP53* and its well-known role in DNA repair and apoptosis, we found that only a subset of essential lncRNA perturbations upregulate genes involved in DNA repair. Taken together, transcriptome profiling in MDA-MB-231 and HAP1 cells revealed several common and distinct mechanisms related to cell survival and proliferation, further reinforcing their role as essential lncRNAs as identified in the initial pooled screens.

### Essential lncRNA expression during development

Given recent efforts to comprehensively map lncRNA expression across development and in different tissues (Figures 6A and S10A),<sup>19</sup> we wondered whether essential lncRNAs may have distinct patterns of expression *in vivo*. Essential lncRNAs showed 5- to 7-fold increased expression across organs and developmental stages *in vivo* (Figure S10B, Mann-Whitney U,  $p < 0.05$ ). We also found that essential lncRNAs tend to exhibit widespread expression across different tissues and are broadly expressed at various time points during development (Figure 6B). Non-essential lncRNAs, on the other hand, show more restricted expression across different tissues and developmental periods (Figure 6B), suggesting specialized functions distinct from cell survival/proliferation.

Interestingly, we also observed a significant enrichment of developmentally dynamic transcripts—those exhibiting differential expression across developmental stages—in essential lncRNAs (Fisher's exact test,  $p < 0.05$ , Figures 6C, S10C, and S10D). By profiling their expression across different developmental stages in the brain, heart, liver, and kidney, we found that those essential lncRNAs with dynamic expression profiles are most highly expressed in the early stages of human development with decreased expression in later stages (Figures 6D, S10E, and S10F). These lncRNAs may be important during embryonic development, where cell proliferation is high. By contrast, non-essential lncRNAs tended to show an opposite pattern: lower expression levels in early development and higher expression at later stages.

In human development, we found a stronger correlation between shared essential lncRNAs and genes that serve as markers of proliferation, such as *PCNA* and *MK167* (Figure S11A). Therefore, we examined co-expression patterns between each lncRNA targeted in the Cas13 library and all PCGs throughout development (from 4 weeks post-conception to old age). We found that co-expressed PCGs for the shared essential lncRNAs were enriched for genes involved in cell proliferation, such as cell-cycle, *MYC* targets, and mitotic spindle organization during brain, heart, liver, and kidney development (Figures 6E and S11B; Tables S5A–S5D). In brain development, 61% of the shared essential lncRNAs (28 of the 46) are co-expressed with PCGs in proliferation pathways; we found similar enrichments across all organs (Figures 6F and S11B). Overall, essential lncRNAs have higher expression *in vivo* than non-essential lncRNAs and tend to be more highly expressed during early stages of development.

### Essential lncRNAs in cancer progression

Given the strong association with proliferation, we hypothesized that essential lncRNAs may also play a role in cancer progres-

sion. Previous genome-scale CRISPR screens to knockout PCGs found that cancer-associated genes are over-represented in essential PCGs,<sup>56,57</sup> suggesting a fundamental link between cell viability and tumorigenesis. We delved into the role of essential lncRNAs in human tumors by re-aligning RNA-seq data from 8,878 primary tumors and 686 matched normal tissues spanning 29 cancer types from The Cancer Genome Atlas (TCGA) to a reference lncRNA transcriptome (Figures 7A and S12A; Table S6A). We found that essential lncRNAs displayed elevated expression in both tumors and matched normal tissues—with greater increases for more essential lncRNAs (Figures 7B and S12B).

When comparing tumors to normal tissues (Figure S12C; Table S6B), we found that essential lncRNAs are more often differentially expressed in tumors compared with non-essential lncRNAs (Figure 7C, Fisher's exact test,  $p < 0.05$ ). Among the 164 differentially expressed essential lncRNAs, 76 were upregulated, 78 lncRNAs were downregulated, and 10 exhibited mixed expression patterns in various tumors. Reassuringly, we also identified several lncRNAs with established roles in cancer progression. For example, *MALAT1*, which was significantly downregulated in breast cancer, colon cancer, lung cancer, and endometrial cancer, has previously been shown to have decreased expression in breast cancer metastases.<sup>38,40</sup> Similarly, *KCNQ1OT1* was significantly upregulated in colon and prostate cancer, as others have shown.<sup>58,59</sup>

To understand the functional roles of essential lncRNAs, we identified PCGs with correlated expression patterns in TCGA primary tumors for each lncRNA. We found that the co-expressed PCGs of essential lncRNAs were enriched for cell proliferation and that the enrichment was greatest for shared essential lncRNAs (Figure 7D; Table S7). For example, oncogenic lncRNAs *OIP5-AS1* (*XLOC\_016293*) and *ZFAS1* (*XLOC\_030849*) are co-expressed with PCGs in *MYC*, E2F, cell-cycle checkpoint, and mTOR pathways (Figure S12D) and have been shown to promote tumorigenesis in multiple tumor types.<sup>60–63</sup> Other lncRNAs, such as *CALCRL-AS1* (*XLOC\_027685*) and *LINC02821* (*XLOC\_010832*), are co-expressed with PCGs that are in immune-related pathways (Figure S12D), suggesting distinct co-expressed genes and functional roles for different essential lncRNAs.

To further assess the clinical relevance of essential lncRNA expression, we categorized tumors as either lncRNA-high or lncRNA-low based on lncRNA expression and then examined whether these groups showed significant differences in overall or progression-free survival. Each cancer cohort was analyzed individually to mitigate bias arising from the distinct features of various cancer types. We found that 34 out of the 46 shared essential lncRNAs were associated with improved or worsened survival (Figures 7E, 7F, and S12E–S12G; Table S8). For instance, increased expression of *SLC16A1-AS1* is correlated with worse overall survival in three cancer types (glioma, renal clear cell carcinoma, and uterine endometrial carcinoma) and worse progression-free survival in two cancer types (glioma and prostate adenocarcinoma) (Figure 7G). This agrees with our *in vitro* data, showing that knockdown of *SLC16A1-AS1* (*XLOC\_001308*) is lethal in leukemia cells (Figure 4E). When more closely matching the tumor samples to

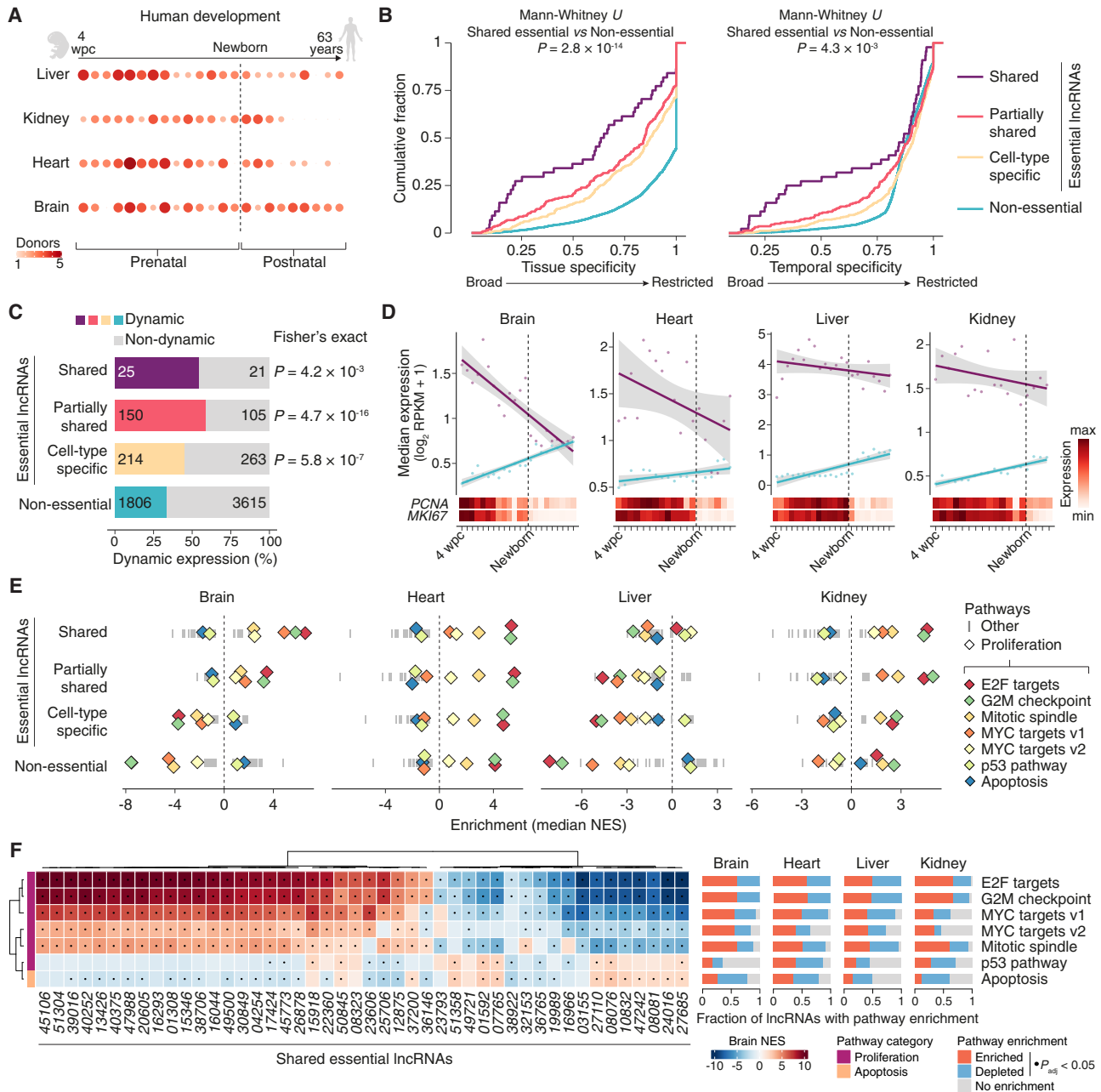


**Figure 6. Essential lncRNAs are expressed broadly across different tissues and at early stages of development**

(A) Transcriptome profiles for each tissue at various developmental time points from recent developmental atlases of lncRNA and PCG expression ( $n = 182$  tissue samples).<sup>19,55</sup>

(B) Empirical cumulative distributions of tissue-specificity (left) and time-specificity (right) indices for essential and non-essential lncRNAs (two-sided Mann-Whitney U test).

(C) The proportion of dynamic lncRNAs for essential and non-essential lncRNAs (Fisher's exact test in comparison to non-essential lncRNAs).

(D) The median expression of dynamic shared essential (purple) and non-essential (turquoise) lncRNAs at different developmental time points in each tissue. The heatmaps below provide annotations for the relative abundance of proliferation markers *PCNA* and *MKI67*.

(E) Gene set enrichment analysis (GSEA) of co-expressed PCGs for essential and non-essential lncRNAs across tissues, represented by the median normalized enrichment scores (NESs) across 50 GSEA hallmark pathways.

(F) NES of proliferation- or apoptosis-associated pathways (a subset of MSigDB Hallmark pathways<sup>51</sup>) for each of the shared essential lncRNAs in brain (left). The fraction of shared essential lncRNAs with proliferation- or apoptosis-associated pathways enriched or depleted ( $p_{adj} < 0.05$ , black dots) across different tissues (right). Statistical significance was determined by a Kolmogorov-Smirnov test with Benjamini-Hochberg correction.

See also [Figures S10](#) and [S11](#).

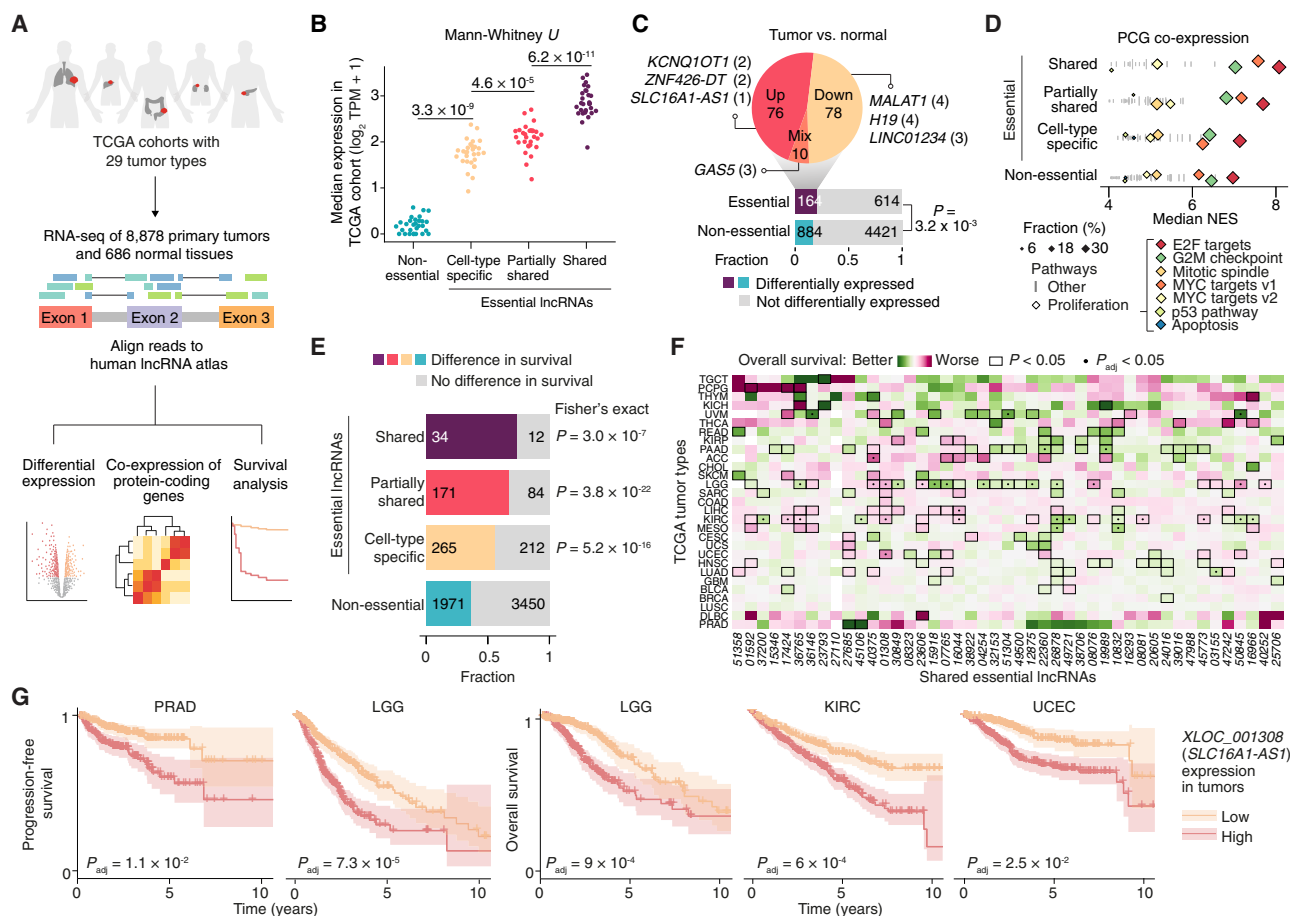


**Figure 7. Essential lncRNAs are differentially expressed in tumors and correlate with survival**

(A) Computational workflow to identify functional lncRNAs across 29 cancer types from The Cancer Genome Atlas (TCGA).

(B) Median expression of essential and non-essential lncRNAs in primary tumors from 29 cancer types (two-sided Mann-Whitney U test).

(C) The fraction of differentially expressed lncRNAs in primary tumors compared with normal tissue across 22 cancer types (bottom). The pie chart (top) separates differentially expressed essential lncRNAs by expression level: high (increased expression in tumor), low (decreased expression in tumor), and mix (varying expression in different cancer types). The number of cancer types with significant differential expression for the example lncRNAs is indicated in parentheses (Fisher's exact test).

(D) Gene set enrichment analysis (GSEA) of co-expressed protein-coding genes (PCGs) for essential and non-essential lncRNAs, represented by the median normalized enrichment scores (NESs) across 50 MSigDB Hallmark pathways.<sup>51</sup> Marker size represents the fraction of lncRNAs within each respective group. Only enriched pathways in the top quartile (by NES) are plotted. Statistical significance was determined by a Kolmogorov-Smirnov test with Benjamini-Hochberg (BH) correction.

(E) The proportion of lncRNAs associated with better or worse overall survival or progression-free survival.

(F) Survival analysis coefficients for TCGA tumor types for the 46 shared essential lncRNAs. lncRNAs with negative coefficients (pink) are associated with worse survival outcomes (increased hazard). lncRNAs with positive coefficients (green) are associated with better survival outcomes (decreased hazard). Rectangles denote  $p < 0.05$  (log rank test), and black dots denote  $p_{adj} < 0.05$  (BH-adjusted log rank test).

(G) Kaplan-Meier progression-free (left) and overall survival (right) estimates for patients with prostate adenocarcinoma (PRAD), low-grade glioma (LGG), kidney renal clear cell carcinoma (KIRC), and uterine corpus endometrial carcinoma (UCEC) stratified by the expression of *SLC16A1-AS1* (BH-adjusted log rank test). Sample sizes for high and low expression groups: LGG:  $n = 257$  (high),  $n = 259$  (low). KIRC:  $n = 265$  (high),  $n = 265$  (low). UCEC:  $n = 272$  (high),  $n = 263$  (low). See also Figure S12.

the cells with Cas13 perturbations (breast invasive carcinomas [BRCA] and MDA-MB-231 pooled screens), we found similar results for essential lncRNAs for expression and survival analyses (Figures S12H–S12J). These analyses link essential lncRNAs to cancer progression and yield new transcriptomic biomarkers that can be tied to function via perturbation screens.

## DISCUSSION

The recent advent of RNA-targeting CRISPR nucleases and pooled screens using these tools have made it possible to perturb thousands of noncoding RNAs in a precise manner and profile their function.<sup>23,64</sup> Since the discovery of pervasive transcription in the genome more than a decade ago,<sup>1,2,65</sup> one

striking puzzle has been to identify the functional role, if any, of the thousands of transcribed lncRNAs. Here, transcriptome-scale RNA-targeting CRISPR screens provide a functional survey at the RNA level and pinpoint which lncRNAs are required across five human cell lines. This systematic approach, combined with comprehensive validation of the pooled screens and integration with multiple independent datasets, suggests a role for lncRNAs as important players in cell proliferation, human development, and cancer.

Out of more than 6,000 targeted lncRNAs, we identified 778 lncRNAs as essential for cell viability, with 61% as cell-type-specific essential lncRNAs and 39% as essential in multiple cell lines. For essential lncRNAs, we found that, in most cases, their nearest PCGs were dispensable, suggesting that these lncRNAs do not function exclusively through the regulation of nearby PCGs. Even for those lncRNAs that do regulate nearby PCGs, it can be challenging to distinguish regulatory activity due to DNA *cis*-regulatory elements from regulation due to the transcript itself. For example, a recent study at the *Lockd-Cdkn1b* locus in mouse erythroblasts reconciled phenotypic differences between insertion of a poly-adenylation signal near the beginning of the lncRNA *Lockd* to abrogate transcription (no change in *Cdkn1b* expression) and deletion of the lncRNA (reduced *Cdkn1b* expression): regulation of *Cdkn1b* expression was mediated entirely by a DNA *cis*-regulatory element at the 5' end of *Lockd* without any involvement of the transcript.<sup>22</sup> This example—along with several others from our study—demonstrates the unmet need for precise, scalable perturbations at the RNA level to avoid potential confounders from nearby PCGs or genomic *cis*-regulatory elements.

By examining the expression and distribution of lncRNAs *in vivo*, we found that essential lncRNAs are highly expressed early in development, which contrasts with non-essential lncRNAs that are more highly expressed in later stages of development and with greater tissue-specificity. We also extended our analyses from organismal development to disease states using primary tumors from 29 human cancers. After re-aligning expression data from ~9,000 TCGA primary tumors to a lncRNA-inclusive reference transcriptome, we were able to show that essential lncRNAs are more often differentially expressed in tumors than other lncRNAs and that nearly all of the shared essential lncRNAs can serve as biomarkers for survival in certain tumor types.

Although our study focused on correlation between oncogenesis and essential lncRNAs, these observations raise a tantalizing possibility: namely, that lncRNAs may be targetable dependencies in cancer. In the decade since the development of genome-scale CRISPR screens to perturb PCGs, many groups have deployed these methods to identify synthetic lethal interactions, such as PARP and Pol $\theta$  inhibition in BRCA-mutant tumors,<sup>66–69</sup> ATR inhibition in ATM mutant tumors,<sup>69</sup> PRMT5 inhibition in *MTAP/CDKN2A*-deleted cancers,<sup>70,71</sup> and PKMYT1 inhibition in *CCNE1*-amplified cancers.<sup>72</sup> With this work, we hope that similar progress might be possible using synthetic lethal lncRNA interactions. Recent successes with antisense oligonucleotides (ASOs) targeting cancer-specific miRNAs underscore the potential of ASOs as effective therapeutics toward lncRNAs.<sup>73</sup> The prospect of designing ASOs to inhibit functional

lncRNAs in tumorigenesis opens an unexplored avenue for therapeutic intervention. The essential lncRNAs identified in this study, implicated in various tumor phenotypes, emerge as potential targets with clinical applications.<sup>74</sup> Conducting further studies, especially in pre-clinical platforms such as tumor-derived organoids or mouse models, will be instrumental in systematically exploring these clinical applications.

The framework of transcriptome-scale RNA-targeting CRISPR screens established in this study is broadly applicable and not limited to lncRNAs. It can be directly applied to other noncoding RNAs, including enhancer RNAs and circular RNAs,<sup>75,76</sup> for interrogating the functional contribution of noncoding transcripts. As we have shown, a major advantage of Cas13 and RNA-targeting CRISPR nucleases is their ability to dissect complex and gene-dense loci situated in close proximity to PCGs. Overall, transcriptome-wide Cas13 pooled transcriptomic screens represent a powerful tool for the systematic investigation of the functional contributions of noncoding transcripts and pave the way to identify functional lncRNAs for any phenotype or disease.

#### Limitations of the study

In this study, we used an RNA-targeting CRISPR (Cas13) to assess lncRNA essentiality, laying the groundwork for a DepMap-like categorization of lncRNAs across various cell types. We were limited by the single phenotypic readout—essentiality as measured by growth in cell culture—and that only those lncRNAs that are expressed in the selected cell lines can be assayed with loss-of-function perturbations. Due to the low abundance and tissue-specificity of lncRNAs, approximately one-third of lncRNAs were not expressed in the cell lines and thus served as negative controls in our screens. Future studies in cells/tissues where these lncRNAs are expressed will be required to probe their essentiality. In addition, our Cas13 library, though extensive, does not cover every lncRNA among the growing number of noncoding RNAs identified through deeper transcriptomic profiling. For this study, we used a recent *de novo* pan-tissue reference based on lncRNAs expressed during human development in multiple tissues. We also re-aligned TCGA tumor samples to this developmental lncRNA reference, which may omit lncRNAs that are expressed exclusively in cancer. Other annotation sources, such as GENCODE, include lncRNAs that are expressed in cell lines or primary tumors. Many of these were omitted from our library due to their low expression levels, but this highlights the importance of the chosen lncRNA reference in the Cas13 library design. To avoid false negatives, future studies should include a broader range of cell types and utilize Cas13 libraries designed using more inclusive reference assemblies—although there is always a trade-off between numbers of gene targets/perturbations and screen feasibility. Finally, each cell received only a single lncRNA perturbation, potentially missing interactions between lncRNAs or between lncRNAs and PCGs. In the future, pooled or single-cell screens using Cas13 gRNA arrays with combinatorial perturbations could reveal these interactions. Despite these limitations, our study offers a valuable resource and a roadmap for more expansive Cas13 libraries targeting more transcripts (with individual and combinatorial perturbations) to further elucidate the complex regulatory networks of the human transcriptome.

## RESOURCE AVAILABILITY

### Lead contact

Further information and requests for resources and reagents should be directed to and will be fulfilled by the lead contact, Neville Sanjana ([neville@sanjanalab.org](mailto:neville@sanjanalab.org)).

### Materials availability

The Cas13 lncRNA pooled gRNA library and plasmids are available through Addgene.

### Data and code availability

Genomic datasets (Cas13 pooled screens, RNA-seq, and CaRPool-seq) are available via BioProject (PRJNA1161603). TCGA data were downloaded from the Genomic Data Commons (GDC) portal (<https://portal.gdc.cancer.gov/>, [https://www.ncbi.nlm.nih.gov/projects/gap/cgi-bin/study.cgi?study\\_id=phs000178.v11.p8](https://www.ncbi.nlm.nih.gov/projects/gap/cgi-bin/study.cgi?study_id=phs000178.v11.p8)). Reference genomes were downloaded from GDC (<https://gdc.cancer.gov/about-data/gdc-data-processing/gdc-reference-files>), 10x Genomics (<https://www.10xgenomics.com/support/software/cell-ranger/downloads>), and HISAT2 (<https://daehwankimlab.github.io/hisat2/download/>). Hi-C TADs were downloaded from the Yue lab (<http://3dgenome.fsm.northwestern.edu/publications.html>).

## ACKNOWLEDGMENTS

We thank the entire Sanjana laboratory for support and advice. We are also grateful to G. Gürsoy, I. Sarropoulos, S. Liu, A. Ellingwood, A. Stirn, and X. Guo and to the NYU Biology Genomics Core for sequencing resources. The results presented are partially based upon data generated by the TCGA Research Network: <https://www.cancer.gov/tcga>. N.E.S. is supported by the NIH/NHGRI (DP2HG010099 and R01HG012790), the NIH/National Cancer Institute (NCI) (R01CA279135 and R01CA218668), the NIH/National Institute of Allergy and Infectious Diseases (NIAID) (R01AI176601), the NIH/National Heart Lung and Blood Institute (NHLBI) (R01HL168247), the Simons Foundation for Autism Research, the MacMillan Center for the Study of the Noncoding Cancer Genome, New York University, and the New York Genome Center.

## AUTHOR CONTRIBUTIONS

W.-W.L., S.M., and N.E.S. conceived the project. H.-H.W., A.S., and N.E.S. designed the lncRNA library. W.-W.L., S.M., S.K.H., H.-H.W., A.M.-M., O.C., L.L., and B.W. performed pooled Cas13 screens. W.-W.L., S.M., and S.K.H. analyzed pooled Cas13 screens. S.M., S.K.H., A.M.-M., O.C., O.K., and A.C. conducted validation assays. C.M.C. and W.-W.L. performed and analyzed the H3K27ac AQuA-HiChIP assay. S.M. and S.K.H. conducted the CaRPool-seq, and W.-W.L. and S.M. analyzed the data. N.E.S. supervised the work. W.-W.L., S.M., and N.E.S. wrote the manuscript with input from all authors.

## DECLARATION OF INTERESTS

The New York Genome Center and New York University have applied for patents related to the work in this article. H.-H.W. is a cofounder of Neptune Bio. N.E.S. is an advisor to Qiagen and a cofounder and advisor of OverT Bio and TruEdit Bio.

## STAR★METHODS

Detailed methods are provided in the online version of this paper and include the following:

- **KEY RESOURCES TABLE**
- **EXPERIMENTAL MODEL AND STUDY PARTICIPANT DETAILS**
  - Monoclonal Cas13 cell line generation and cell culture
- **METHOD DETAILS**
  - Transcriptome-scale and CaRPool-seq Cas13 libraries: Design and cloning
  - Pooled lentiviral production
  - Pooled Cas13 library CRISPR screens

- Single-cell sequencing coupled with Cas13 perturbations (CaRPool-seq)
- Arrayed gRNA cloning and lentiviral production
- Competitive cell growth assays
- Cell cycle analyses
- Apoptosis assays
- RNA interference
- RNA-sequencing
- H3K27ac AQuA-HiChIP
- Quantitative reverse-transcription PCR (RT-qPCR)
- **QUANTIFICATION AND STATISTICAL ANALYSIS**
  - Pooled screen analysis
  - Total RNA-sequencing analyses
  - H3K27ac AQuA-HiChIP and Hi-C analysis
  - CaRPool-seq analysis: Pooled screen
  - CaRPool-seq analysis: Single-cell
  - Bulk mRNA-seq processing
  - Developmental gene expression analyses
  - Tumor gene expression and survival analyses
  - Matched expression lncRNA analyses
  - Gene set enrichment analyses

## SUPPLEMENTAL INFORMATION

Supplemental information can be found online at <https://doi.org/10.1016/j.cell.2024.10.021>.

Received: January 4, 2024

Revised: July 9, 2024

Accepted: October 12, 2024

Published: November 7, 2024

## REFERENCES

1. ENCODE; Project Consortium, Birney, E., Stamatoyannopoulos, J.A., Dutta, A., Guigó, R., Gingeras, T.R., Margulies, E.H., Weng, Z., Snyder, M., Dermitzakis, E.T., et al. (2007). Identification and analysis of functional elements in 1% of the human genome by the ENCODE pilot project. *Nature* 447, 799–816. <https://doi.org/10.1038/nature05874>.
2. Carninci, P., Kasukawa, T., Katayama, S., Gough, J., Frith, M.C., Maeda, N., Oyama, R., Ravasi, T., Lenhard, B., Wells, C., et al. (2005). The transcriptional landscape of the mammalian genome. *Science* 309, 1559–1563. <https://doi.org/10.1126/science.1112014>.
3. Ulitsky, I., and Bartel, D.P. (2013). lincRNAs: genomics, evolution, and mechanisms. *Cell* 154, 26–46. <https://doi.org/10.1016/j.cell.2013.06.020>.
4. Kopp, F., and Mendell, J.T. (2018). Functional classification and experimental dissection of long noncoding RNAs. *Cell* 172, 393–407. <https://doi.org/10.1016/j.cell.2018.01.011>.
5. Tay, Y., Rinn, J., and Pandolfi, P.P. (2014). The multilayered complexity of ceRNA crosstalk and competition. *Nature* 505, 344–352. <https://doi.org/10.1038/nature12986>.
6. Tichon, A., Gil, N., Lubelsky, Y., Havkin Solomon, T., Lemze, D., Itzkovitz, S., Stern-Ginossar, N., and Ulitsky, I. (2016). A conserved abundant cytoplasmic long noncoding RNA modulates repression by Pumilio proteins in human cells. *Nat. Commun.* 7, 12209. <https://doi.org/10.1038/ncomms12209>.
7. Daneshvar, K., Ardehali, M.B., Klein, I.A., Hsieh, F.-K., Kratkiewicz, A.J., Mahpour, A., Cancelliere, S.O.L., Zhou, C., Cook, B.M., Li, W., et al. (2020). lncRNA DIGIT and BRD3 protein form phase-separated condensates to regulate endoderm differentiation. *Nat. Cell Biol.* 22, 1211–1222. <https://doi.org/10.1038/s41556-020-0572-2>.
8. Anderson, D.M., Anderson, K.M., Chang, C.-L., Makarewich, C.A., Nelson, B.R., McAnally, J.R., Kasaragod, P., Shelton, J.M., Liou, J., Bassey-Duby, R., et al. (2015). A micropeptide encoded by a putative long

- noncoding RNA regulates muscle performance. *Cell* 160, 595–606. <https://doi.org/10.1016/j.cell.2015.01.009>.
9. Matsumoto, A., Pasut, A., Matsumoto, M., Yamashita, R., Fung, J., Monteleone, E., Saghatelian, A., Nakayama, K.I., Clohessy, J.G., and Pandolfi, P.P. (2017). mTORC1 and muscle regeneration are regulated by the LINC00961-encoded SPAR polypeptide. *Nature* 541, 228–232. <https://doi.org/10.1038/nature21034>.
  10. Mercer, T.R., and Mattick, J.S. (2013). Structure and function of long non-coding RNAs in epigenetic regulation. *Nat. Struct. Mol. Biol.* 20, 300–307. <https://doi.org/10.1038/nsmb.2480>.
  11. Statello, L., Guo, C.-J., Chen, L.-L., and Huarte, M. (2021). Gene regulation by long non-coding RNAs and its biological functions. *Nat. Rev. Mol. Cell Biol.* 22, 96–118. <https://doi.org/10.1038/s41580-020-00315-9>.
  12. Djebali, S., Davis, C.A., Merkel, A., Dobin, A., Lassmann, T., Mortazavi, A., Tanzer, A., Lagarde, J., Lin, W., Schlesinger, F., et al. (2012). Landscape of transcription in human cells. *Nature* 489, 101–108. <https://doi.org/10.1038/nature11233>.
  13. Derrien, T., Johnson, R., Bussotti, G., Tanzer, A., Djebali, S., Tilgner, H., Guernec, G., Martin, D., Merkel, A., Knowles, D.G., et al. (2012). The GENCODE v7 catalog of human long noncoding RNAs: analysis of their gene structure, evolution, and expression. *Genome Res.* 22, 1775–1789. <https://doi.org/10.1101/gr.132159.111>.
  14. Mukherjee, N., Calviello, L., Hirsekorn, A., de Pretis, S., Pelizzola, M., and Ohler, U. (2017). Integrative classification of human coding and noncoding genes through RNA metabolism profiles. *Nat. Struct. Mol. Biol.* 24, 86–96. <https://doi.org/10.1038/nsmb.3325>.
  15. Schlackow, M., Nojima, T., Gomes, T., Dhir, A., Carmo-Fonseca, M., and Proudfoot, N.J. (2017). Distinctive patterns of transcription and RNA processing for human lincRNAs. *Mol. Cell* 65, 25–38. <https://doi.org/10.1016/j.molcel.2016.11.029>.
  16. Mattioli, K., Volders, P.-J., Gerhardinger, C., Lee, J.C., Maass, P.G., Melé, M., and Rinn, J.L. (2019). High-throughput functional analysis of lncRNA core promoters elucidates rules governing tissue specificity. *Genome Res.* 29, 344–355. <https://doi.org/10.1101/gr.242222.118>.
  17. Ponting, C.P., and Haerty, W. (2022). Genome-wide analysis of human long noncoding RNAs: A provocative review. *Annu. Rev. Genomics Hum. Genet.* 23, 153–172. <https://doi.org/10.1146/annurev-genom-112921-123710>.
  18. Ponjavic, J., Ponting, C.P., and Lunter, G. (2007). Functionality or transcriptional noise? Evidence for selection within long noncoding RNAs. *Genome Res.* 17, 556–565. <https://doi.org/10.1101/gr.6036807>.
  19. Sarropoulos, I., Marin, R., Cardoso-Moreira, M., and Kaessmann, H. (2019). Developmental dynamics of lncRNAs across mammalian organs and species. *Nature* 571, 510–514. <https://doi.org/10.1038/s41586-019-1341-x>.
  20. Liu, S.-J., Horlbeck, M.A., Cho, S.W., Birk, H.S., Malatesta, M., He, D., Atenello, F.J., Villalta, J.E., Cho, M.Y., Chen, Y., et al. (2017). CRISPRi-based genome-scale identification of functional long noncoding RNA loci in human cells. *Science* 355, aah7111. <https://doi.org/10.1126/science.aah7111>.
  21. Joung, J., Engreitz, J.M., Konermann, S., Abudayyeh, O.O., Verdine, V.K., Aguet, F., Gootenberg, J.S., Sanjana, N.E., Wright, J.B., Fulco, C.P., et al. (2017). Genome-scale activation screen identifies a lncRNA locus regulating a gene neighbourhood. *Nature* 548, 343–346. <https://doi.org/10.1038/nature23451>.
  22. Paralkar, V.R., Taborda, C.C., Huang, P., Yao, Y., Kossenkov, A.V., Prasad, R., Luan, J., Davies, J.J., Hughes, J.R., Hardison, R.C., et al. (2016). Unlinking an lncRNA from its Associated cis Element. *Mol. Cell* 62, 104–110. <https://doi.org/10.1016/j.molcel.2016.02.029>.
  23. Wessels, H.-H., Méndez-Mancilla, A., Guo, X., Legut, M., Daniloski, Z., and Sanjana, N.E. (2020). Massively parallel Cas13 screens reveal principles for guide RNA design. *Nat. Biotechnol.* 38, 722–727. <https://doi.org/10.1038/s41587-020-0456-9>.
  24. Guo, X., Rahman, J.A., Wessels, H.-H., Méndez-Mancilla, A., Haro, D., Chen, X., and Sanjana, N.E. (2021). Transcriptome-wide Cas13 guide RNA design for model organisms and viral RNA pathogens. *Cell Genom.* 1, 100001. <https://doi.org/10.1016/j.xgen.2021.100001>.
  25. Méndez-Mancilla, A., Wessels, H.-H., Legut, M., Kadina, A., Mabuchi, M., Walker, J., Robb, G.B., Holden, K., and Sanjana, N.E. (2022). Chemically modified guide RNAs enhance CRISPR-Cas13 knockdown in human cells. *Cell Chem. Biol.* 29, 321–327.e4. <https://doi.org/10.1016/j.chembiol.2021.07.011>.
  26. Abudayyeh, O.O., Gootenberg, J.S., Essletzbichler, P., Han, S., Joung, J., Belanto, J.J., Verdine, V., Cox, D.B.T., Kellner, M.J., Regev, A., et al. (2017). RNA targeting with CRISPR-Cas13. *Nature* 550, 280–284. <https://doi.org/10.1038/nature24049>.
  27. Quek, X.C., Thomson, D.W., Maag, J.V., Bartonicek, N., Signal, B., Clark, M.B., Gloss, B.S., and Dinger, M.E. (2015). lncRNADB v2.0: expanding the reference database for functional long noncoding RNAs. *Nucleic Acids Res.* 43, D168–D173. <https://doi.org/10.1093/nar/gku988>.
  28. Ji, P., Diederichs, S., Wang, W., Böing, S., Metzger, R., Schneider, P.M., Tidow, N., Brandt, B., Buerger, H., Bulk, E., et al. (2003). MALAT-1, a novel noncoding RNA, and thymosin beta4 predict metastasis and survival in early-stage non-small cell lung cancer. *Oncogene* 22, 8031–8041. <https://doi.org/10.1038/sj.onc.1206928>.
  29. Clemson, C.M., Hutchinson, J.N., Sara, S.A., Ensminger, A.W., Fox, A.H., Chess, A., and Lawrence, J.B. (2009). An architectural role for a nuclear noncoding RNA: NEAT1 RNA is essential for the structure of paraspeckles. *Mol. Cell* 33, 717–726. <https://doi.org/10.1016/j.molcel.2009.01.026>.
  30. Tsherniak, A., Vazquez, F., Montgomery, P.G., Weir, B.A., Kryukov, G., Cowley, G.S., Gill, S., Harrington, W.F., Pantel, S., Krill-Burger, J.M., et al. (2017). Defining a cancer dependency map. *Cell* 170, 564–576.e16. <https://doi.org/10.1016/j.cell.2017.06.010>.
  31. Rancati, G., Moffat, J., Typas, A., and Pavelka, N. (2018). Emerging and evolving concepts in gene essentiality. *Nat. Rev. Genet.* 19, 34–49. <https://doi.org/10.1038/nrg.2017.74>.
  32. Wang, T., Birsoy, K., Hughes, N.W., Krupczak, K.M., Post, Y., Wei, J.J., Lander, E.S., and Sabatini, D.M. (2015). Identification and characterization of essential genes in the human genome. *Science* 350, 1096–1101. <https://doi.org/10.1126/science.aac7041>.
  33. Blomen, V.A., Májek, P., Jae, L.T., Bigenzahn, J.W., Nieuwenhuis, J., Staring, J., Sacco, R., van Diemen, F.R., Olk, N., Stukalov, A., et al. (2015). Gene essentiality and synthetic lethality in haploid human cells. *Science* 350, 1092–1096. <https://doi.org/10.1126/science.aac7557>.
  34. Hart, T., Chandrashekar, M., Aregger, M., Steinhart, Z., Brown, K.R., MacLeod, G., Mis, M., Zimmermann, M., Fradet-Turcotte, A., Sun, S., et al. (2015). High-resolution CRISPR screens reveal fitness genes and genotype-specific cancer liabilities. *Cell* 163, 1515–1526. <https://doi.org/10.1016/j.cell.2015.11.015>.
  35. Nojima, T., and Proudfoot, N.J. (2022). Mechanisms of lncRNA biogenesis as revealed by nascent transcriptomics. *Nat. Rev. Mol. Cell Biol.* 23, 389–406. <https://doi.org/10.1038/s41580-021-00447-6>.
  36. Hart, S.K., Wessels, H.-H., Méndez-Mancilla, A., Müller, S., Drabavicius, G., Choi, O., and Sanjana, N.E. (2024). Low copy CRISPR-Cas13d mitigates collateral RNA cleavage. Preprint at bioRxiv. <https://doi.org/10.1101/2024.05.13.594039>.
  37. Gutschner, T., Hämmerle, M., Eissmann, M., Hsu, J., Kim, Y., Hung, G., Revenko, A., Arun, G., Stentrup, M., Gross, M., et al. (2013). The noncoding RNA MALAT1 is a critical regulator of the metastasis phenotype of lung cancer cells. *Cancer Res.* 73, 1180–1189. <https://doi.org/10.1158/0008-5472.CAN-12-2850>.
  38. Xu, S., Sui, S., Zhang, J., Bai, N., Shi, Q., Zhang, G., Gao, S., You, Z., Zhan, C., Liu, F., et al. (2015). Downregulation of long noncoding RNA MALAT1 induces epithelial-to-mesenchymal transition via the PI3K-AKT pathway in breast cancer. *Int. J. Clin. Exp. Pathol.* 8, 4881–4891.

39. Arun, G., Diermeier, S., Akerman, M., Chang, K.-C., Wilkinson, J.E., Hearn, S., Kim, Y., MacLeod, A.R., Krainer, A.R., Norton, L., et al. (2016). Differentiation of mammary tumors and reduction in metastasis upon Malat1 lncRNA loss. *Genes Dev.* 30, 34–51. <https://doi.org/10.1101/gad.270959.115>.
40. Kim, J., Piao, H.-L., Kim, B.-J., Yao, F., Han, Z., Wang, Y., Xiao, Z., Siverly, A.N., Lawhon, S.E., Ton, B.N., et al. (2018). Long noncoding RNA MALAT1 suppresses breast cancer metastasis. *Nat. Genet.* 50, 1705–1715. <https://doi.org/10.1038/s41588-018-0252-3>.
41. Xu, J., Meng, Q., Li, X., Yang, H., Xu, J., Gao, N., Sun, H., Wu, S., Familiari, G., Relucanti, M., et al. (2019). Long noncoding RNA MIR17HG promotes colorectal cancer progression via miR-17-5p. *Cancer Res.* 79, 4882–4895. <https://doi.org/10.1158/0008-5472.CAN-18-3880>.
42. Yuan, G., Liu, B., Han, W., and Zhao, D. (2019). LncRNA-MIR17HG mediated upregulation of miR-17 and miR-18a promotes colon cancer progression via activating Wnt/ $\beta$ -catenin signaling. *Transl. Cancer Res.* 8, 1097–1108. <https://doi.org/10.21037/tcr.2019.06.20>.
43. Morelli, E., Fulcinitti, M., Samur, M.K., Ribeiro, C.F., Wert-Lamas, L., Henninger, J.E., Gullà, A., Aktas-Samur, A., Todoerti, K., Talluri, S., et al. (2023). A MIR17HG-derived long noncoding RNA provides an essential chromatin scaffold for protein interaction and myeloma growth. *Blood* 141, 391–405. <https://doi.org/10.1182/blood.2022016892>.
44. Sakaue-Sawano, A., Kurokawa, H., Morimura, T., Hanyu, A., Hama, H., Osawa, H., Kashiwagi, S., Fukami, K., Miyata, T., Miyoshi, H., et al. (2008). Visualizing spatiotemporal dynamics of multicellular cell-cycle progression. *Cell* 132, 487–498. <https://doi.org/10.1016/j.cell.2007.12.033>.
45. Ando, R., Sakaue-Sawano, A., Shoda, K., and Miyawaki, A. (2023). Two coral fluorescent proteins of distinct colors for sharp visualization of cell-cycle progression. *Cell Struct. Funct.* 48, 135–144. <https://doi.org/10.1247/csf.23028>.
46. Yap, K.L., Li, S., Muñoz-Cabello, A.M., Raguz, S., Zeng, L., Mujtaba, S., Gil, J., Walsh, M.J., and Zhou, M.-M. (2010). Molecular interplay of the noncoding RNA ANRIL and methylated histone H3 lysine 27 by polycomb CBX7 in transcriptional silencing of INK4a. *Mol. Cell* 38, 662–674. <https://doi.org/10.1016/j.molcel.2010.03.021>.
47. Brown, C.J., Ballabio, A., Rupert, J.L., Lafreniere, R.G., Grompe, M., Tonlorenzi, R., and Willard, H.F. (1991). A gene from the region of the human X inactivation centre is expressed exclusively from the inactive X chromosome. *Nature* 349, 38–44. <https://doi.org/10.1038/349038a0>.
48. Rao, S.S.P., Huntley, M.H., Durand, N.C., Stamenova, E.K., Bochkov, I.D., Robinson, J.T., Sanborn, A.L., Machol, I., Omer, A.D., Lander, E.S., et al. (2014). A 3D map of the human genome at kilobase resolution reveals principles of chromatin looping. *Cell* 159, 1665–1680. <https://doi.org/10.1016/j.cell.2014.11.021>.
49. Morris, J.A., Caragine, C., Daniloski, Z., Domingo, J., Barry, T., Lu, L., Davis, K., Ziosi, M., Glios, D.A., Hao, S., et al. (2023). Discovery of target genes and pathways at GWAS loci by pooled single-cell CRISPR screens. *Science* 380, eadh7699. <https://doi.org/10.1126/science.adh7699>.
50. Wessels, H.-H., Méndez-Mancilla, A., Hao, Y., Papalexi, E., Mauck, W.M., 3rd, Lu, L., Morris, J.A., Mimitou, E.P., Smibert, P., Sanjana, N.E., et al. (2023). Efficient combinatorial targeting of RNA transcripts in single cells with Cas13 RNA Perturb-seq. *Nat. Methods* 20, 86–94. <https://doi.org/10.1038/s41592-022-01705-x>.
51. Liberzon, A., Birger, C., Thorvaldsdóttir, H., Ghandi, M., Mesirov, J.P., and Tamayo, P. (2015). The Molecular Signatures Database (MSigDB) hallmark gene set collection. *Cell Syst.* 7, 417–425. <https://doi.org/10.1016/j.cels.2015.12.004>.
52. Sack, L.M., Davoli, T., Li, M.Z., Li, Y., Xu, Q., Naxerova, K., Wooten, E.C., Bernardi, R.J., Martin, T.D., Chen, T., et al. (2018). Profound tissue specificity in proliferation control underlies cancer drivers and aneuploidy patterns. *Cell* 173, 499–514.e23. <https://doi.org/10.1016/j.cell.2018.02.037>.
53. Gardner, L.B., Li, Q., Park, M.S., Flanagan, W.M., Semenza, G.L., and Dang, C.V. (2001). Hypoxia inhibits G1/S transition through regulation of p27 expression. *J. Biol. Chem.* 276, 7919–7926. <https://doi.org/10.1074/jbc.M010189200>.
54. Haupt, Y., Maya, R., Kazaz, A., and Oren, M. (1997). Mdm2 promotes the rapid degradation of p53. *Nature* 387, 296–299. <https://doi.org/10.1038/387296a0>.
55. Cardoso-Moreira, M., Halbert, J., Valloton, D., Velten, B., Chen, C., Shao, Y., Liechti, A., Ascensão, K., Rummel, C., Ovchinnikova, S., et al. (2019). Gene expression across mammalian organ development. *Nature* 571, 505–509. <https://doi.org/10.1038/s41586-019-1338-5>.
56. Dickerson, J.E., Zhu, A., Robertson, D.L., and Hentges, K.E. (2011). Defining the role of essential genes in human disease. *PLoS One* 6, e27368. <https://doi.org/10.1371/journal.pone.0027368>.
57. Bartha, I., di Iulio, J., Venter, J.C., and Telenti, A. (2018). Human gene essentiality. *Nat. Rev. Genet.* 19, 51–62. <https://doi.org/10.1038/nrg.2017.75>.
58. Duan, Q., Cai, L., Zheng, K., Cui, C., Huang, R., Zheng, Z., Xie, L., Wu, C., Yu, X., and Yu, J. (2020). lncRNA KCNQ1OT1 knockdown inhibits colorectal cancer cell proliferation, migration and invasiveness via the PI3K/AKT pathway. *Oncol. Lett.* 20, 601–610. <https://doi.org/10.3892/ol.2020.11619>.
59. Hao, H., Chen, H., Xie, L., Liu, H., and Wang, D. (2021). LncRNA KCNQ1OT1 promotes proliferation, invasion and metastasis of prostate cancer by regulating miR-211-5p/CHI3L1 pathway. *OncoTargets Ther.* 14, 1659–1671. <https://doi.org/10.2147/OTT.S288785>.
60. Kim, J., Abdelmohsen, K., Yang, X., De, S., Grammatikakis, I., Noh, J.H., and Gorospe, M. (2016). LncRNA OIP5-AS1/cyranos sponges RNA-binding protein HuR. *Nucleic Acids Res.* 44, 2378–2392. <https://doi.org/10.1093/nar/gkw017>.
61. Ghafouri-Fard, S., Dashti, S., Farsi, M., Hussen, B.M., and Taheri, M. (2021). A review on the role of oncogenic lncRNA OIP5-AS1 in human malignancies. *Biomed. Pharmacother.* 137, 111366. <https://doi.org/10.1016/j.biopha.2021.111366>.
62. Rao, M., Xu, S., Zhang, Y., Liu, Y., Luan, W., and Zhou, J. (2021). Long non-coding RNA ZFAS1 promotes pancreatic cancer proliferation and metastasis by sponging miR-497-5p to regulate HMGA2 expression. *Cell Death Dis.* 12, 859. <https://doi.org/10.1038/s41419-021-04123-7>.
63. Wang, H., Chen, Y., Liu, Y., Li, Q., Luo, J., Wang, L., Chen, Y., Sang, C., Zhang, W., Ge, X., et al. (2022). The lncRNA ZFAS1 regulates lipogenesis in colorectal cancer by binding polyadenylate-binding protein 2 to stabilize SREBP1 mRNA. *Mol. Ther. Nucleic Acids* 27, 363–374. <https://doi.org/10.1016/j.omtn.2021.12.010>.
64. Konermann, S., Lotfy, P., Brideau, N.J., Oki, J., Shokhirev, M.N., and Hsu, P.D. (2018). Transcriptome engineering with RNA-targeting Type VI-D CRISPR effectors. *Cell* 173, 665–676.e14. <https://doi.org/10.1016/j.cell.2018.02.033>.
65. ENCODE Project Consortium (2012). An integrated encyclopedia of DNA elements in the human genome. *Nature* 489, 57–74. <https://doi.org/10.1038/nature11247>.
66. Farmer, H., McCabe, N., Lord, C.J., Tutt, A.N.J., Johnson, D.A., Richardson, T.B., Santarosa, M., Dillon, K.J., Hickson, I., Knights, C., et al. (2005). Targeting the DNA repair defect in BRCA mutant cells as a therapeutic strategy. *Nature* 434, 917–921. <https://doi.org/10.1038/nature03445>.
67. Fong, P.C., Boss, D.S., Yap, T.A., Tutt, A., Wu, P., Mergui-Roelvink, M., Mortimer, P., Swaisland, H., Lau, A., O'Connor, M.J., et al. (2009). Inhibition of poly(ADP-ribose) polymerase in tumors from BRCA mutation carriers. *N. Engl. J. Med.* 361, 123–134. <https://doi.org/10.1056/NEJMoa0900212>.
68. Ceccaldi, R., Liu, J.C., Amunugama, R., Hajdu, I., Primack, B., Petalcorin, M.I.R., O'Connor, K.W., Konstantinopoulos, P.A., Elledge, S.J., Boulton, S.J., et al. (2015). Homologous-recombination-deficient tumours are

- dependent on Pol $\theta$ -mediated repair. *Nature* 518, 258–262. <https://doi.org/10.1038/nature14184>.
69. Mateos-Gomez, P.A., Gong, F., Nair, N., Miller, K.M., Lazerini-Denchi, E., and Sfeir, A. (2015). Mammalian polymerase  $\theta$  promotes alternative NHEJ and suppresses recombination. *Nature* 518, 254–257. <https://doi.org/10.1038/nature14157>.
70. Mavrakis, K.J., McDonald, E.R., 3rd, Schlabach, M.R., Billy, E., Hoffman, G.R., deWeck, A., Ruddy, D.A., Venkatesan, K., Yu, J., McAllister, G., et al. (2016). Disordered methionine metabolism in MTAP/CDKN2A-deleted cancers leads to dependence on PRMT5. *Science* 351, 1208–1213. <https://doi.org/10.1126/science.aad5944>.
71. Kryukov, G.V., Wilson, F.H., Ruth, J.R., Paulk, J., Tsherniak, A., Marlow, S.E., Vazquez, F., Weir, B.A., Fitzgerald, M.E., Tanaka, M., et al. (2016). MTAP deletion confers enhanced dependency on the PRMT5 arginine methyltransferase in cancer cells. *Science* 351, 1214–1218. <https://doi.org/10.1126/science.aad5214>.
72. Gallo, D., Young, J.T.F., Fourtounis, J., Martino, G., Álvarez-Quilón, A., Bernier, C., Duffy, N.M., Papp, R., Roulston, A., Stocco, R., et al. (2022). CCNE1 amplification is synthetic lethal with PKMYT1 kinase inhibition. *Nature* 604, 749–756. <https://doi.org/10.1038/s41586-022-04638-9>.
73. Winkle, M., El-Daly, S.M., Fabbri, M., and Calin, G.A. (2021). Noncoding RNA therapeutics - challenges and potential solutions. *Nat. Rev. Drug Discov.* 20, 629–651. <https://doi.org/10.1038/s41573-021-00219-z>.
74. Chang, L., Ruiz, P., Ito, T., and Sellers, W.R. (2021). Targeting pan-essential genes in cancer: challenges and opportunities. *Cancer Cell* 39, 466–479. <https://doi.org/10.1016/j.ccell.2020.12.008>.
75. Li, S., Li, X., Xue, W., Zhang, L., Yang, L.-Z., Cao, S.-M., Lei, Y.-N., Liu, C.-X., Guo, S.-K., Shan, L., et al. (2021). Screening for functional circular RNAs using the CRISPR-Cas13 system. *Nat. Methods* 18, 51–59. <https://doi.org/10.1038/s41592-020-01011-4>.
76. Liu, C.-X., and Chen, L.-L. (2022). Circular RNAs: characterization, cellular roles, and applications. *Cell* 185, 2016–2034. <https://doi.org/10.1016/j.cell.2022.04.021>.
77. Lorenzi, L., Chiu, H.-S., Avila Cobos, F., Gross, S., Volders, P.-J., Cannoodt, R., Nuytens, J., Vanderheyden, K., Anckaert, J., Lefever, S., et al. (2021). The RNA Atlas expands the catalog of human non-coding RNAs. *Nat. Biotechnol.* 39, 1453–1465. <https://doi.org/10.1038/s41587-021-00936-1>.
78. Wang, Y., Song, F., Zhang, B., Zhang, L., Xu, J., Kuang, D., Li, D., Choudhary, M.N.K., Li, Y., Hu, M., et al. (2018). The 3D Genome Browser: a web-based browser for visualizing 3D genome organization and long-range chromatin interactions. *Genome Biol.* 19, 151. <https://doi.org/10.1186/s13059-018-1519-9>.
79. Wessels, H.-H., Stirn, A., Méndez-Mancilla, A., Kim, E.J., Hart, S.K., Knowles, D.A., and Sanjana, N.E. (2024). Prediction of on-target and off-target activity of CRISPR-Cas13d guide RNAs using deep learning. *Nat. Biotechnol.* 42, 628–637. <https://doi.org/10.1038/s41587-023-01830-8>.
80. Martin, M. (2011). Cutadapt removes adapter sequences from high-throughput sequencing reads. *EMBnet J.* 17, 10. <https://doi.org/10.14806/ej.17.1.200>.
81. Langmead, B., Trapnell, C., Pop, M., and Salzberg, S.L. (2009). Ultrafast and memory-efficient alignment of short DNA sequences to the human genome. *Genome Biol.* 10, R25. <https://doi.org/10.1186/gb-2009-10-3-r25>.
82. Leek, J.T., Johnson, W.E., Parker, H.S., Jaffe, A.E., and Storey, J.D. (2012). The sva package for removing batch effects and other unwanted variation in high-throughput experiments. *Bioinformatics* 28, 882–883. <https://doi.org/10.1093/bioinformatics/bts034>.
83. Kolde, R., Laur, S., Adler, P., and Vilo, J. (2012). Robust rank aggregation for gene list integration and meta-analysis. *Bioinformatics* 28, 573–580. <https://doi.org/10.1093/bioinformatics/btr709>.
84. Dobin, A., Davis, C.A., Schlesinger, F., Drenkow, J., Zaleski, C., Jha, S., Batut, P., Chaisson, M., and Gingeras, T.R. (2013). STAR: ultrafast universal RNA-seq aligner. *Bioinformatics* 29, 15–21. <https://doi.org/10.1093/bioinformatics/bts635>.
85. Li, B., and Dewey, C.N. (2011). RSEM: accurate transcript quantification from RNA-Seq data with or without a reference genome. *BMC Bioinformatics* 12, 323. <https://doi.org/10.1186/1471-2105-12-323>.
86. Sonesson, C., Love, M.I., and Robinson, M.D. (2015). Differential analyses for RNA-seq: transcript-level estimates improve gene-level inferences. *F1000Res* 4, 1521.
87. Love, M.I., Huber, W., and Anders, S. (2014). Moderated estimation of fold change and dispersion for RNA-seq data with DESeq2. *Genome Biol.* 15, 550. <https://doi.org/10.1186/s13059-014-0550-8>.
88. Therneau, T.M., and Grambsch, P.M. (2000). *Modeling Survival Data: Extending the Cox Model* (Springer).
89. Therneau, T.M. (2024). A Package for Survival Analysis in R. <https://cran.r-project.org/web/packages/survival/vignettes/survival.pdf>.
90. Kassambara, A., Kosinski, M., and Biecek, P. (2021). *Survminer: drawing Survival Curves using “ggplot2.”* <https://cran.r-project.org/web/packages/survminer/survminer.pdf>.
91. Wu, T., Hu, E., Xu, S., Chen, M., Guo, P., Dai, Z., Feng, T., Zhou, L., Tang, W., Zhan, L., et al. (2021). clusterProfiler 4.0: A universal enrichment tool for interpreting omics data. *Innovation (Camb.)* 2, 100141. <https://doi.org/10.1016/j.xinn.2021.100141>.
92. Zheng, G.X.Y., Terry, J.M., Belgrader, P., Ryvkin, P., Bent, Z.W., Wilson, R., Ziraldo, S.B., Wheeler, T.D., McDermott, G.P., Zhu, J., et al. (2017). Massively parallel digital transcriptional profiling of single cells. *Nat. Commun.* 8, 14049. <https://doi.org/10.1038/ncomms14049>.
93. Hao, Y., Hao, S., Andersen-Nissen, E., Mauck, W.M., 3rd, Zheng, S., Butler, A., Lee, M.J., Wilk, A.J., Darby, C., Zager, M., et al. (2021). Integrated analysis of multimodal single-cell data. *Cell* 184, 3573–3587.e29. <https://doi.org/10.1016/j.cell.2021.04.048>.
94. Liao, Y., Smyth, G.K., and Shi, W. (2014). featureCounts: an efficient general purpose program for assigning sequence reads to genomic features. *Bioinformatics* 30, 923–930. <https://doi.org/10.1093/bioinformatics/btt656>.
95. Kim, D., Paggi, J.M., Park, C., Bennett, C., and Salzberg, S.L. (2019). Graph-based genome alignment and genotyping with HISAT2 and HISAT-genotype. *Nat. Biotechnol.* 37, 907–915. <https://doi.org/10.1038/s41587-019-0201-4>.
96. Conway, J.R., Lex, A., and Gehlenborg, N. (2017). UpSetR: an R package for the visualization of intersecting sets and their properties. *Bioinformatics* 33, 2938–2940. <https://doi.org/10.1093/bioinformatics/btx364>.
97. Gu, Z., Eils, R., and Schlesner, M. (2016). Complex heatmaps reveal patterns and correlations in multidimensional genomic data. *Bioinformatics* 32, 2847–2849. <https://doi.org/10.1093/bioinformatics/btw313>.
98. Gu, Z., Gu, L., Eils, R., Schlesner, M., and Brors, B. (2014). circize Implements and enhances circular visualization in R. *Bioinformatics* 30, 2811–2812. <https://doi.org/10.1093/bioinformatics/btu393>.
99. Servant, N., Varoquaux, N., Lajoie, B.R., Viara, E., Chen, C.-J., Vert, J.-P., Heard, E., Dekker, J., and Barillot, E. (2015). HiC-Pro: an optimized and flexible pipeline for Hi-C data processing. *Genome Biol.* 16, 259. <https://doi.org/10.1186/s13059-015-0831-x>.
100. Quinlan, A.R., and Hall, I.M. (2010). BEDTools: a flexible suite of utilities for comparing genomic features. *Bioinformatics* 26, 841–842. <https://doi.org/10.1093/bioinformatics/btq033>.
101. Dale, R.K., Pedersen, B.S., and Quinlan, A.R. (2011). Pybedtools: a flexible Python library for manipulating genomic datasets and annotations. *Bioinformatics* 27, 3423–3424. <https://doi.org/10.1093/bioinformatics/btr539>.
102. Robinson, J.T., Thorvaldsdóttir, H., Winckler, W., Guttman, M., Lander, E.S., Getz, G., and Mesirov, J.P. (2011). Integrative genomics viewer. *Nat. Biotechnol.* 29, 24–26. <https://doi.org/10.1038/nbt.1754>.

103. Putri, G.H., Anders, S., Pyl, P.T., Pimanda, J.E., and Zanini, F. (2022). Analysing high-throughput sequencing data in Python with HTSeq 2.0. *Bioinformatics* *38*, 2943–2945. <https://doi.org/10.1093/bioinformatics/btac166>.
104. Danecek, P., Bonfield, J.K., Liddle, J., Marshall, J., Ohan, V., Pollard, M.O., Whitwham, A., Keane, T., McCarthy, S.A., Davies, R.M., et al. (2021). Twelve years of SAMtools and BCFtools. *GigaScience* *10*, giab008. <https://doi.org/10.1093/gigascience/giab008>.
105. Mölder, F., Jablonski, K.P., Letcher, B., Hall, M.B., Tomkins-Tinch, C.H., Sochat, V., Forster, J., Lee, S., Twardziok, S.O., Kanitz, A., et al. (2021). Sustainable data analysis with Snakemake. *F1000Res* *10*, 33.
106. Hinrichs, A.S., Karolchik, D., Baertsch, R., Barber, G.P., Bejerano, G., Clawson, H., Diekhans, M., Furey, T.S., Harte, R.A., Hsu, F., et al. (2006). The UCSC Genome Browser Database: update 2006. *Nucleic Acids Res.* *34*, D590–D598. <https://doi.org/10.1093/nar/gkj144>.
107. Chen, S., Sanjana, N.E., Zheng, K., Shalem, O., Lee, K., Shi, X., Scott, D.A., Song, J., Pan, J.Q., Weissleder, R., et al. (2015). Genome-wide CRISPR screen in a mouse model of tumor growth and metastasis. *Cell* *160*, 1246–1260. <https://doi.org/10.1016/j.cell.2015.02.038>.
108. Gryder, B.E., Khan, J., and Stanton, B.Z. (2020). Measurement of differential chromatin interactions with absolute quantification of architecture (AQuA-HiChIP). *Nat. Protoc.* *15*, 1209–1236. <https://doi.org/10.1038/s41596-019-0285-9>.
109. Ewels, P., Magnusson, M., Lundin, S., and Käller, M. (2016). MultiQC: summarize analysis results for multiple tools and samples in a single report. *Bioinformatics* *32*, 3047–3048. <https://doi.org/10.1093/bioinformatics/btw354>.
110. Subramanian, A., Tamayo, P., Mootha, V.K., Mukherjee, S., Ebert, B.L., Gillette, M.A., Paulovich, A., Pomeroy, S.L., Golub, T.R., Lander, E.S., et al. (2005). Gene set enrichment analysis: a knowledge-based approach for interpreting genome-wide expression profiles. *Proc. Natl. Acad. Sci. USA* *102*, 15545–15550. <https://doi.org/10.1073/pnas.0506580102>.
111. Mootha, V.K., Lindgren, C.M., Eriksson, K.-F., Subramanian, A., Sihag, S., Lehar, J., Puigserver, P., Carlsson, E., Ridderstråle, M., Laurila, E., et al. (2003). PGC-1 $\alpha$ -responsive genes involved in oxidative phosphorylation are coordinately downregulated in human diabetes. *Nat. Genet.* *34*, 267–273. <https://doi.org/10.1038/ng1180>.
112. Cancer; Genome; Atlas; Research Network, Weinstein, J.N., Collisson, E.A., Mills, G.B., Shaw, K.R.M., Ozenberger, B.A., Ellrott, K., Shmulevich, I., Sander, C., and Stuart, J.M. (2013). The cancer genome atlas pan-cancer analysis project. *Nat. Genet.* *45*, 1113–1120. <https://doi.org/10.1038/ng.2764>.

## STAR★METHODS

### KEY RESOURCES TABLE

REAGENT or RESOURCE	SOURCE	IDENTIFIER
<b>Antibodies</b>		
anti-HA peptide antibody	Cell Signaling Technology	2367S
Anti-H3k27ac antibody	Active Motif	39133; RRID: AB_2561016
<b>Bacterial and virus strains</b>		
NEB Stable Cells	New England Biolabs	C30401
Endura Electrocompetent Cells	Lucigen	60242-2
<b>Chemicals, peptides, and recombinant proteins</b>		
Polyethyleneimine	Polysciences	23966
Puromycin	Invivogen	ant-pr-1
Blasticidin S	A.G. Scientific	B-1247-SOL
Doxycycline	Sigma-Aldrich	D3447
Doxorubicin	MedChemExpress	HY-15142
Dinaciclib	MedChemExpress	HY-10492
<b>Critical commercial assays</b>		
KAPA Total RNA-seq kit with RiboErase	Roche	07962282001
Stranded mRNA Prep	Illumina	20040532
RNA UD Indexes, Set A	Illumina	20040553
Chromium Single Cell 3' Gene Expression v3.1 with feature barcoding technology for CRISPR screening	10x Genomics	10000127, 10000268 and 10000262
TaqB polymerase	Enzymatics	P7250L
2× Rapid Ligase Buffer	Enzymatics	B1010L
Q5 High-Fidelity DNA Polymerase	NEB	M0491
T7 DNA Ligase	NEB	M0318L
T4 DNA Ligase	NEB	B0202S
Gibson Assembly Master Mix	NEB	E2611L
KAPA HiFi HotStart ReadyMix PCR Kit	Roche	07958935001
SPRI beads	Beckman	B23317
MAXI Fast-Ion Plasmid Purification Kit	IBI Scientific	IB47125
QIAGEN Plasmid Mini Kit	Qiagen	12123
QiaQuick Gel Extraction Kit	Qiagen	28704
DNA Clean & Concentrator	Zymo	D4014
Qubit RNA XR Assay Kit	Thermo	Q10210
Qubit dsDNA HS Assay Kit	Thermo	Q32851
FastDigest <i>Esp3I</i>	Thermo	FD0454
FastDigest <i>LguI</i>	Thermo	FD1934
FastDigest <i>NheI</i>	Thermo	FD0974
FastDigest <i>ApaI</i>	Thermo	FD1414
FastDigest <i>BamHI</i>	Thermo	FD0055
FastDigest <i>KpnI</i>	Thermo	FD0524
FastAP Thermosensitive Alkaline Phosphatase	Thermo	EF0651
Qubit RNA XR Assay Kit	Thermo	Q10210
<i>MboI</i>	NEB	R0147M
DNA Polymerase I Large (Klenow) Fragment	NEB	M0210L
Biotin-14-dATP	Thermo	19524016

(Continued on next page)

**Continued**

REAGENT or RESOURCE	SOURCE	IDENTIFIER
Direct-zol RNA Purification Kit	Zymo	R2062
Agilent High Sensitivity DNA Kit	Agilent	5067-4626
RevertAid Reverse Transcriptase	Thermo	EP0442
Luna Universal qPCR Master Mix	NEB	M3003E
Lipofectamine RNAiMAX	Thermo	13778075
LIVE/DEAD Fixable Violet Dead Cell Stain Kit	Thermo	L34963
Incucyte Annexin V Dye for Apoptosis	Sartorius	4642
Proteinase K	NEB	P8107S
RNase A	A.G.Scientific	R-2000
TE Buffer	Sigma	93283
Dynabeads Protein A	Thermo	10001D
Dynabeads M-280 Streptavidin	Thermo	11205D

**Deposited data**

MDA-MB-231 total RNA-seq fastq	RNA atlas <sup>77</sup>	N/A
Developmental lncRNA annotation (human.lncRNA.gtf)	Sarropoulos et al. <sup>19</sup>	N/A
Developmental samples	Sarropoulos et al. <sup>19</sup> and Cardoso-Moreira et al. <sup>55</sup>	N/A
Fastq files of TCGA RNA-seq samples	TCGA, dbGaP (phs000178.v11.p8)	<a href="https://portal.gdc.cancer.gov/">https://portal.gdc.cancer.gov/</a> , <a href="https://www.ncbi.nlm.nih.gov/projects/gap/cgi-bin/study.cgi?study_id=phs000178.v11.p8">https://www.ncbi.nlm.nih.gov/projects/gap/cgi-bin/study.cgi?study_id=phs000178.v11.p8</a>
GRCh38 reference genome (GRCh38.d1.vd1.fa.tar)	GENCODE	<a href="https://gdc.cancer.gov/about-data/gdc-data-processing/gdc-reference-files">https://gdc.cancer.gov/about-data/gdc-data-processing/gdc-reference-files</a>
GENCODE v36 (gencode.v36.annotation.gtf.gz)	GENCODE	<a href="https://gdc.cancer.gov/about-data/gdc-data-processing/gdc-reference-files">https://gdc.cancer.gov/about-data/gdc-data-processing/gdc-reference-files</a>
10x Genomics reference (refdata-gex-GRCh38-2024-A)	10x Genomics	<a href="https://www.10xgenomics.com/support/software/cell-ranger/downloads">https://www.10xgenomics.com/support/software/cell-ranger/downloads</a>
HISAT2 indexes (UCSC hg38)	HISAT2	<a href="https://daehwankimlab.github.io/hisat2/download/">https://daehwankimlab.github.io/hisat2/download/</a>
K562 and KBM7 Hi-C TADs bed files (TADs in hg38)	Hi-C genome Browser <sup>78</sup>	<a href="http://3dgenome.fsm.northwestern.edu/publications.html">http://3dgenome.fsm.northwestern.edu/publications.html</a> )
Pooled transcriptome-scale RNA-targeting Cas13 screens	This study	BioProject accession: PRJNA1161603
Total RNA-seq of parental and Cas13-engineered cells	This study	BioProject accession: PRJNA1161603
CaRPool-seq of MDA-MB-231 and HAP1 perturbed cells	This study	BioProject accession: PRJNA1161603
mRNA-seq of MDA-MB-231 perturbed cells	This study	BioProject accession: PRJNA1161603
H3K27ac AQuA-HiChIP of HAP1 cells	This study	BioProject accession: PRJNA1161603

**Experimental models: Cell lines**

HAP1	Guo et al. <sup>24</sup>	N/A
HEK293FT	Thermo	R70007
K562	ATCC	CCL-243
MDA-MB-231	ATCC	HTB-26
THP1	Wessels and Méndez-Mancilla et al. <sup>50</sup>	N/A
HAP1 <i>RfxCas13d</i>	Guo et al. <sup>24</sup>	N/A
HEK293FT <i>RfxCas13d</i>	Wessels and Méndez-Mancilla et al. <sup>23</sup>	N/A
K562 <i>RfxCas13d</i>	This study	N/A
MDA-MB-231 <i>RfxCas13d</i>	This study	N/A
THP1 <i>RfxCas13d</i>	Wessels and Méndez-Mancilla et al. <sup>50</sup>	N/A

(Continued on next page)

**Continued**

REAGENT or RESOURCE	SOURCE	IDENTIFIER
<b>Oligonucleotides</b>		
Guide RNA sequences, see <a href="#">Tables S1B, S3A, and S4A</a>	This study	N/A
lncRNA-targeting siRNA sequences, see <a href="#">Table S3D</a>	This study	N/A
RT-qPCR oligo sequences, see <a href="#">Table S3B</a>	This study	N/A
<b>Recombinant DNA</b>		
pLentiRNACRISPR_007 - TetO-NLS-RfxCas13d-NLS-WPRE-EFS-rtTA3-2A-Blast	Wessels and Méndez-Mancilla et al. <sup>23</sup>	Addgene 138149
pLentiRNAGuide_001 - hU6-RfxCas13d-DR1-BsmBI-EFS-Puro-WPRE	Wessels et al. <sup>23</sup>	Addgene 138150
pLentiRNAGuide_004 - hU6-RfxCas13d-DR1-EGFP-P2A-PuroR	Hart et al. <sup>36</sup>	Addgene 223175
Human Cas13 Pooled Long-Noncoding RNA (lncRNA) Library	This study	Addgene 227014
tFUCCI(CA)5	Ando et al. <sup>45</sup>	Addgene 153521
pLentiFUCCI(CA)5	This study	Addgene 223176
pMD2.G	Didier Trono	Addgene 12259
psPAX2	Didier Trono	Addgene 12260
<b>Software and algorithms</b>		
Cas13 design tool	Guo et al. <sup>24</sup>	<a href="https://cas13design.nygenome.org/">https://cas13design.nygenome.org/</a>
Cas13 guide design algorithm	Wessels and Méndez-Mancilla et al. <sup>23</sup>	<a href="https://gitlab.com/sanjanalab/cas13">https://gitlab.com/sanjanalab/cas13</a>
TIGER gRNA design	Wessels and Stirn et al. <sup>79</sup>	<a href="https://tiger.nygenome.org/">https://tiger.nygenome.org/</a>
Cutadapt v.1.13	Martin <sup>80</sup>	<a href="https://cutadapt.readthedocs.io/en/stable/">https://cutadapt.readthedocs.io/en/stable/</a>
Bowtie v.1.1.2	Langmead et al. <sup>81</sup>	<a href="https://bowtie-bio.sourceforge.net/index.shtml">https://bowtie-bio.sourceforge.net/index.shtml</a>
SVA v.3.34.0	Leek et al. <sup>82</sup>	<a href="https://bioconductor.org/packages/release/bioc/html/sva.html">https://bioconductor.org/packages/release/bioc/html/sva.html</a>
RobustRankAggreg v1.2.1	Kolde et al. <sup>83</sup>	<a href="https://cran.r-project.org/web/packages/RobustRankAggreg/index.html">https://cran.r-project.org/web/packages/RobustRankAggreg/index.html</a>
STAR	Dobin et al. <sup>84</sup>	<a href="https://github.com/alexdobin/STAR">https://github.com/alexdobin/STAR</a>
RSEM	Li and Dewey <sup>85</sup>	<a href="https://github.com/deweylab/RSEM">https://github.com/deweylab/RSEM</a>
Tximport	Soneson et al. <sup>86</sup>	<a href="https://bioconductor.org/packages/release/bioc/html/tximport.html">https://bioconductor.org/packages/release/bioc/html/tximport.html</a>
DESeq2 v.3.19	Love et al. <sup>87</sup>	<a href="https://bioconductor.org/packages/release/bioc/html/DESeq2.html">https://bioconductor.org/packages/release/bioc/html/DESeq2.html</a>
survival v.3.2.7	Therneau et al. <sup>88,89</sup>	<a href="https://CRAN.R-project.org/package=survival">https://CRAN.R-project.org/package=survival</a>
survminer v.0.4.9	Kassambara et al. <sup>90</sup>	<a href="https://rpkgs.datanovia.com/survminer/index.html">https://rpkgs.datanovia.com/survminer/index.html</a>
clusterProfiler v4.10.0	Wu et al. <sup>91</sup>	<a href="https://bioconductor.org/packages/release/bioc/html/clusterProfiler.html">https://bioconductor.org/packages/release/bioc/html/clusterProfiler.html</a>
MSigDB v2023.2	Subramanian et al.	<a href="https://www.gsea-msigdb.org/gsea/msigdb/collections.jsp">https://www.gsea-msigdb.org/gsea/msigdb/collections.jsp</a>
10x Genomics Cell Ranger v6.0.0	Zheng et al. <sup>92</sup>	<a href="https://www.10xgenomics.com/support/software/cell-ranger/latest">https://www.10xgenomics.com/support/software/cell-ranger/latest</a>
Seurat v4.1.1	Hao et al. <sup>93</sup>	<a href="https://satijalab.org/seurat/">https://satijalab.org/seurat/</a>
FeatureCounts v2.0.4	Liao et al. <sup>94</sup>	<a href="https://subread.sourceforge.net/featureCounts.html">https://subread.sourceforge.net/featureCounts.html</a>
HiSat2 v2.1.0	Kim et al. <sup>95</sup>	<a href="https://daehwankimlab.github.io/hisat2/">https://daehwankimlab.github.io/hisat2/</a>

(Continued on next page)

**Continued**

REAGENT or RESOURCE	SOURCE	IDENTIFIER
ggplot2 v3.5.1	Wickham	<a href="https://cran.r-project.org/web/packages/ggplot2/index.html">https://cran.r-project.org/web/packages/ggplot2/index.html</a>
UpSetR v1.4.0	Conway et al. <sup>96</sup>	<a href="https://cran.rstudio.com/web/packages/UpSetR/">https://cran.rstudio.com/web/packages/UpSetR/</a>
ComplexHeatmap v2.20.0	Gu et al. <sup>97</sup>	<a href="https://bioconductor.org/packages/release/bioc/html/ComplexHeatmap.html">https://bioconductor.org/packages/release/bioc/html/ComplexHeatmap.html</a>
circlize v0.4.16	Gu et al. <sup>98</sup>	<a href="https://cran.r-project.org/web/packages/circlize/index.html">https://cran.r-project.org/web/packages/circlize/index.html</a>
ggraph v2.2.1	Pedersen	<a href="https://cran.r-project.org/web/packages/ggraph/index.html">https://cran.r-project.org/web/packages/ggraph/index.html</a>
igraph v2.0.3	Csardi and Nepusz	<a href="https://cran.r-project.org/web/packages/igraph/index.html">https://cran.r-project.org/web/packages/igraph/index.html</a>
Incucyte Cell-by-Cell Analysis Software Module	Sartorius	9600-0031
HiC-Pro	Servant et al. <sup>99</sup>	<a href="https://nservant.github.io/HiC-Pro/">https://nservant.github.io/HiC-Pro/</a>
Pybedtools	Quinlan and Hall <sup>100</sup> and Dale et al. <sup>101</sup>	<a href="https://daler.github.io/pybedtools/">https://daler.github.io/pybedtools/</a>
IGV: Integrative Genomics Viewer	Robinson et al. <sup>102</sup>	<a href="https://igv.org/">https://igv.org/</a>
HTSeq	Putri et al. <sup>103</sup>	<a href="https://htseq.readthedocs.io/">https://htseq.readthedocs.io/</a>
FlowJo v10	BD Biosciences	<a href="https://www.bdbiosciences.com/en-us/products/software/flowjo-v10-software">https://www.bdbiosciences.com/en-us/products/software/flowjo-v10-software</a>
Samtools	Danecek et al. <sup>104</sup>	<a href="https://www.htslib.org/">https://www.htslib.org/</a>
Snakemake	Mölder et al. <sup>105</sup>	<a href="https://snakemake.github.io/">https://snakemake.github.io/</a>
UCSC Lift Genome Annotations	UCSC <sup>106</sup>	<a href="https://genome.ucsc.edu/cgi-bin/hgLiftOver">https://genome.ucsc.edu/cgi-bin/hgLiftOver</a>
Python v3.7	Python Software Foundation	<a href="https://www.python.org/">https://www.python.org/</a>
R v3.6	R Development Core Team	<a href="https://www.R-project.org/">https://www.R-project.org/</a>
<b>Other</b>		
Serum Plus II Supplement	Sigma	14009C
Gibco Fetal Bovine Serum, Tet system approved	Thermo	A4736201
HyClone Dulbecco's Modified Eagle's Medium	Cytiva	SH30022.01
HyClone Iscove's Modified Dulbecco's Medium	Cytiva	SH30228.FS
HyClone RPMI 1640 Medium	Cytiva	SH30255.FS

**EXPERIMENTAL MODEL AND STUDY PARTICIPANT DETAILS**

**Monoclonal Cas13 cell line generation and cell culture**

MDA-MB-231 and K562 cell lines were acquired from American Type Culture Collection (HTB-26 and CCL-243, respectively). Monoclonal doxycycline-inducible *RfxCas13d* MDA-MB-231 and K562 cells were generated by transducing cells with a lentivirus produced using pLentiRNACRISPR\_007 (Addgene 138149) at a low multiplicity of infection (MOI < 0.1) and selected with 5 μg/ml of blasticidin S (A.G. Scientific B-1247). Single-cell colonies were isolated by low-density plating and then expression of HA-tagged Cas13 was confirmed by immunoblot using an anti-HA peptide antibody (Cell Signaling Technology 2367S). Monoclonal doxycycline-inducible *RfxCas13d*-NLS HEK293FT cells were obtained from Wessels and Méndez-Mancilla et al.,<sup>23</sup> *RfxCas13d*-NLS HAP1 cells were obtained from Guo et al.,<sup>24</sup> and *RfxCas13d*-NLS THP1 cells were obtained from Wessels and Méndez-Mancilla et al.<sup>50</sup>

HEK293FT and MDA-MB-231 cells were cultured in D10 medium: Dulbecco's Modified Eagle Medium with high glucose and stabilized L-glutamine (Cytiva SH30022.01) supplemented with 10% Serum Plus II (Sigma-Aldrich 14009C) and 5 μg/ml blasticidin. HAP1 and K562 cells were cultured in I10 medium: Iscove's Modified Dulbecco's Medium with L-glutamine (Cytiva SH30228.FS) supplemented with 10% Serum Plus II and 5 μg/ml blasticidin. THP-1 cells were cultured in R10 medium: HyClone RPMI 1640 Medium (Cytiva SH30255.FS) supplemented with 10% Serum Plus II and 5 μg/ml blasticidin. All cells were incubated at 37 °C with 5% carbon dioxide.

## METHOD DETAILS

### Transcriptome-scale and CaRPool-seq Cas13 libraries: Design and cloning

To rationally select lncRNAs to perturb, we used a developmental atlas profiling 31,687 lncRNAs across developmental stages and different species<sup>19</sup> and essential lncRNAs identified in prior CRISPRi screens.<sup>20</sup> We first filtered out lowly expressed lncRNAs, which we defined as those expressed that were not expressed above at least 5 reads per kilobase of transcript per million mapped reads (RPKM) in at least one sample from the developmental atlas. To identify matching lncRNAs between the developmental atlas and CRISPRi screen annotations, we used the primary transcription start site (TSS) from the CRISPRi screens. We extended the TSS by 500 bp in each direction and intersected it with the first exon of the lncRNA annotations from the developmental atlas in a strand-specific manner. In total, the final library included 6,199 lncRNA targets, 4,309 closest protein-coding gene (PCG) targets, and 100 essential gene targets (positive controls). The 100 essential genes were selected as those that were essential in all CRISPR-Cas9 screens from Hart et al.<sup>34</sup> For each lncRNA, we used annotations (e.g., genomic location, time- and tissue-specificity, dynamic/non-dynamic) provided by the developmental atlas.<sup>19</sup>

For each lncRNA/PCG, we selected the transcript with the highest isoform expression and designed optimized gRNAs using a machine learning model for Cas13 gRNA design that previously was trained on thousands of gRNAs (<http://cas13design.nygenome.org>).<sup>23</sup> For each lncRNA/PCG, we selected 8 gRNAs from the highest (or second-highest as needed) efficacy quartile (as given by cas13design) and made sure that the selected gRNAs had no secondary target sites in the human transcriptome with 0 to 2 mismatches to the cognate site.<sup>24</sup> Wherever possible, we aimed to select 2 gRNAs from each of the first three exons of the lncRNA/PCG to minimize false negatives due to alternative exon usage/splicing. We also embedded 1,000 non-targeting gRNAs as negative controls, which we ensured had 3 or more mismatches to any other transcripts (hg19). In total, the library included 75,065 gRNAs. Each gRNA was flanked with constant regions (for PCR amplification and Gibson cloning) and synthesized as 106mer single-stranded oligonucleotides (Twist Biosciences). A full list of gRNA sequences in the library can be found in [Table S1B](#) as a pooled library via Addgene (227014).

For library cloning, we amplified pooled oligonucleotides (Twist) using a nested PCR. PCR1 amplifies the oligo pool and PCR2 adds overhangs for Gibson cloning. For PCR1, the oligo pool was amplified using Q5 High-Fidelity DNA Polymerase (NEB M0491L) with 0.2  $\mu$ l of enzyme and 1 ng (1 ng/ $\mu$ l) of the oligo pool per reaction in four 20  $\mu$ l reaction: 98 °C for 30s, 7  $\times$  (98 °C for 10 s, 63 °C for 10 s, 72 °C for 15 s), 72 °C for 1 min. For PCR1 1  $\mu$ l of the following primers (10  $\mu$ M) were used:

5'-TAGAAGGTCTATGTTTCGCCA-3'

5'-TAACGAGTCCTAAACGGGAT-3'

After PCR1, the replicate reactions were combined. Then, for PCR2, 2  $\mu$ l of pooled PCR1 product was used in each (20- $\mu$ l) PCR2 reaction. In total, we performed 26 PCR2 reactions (20- $\mu$ l each) with 7 amplification cycles using Q5 High-Fidelity DNA Polymerase (NEB M0491) as follows: 98 °C for 30s, 7  $\times$  (98 °C for 10 s, 63 °C for 15 s, 72 °C for 15 s), 72 °C for 1 min. For PCR2 1  $\mu$ l of the following primers (10  $\mu$ M) were used:

5'-TATATATCTTGTGGAAAGGACGAAACACCGAACCCCTACCAACTGGTCGGGGTTTGAAC-3'

5'-ACTGACGGGCACCGGAGCCAATTCCTCTTTCAAGACCTAGCTAGCGAATTCAAAAA-3'

The PCR2 amplicon was purified using the DNA Clean & Concentrator (Zymo D4014). The purified amplicon was Gibson-cloned into a puromycin-resistant lentiviral vector with an enhanced Cas13 direct repeat (DR1), pLentiRNAguide\_001 (Addgene 138150). For that, 40  $\mu$ g plasmid was digested using 10  $\mu$ l *Esp3I* (Thermo FD0454) at 37 °C for 2 hours and dephosphorylated using 10  $\mu$ l FastAP (Thermo EF0651) at 37 °C for 30 minutes. The digested plasmid backbone was gel-purified using a 1% E-Gel (Thermo G401001) and QiaQuick Gel Extraction Kit (Qiagen 28704). We performed three 20  $\mu$ l Gibson reactions using 10  $\mu$ l 2  $\times$  Gibson Assembly Master Mix (NEB E2611L): Each Gibson reaction included 500 ng digested and dephosphorylated pLentiRNAguide\_001 plasmid and 80 ng PCR2 amplicon at 50 °C for 1 hour. We purified the plasmid library using isopropanol precipitation at room temperature for 15 minutes and transformed the purified library into Endura electrocompetent cells (Lucigen 60242-2) with >1,000 colonies per construct. Following library purification using the MAXI Fast-Ion Plasmid Purification Kit (IBI Scientific IB47125), we verified successful cloning via Illumina sequencing (MiSeq) with a 90:10 ratio (90th percentile/10th percentile crRNA read ratio) of 1.9 and a recovery rate of 99.94%. This transcriptome-scale pooled Cas13 library has been deposited at Addgene (227014).

For each target gene in the CaRPool-seq library, we picked the three most depleted gRNAs from the transcriptome-scale screen that target expressed exons. The gRNAs chosen were non-overlapping. Since every gRNA array includes two targeting gRNAs, we paired each selected gRNA (from the transcriptome-scale screen) with a newly-designed gRNA using the TIGER gRNA design tool<sup>79</sup> and an array-specific barcode gRNA (bcgRNA). We designed three individual gRNA arrays for 50 essential lncRNAs and 18 closest protein-coding genes (PCGs). We also designed gRNA arrays targeting three known essential genes (*MYC*, *MTOR* and *HSPA9*). We added 10 control (non-targeting) gRNA arrays. For the bcgRNAs, we designed random 15mer sequences with a hamming distance greater than four from any other 15mer. The 225mer single-stranded oligonucleotides were designed in the following way:

PCR-handle:*BsmBI*:gRNA1:DR:gRNA2:DR:TruSeq-PCR-handle:barcode:*Lgul*:PCR-handle

DR indicates wild-type 36nt *RfxCas13d* direct repeat. Pooled oligonucleotides were synthesized as an oPool (IDT) and are shown in [Table S4A](#). The pool was amplified using Q5 High-Fidelity DNA Polymerase (NEB M0491L) using 0.5  $\mu$ l of enzyme and 20 ng (1 ng/ $\mu$ l)

of the oligo pool in a single 50  $\mu$ l reaction: 98 °C for 30s, 8 $\times$  (98 °C for 10 s, 60 °C for 15 s, 72 °C for 15 s), 72 °C for 1 min. For the PCR 2.5  $\mu$ l of the following primers (10  $\mu$ M) were used:

5'-TAGAAGGTCTATGTTCCGCCA-3'

5'-TAACGAGTCCTAACGGGAT-3'

The amplicon was purified using a 2.0 $\times$  solid phase reversible immobilization (SPRI) clean-up. For digestion, all purified PCR product was digested in a 20  $\mu$ l reaction with 1  $\mu$ l each of *Esp31* and *Lgul* at 37 °C for 2 hours. We purified the digested amplicon using a 2.0 $\times$  SPRI cleanup. The purified amplicon was cloned into a puromycin-resistant lentiviral vector with a 5' enhanced Cas13 direct repeat (DR1) and 3' stabilizing pseudoknot element (evopreQ1), pLentiRNAguide\_003 (Addgene 192505). For that, 5  $\mu$ g pLentiRNAguide\_003 plasmid was digested using 2.5  $\mu$ l *Esp31* (Thermo FD0454) and 2.5  $\mu$ l *Lgul* (Thermo FD1934) at 37 °C for 2 hours and dephosphorylated using 2.5  $\mu$ l FastAP (Thermo EF0651) at 37 °C for 30 minutes. The digested plasmid backbone was gel-purified using a 2% E-Gel (Thermo G401002) and QiaQuick Gel Extraction Kit (Qiagen 28704). All of the PCR product was ligated into *Esp31/Lgul*-digested and dephosphorylated pLentiRNAguide\_003 in four 20  $\mu$ l reactions using per reaction: 1  $\mu$ l T7 DNA ligase (NEB M0318), 25 ng digested plasmid and 2 $\times$  Rapid Ligase Buffer (Enzymatics B1010L) for 15 minutes at room temperature. Ligation products were purified using a 2 $\times$  SPRI cleanup and transformed into Endura electrocompetent cells (Lucigen 60242-2) with >10,000 colonies per construct. Following library purification using the MAXI Fast-Inv Plasmid Purification Kit (IBI Scientific IB47125), the complete library representation with minimal bias (90th percentile/10th percentile crRNA read ratio 11.8), and correct gRNA array to barcode linkage (88.3%) was verified by sequencing (Illumina MiSeq).

### Pooled lentiviral production

For both pooled libraries, lentivirus was produced by transfecting the pooled transfer plasmid with packaging plasmids psPAX2 (Addgene 12260) and pMD2.G (Addgene 12259) using linear polyethylenimine MW25000 (Polysciences 23966). We seeded ten million HEK293FT cells per 10 cm dish and transfected them with 60  $\mu$ l polyethylenimine, 9.2  $\mu$ g plasmid pool, 6.4  $\mu$ g psPAX2 and 4.4  $\mu$ g pMD2.G. Three days post-transfection, the viral supernatant was collected, filtered through a 0.45- $\mu$ m filter, and stored at -80 °C until further use. The amount of lentivirus used for transduction was titrated to result in 30-40% transduction efficiency, to minimize the probability of multiple gRNAs being introduced into a single cell.

### Pooled Cas13 library CRISPR screens

We conducted pooled Cas13d screens following established protocols.<sup>23,50</sup> Briefly, Cas13d-expressing cells were transduced with the library lentivirus through separate infection replicates by spinfection at 1000 rpm for 1 hour at 37 °C, followed by overnight incubation. After 24 hours, new media with 1  $\mu$ g/ml puromycin (Invivogen ant-pr-1) was added. Puromycin selection was completed within 48 hours for all cell lines, except for THP1. Because THP1 required an extended selection time, we maintained it in R10 but with 10% Tet-system approved serum (Gibco A4736201) substituted for Serum Plus II and with 1  $\mu$ g/ml puromycin. THP1 cells took approximately two weeks for full selection (using an in-line non-transduced control).

Following puromycin selection, *RfxCas13d* expression was induced by replenishing the growth medium containing 1  $\mu$ g/ml puromycin, 5  $\mu$ g/ml blasticidin and 1  $\mu$ g/ml doxycycline. Cells were passaged every 2 to 4 days and split as needed, ensuring a guide representation of >1,000 $\times$ . Samples with a guide abundance of 1,000-fold were harvested at 0, 7, and 14 days post-Cas13d induction.

Genomic DNA was isolated from cell pellets via a modified salting out procedure.<sup>107</sup> For that, 12 ml of NK Lysis Buffer (50 mM Tris, 50 mM EDTA, 1% SDS, pH 8) and 60  $\mu$ l of 20 mg/ml Proteinase K (QIAGEN 19131) were added to 80 million cells and incubated at 55 °C overnight. The next day, 6  $\mu$ l of 100 mg/ml RNase A (A.G. Scientific R-2000) was added to the lysed sample, which was then inverted 25 times and incubated at 37 °C for 30 min. Samples were cooled on ice before addition of 4 ml of pre-chilled 7.5M ammonium acetate (Sigma A1542) to precipitate proteins. After adding ammonium acetate, the samples were vortexed and centrifuged at 4,000  $\times$  g for 10 minutes. After the spin, 12 ml isopropanol was added to the collected supernatant, inverted 50 times and centrifuged at 4,000  $\times$  g for 10 minutes. The supernatant was discarded, 12 ml of freshly prepared 70% ethanol was added, the tube was inverted 10 times, and then centrifuged at 4,000  $\times$  g for 10 minutes. The supernatant was discarded, and remaining ethanol was removed. After air drying for 30 minutes, 500  $\mu$ l of 0.2 $\times$  TE buffer (Sigma 93283) was added, the tube was incubated at 65 °C for 1 hour and at room temperature overnight to fully resuspend the DNA. The next day, the gDNA samples were vortexed briefly. The gDNA concentration was measured using a Nanodrop (Thermo). We excluded one biological replicate (K562 day 0) due to low recovery after gDNA extraction.

We amplified gRNA cassettes and prepared them for sequencing using a two-step PCR. PCR1 was performed to amplify a region containing the crRNA cassette in the lentiviral genomic integrant using TaqB polymerase (Enzymatics P7250L). We performed 70 PCR1 reactions for each gDNA sample using 5  $\mu$ g gDNA per 100  $\mu$ l PCR1 reaction as follows: 94 °C for 3 min, 20 $\times$  (94 °C for 10 s, 55 °C for 30 s, 68 °C for 45 s), 68 °C for 5 min. For PCR1 the following primers were used:

5'-GAGGGCCTATTTCCCATGATTC-3'

5'-GTTGCGAAAAAGAACGTTCCACGG-3'

We then combined PCR1 products for the same sample together before PCR2, which was done to incorporate Illumina adaptors using Q5 High-Fidelity DNA Polymerase (NEB M0491). We performed 10 PCR2 reactions for each sample using 10  $\mu$ l unpurified

PCR1 product per 50  $\mu$ l reaction as follows: 98 °C for 30 s, 6-10 $\times$  (98 °C for 10 s, 63 °C for 30 s, 72 °C for 45 s), 72 °C for 5 min. For PCR2 the following primers was used:

5'-AATGATACGGCGACCACCGAGATCTACACTCTTCCCTACACGACGCTCTCCGATCT(N<sub>1-9</sub>)(BC<sub>8</sub>)  
TCTTGTGGAAAGGACGAAACACCG-3'  
5'-CAAGCAGAAGACGGCATAACGAGAT(BC<sub>8</sub>)GTGACTGGAGTTCAGACGTGTGCTCTCCGATCT(N<sub>1-9</sub>)  
GAGCCAATCCCACTCCTTTCAAG-3'

where N is a stagger of 1 to 9 nucleotides and BC is a barcode of 8 nucleotides. The resulting amplicons from PCR2 (~270 bp) were pooled and then purified using double-sided SPRI beads clean up (Beckman B23317) or gel extracted using a QiaQuick Gel Extraction kit (Qiagen 28704). For double-sided SPRI clean up, the amplicon was first incubated with 0.6 $\times$  SPRI to remove larger fragments (>350 bp bound to beads and removed), the supernatant was then transferred and further incubated with 0.8 $\times$  SPRI beads (<200 bp in supernatant and removed). The concentration of the purified PCR amplicon was quantified using Qubit dsDNA HS Assay Kit (Thermo Q32851) and sequenced on an Illumina NextSeq 500 using a single-end 150 cycle read.

### Single-cell sequencing coupled with Cas13 perturbations (CaRPool-seq)

RfxCas13d-expressing MDA-MB-231 and HAP1 cells were maintained in their respective media (D10 for MDA-MB-231 and I10 for HAP1), except 10% Tet-system approved serum (Gibco A4736201) was substituted for Serum Plus II. We transduced the CaRPool-seq library at a low multiplicity of infection (MOI < 0.2) by spinfection at 1000  $\times$  g for 1 hour at 37 °C, followed by overnight incubation. After 24 hours, fresh media with 1  $\mu$ g/ml puromycin was added. Puromycin selection was completed within 72 hours for both cell lines and cells were collected for CaRPool-seq readouts at 48 hours after Cas13-induction (1  $\mu$ g/ml doxycycline). The experiment was conducted using one lane per cell line of the 10X Genomics 3' kit (Chromium Single Cell 3' Gene Expression v3.1 with feature barcoding technology for CRISPR screening, 10000127, 10000268 and 10000262). For pooled screen readouts, the cells were passaged every 2 days, ensuring a guide representation of >10,000 $\times$ . Five million cells were harvested at 0 and 12 days post-Cas13 induction. The libraries for bulk readout were prepared as described in *Pooled Cas13 library CRISPR screens*.

Single-cell sequencing library preparation for bcgRNAs and cDNA followed the 10X Genomics manual (CG000316 Rev D) with following modifications to allow for capture of bcgRNAs in our Cas13 CRISPR array configuration type X as previously described.<sup>50</sup> After elution of GEM-RT in 34  $\mu$ L (Step 2.1-s.), we added 1  $\mu$ L ADT additive primer (0.4  $\mu$ M).

5'-CCTTGGCACCCGAGAATTCC-3'

to increase bcgRNA yield during cDNA amplification. The cDNA and bcgRNAs were purified using SPRI cleanup as indicated in steps 2.3A (Pellet Cleanup, 3' GEX) and 2.3B (Transferred Supernatant Cleanup, CRISPR screening library), respectively. 45  $\mu$ L of the purified bcgRNAs was used to construct the bcgRNA library through PCR amplification that adds Illumina P5 and P7 handles and an i7 index to the bcgRNA amplicon. We performed 12 cycles of PCR amplification (PCR1) in 100  $\mu$ l reactions using 50  $\mu$ l of 2 $\times$  KAPA HiFi PCR Mastermix (Roche 07958935001) and 45  $\mu$ l of bcgRNA PCR template as follows: 95 °C for 3 min, 12 $\times$  (95 °C for 20 s, 60 °C for 8 s, 72 °C for 8 s), 72 °C for 1 min). For the PCR 2.5  $\mu$ l of the following primers (10  $\mu$ M) were used:

5'-AATGATACGGCGACCACCGAGATCTACACTCGTCGGCAGCGTCAGATGTGTATAAGAGACAG-3'

5'-CAAGCAGAAGACGGCATAACGAGAT(BC)<sub>8</sub>GTGACTGGAGTTCCTTGGCACCCGAGAATTCCA-3'

where BC is a barcode of 8 nucleotides. After PCR product purification using a 1.6 $\times$  SPRI cleanup, we performed 4 more cycles of PCR amplification using P5 and P7 primers in 100  $\mu$ l reactions using 50  $\mu$ l of 2 $\times$  KAPA HiFi PCR Mastermix (Roche 07958935001) and 45  $\mu$ l of PCR1 product as follows: 95 °C for 3 min, 4 $\times$  (95 °C for 20 s, 60 °C for 8 s, 72 °C for 8 s), 72 °C for 1 min). For the PCR 2.5  $\mu$ l of the following primers (10  $\mu$ M) were used:

5'- AATGATACGGCGACCACCGA-3'

5'- CAAGCAGAAGACGGCATAACGAGA-3'

After purification using a 1.6 $\times$  SPRI cleanup, bcgRNA and cDNA libraries were quantified using the Qubit dsDNA HS Assay Kit (Thermo Q32851). The average amplicon size of each library was quantified using a Bioanalyzer 2100 using the High Sensitivity DNA Kit (Agilent 5067-4626). Using the average amplicon size and concentration, we then diluted both libraries appropriately for sequencing. We mixed the libraries in suitable proportion to achieve ~45,000 reads per cell for the cDNA library and ~5,000 reads per cell for the bcgRNA library. After mixing, the pooled CaRPool-seq libraries were sequenced on an NovaSeq 6000 (Illumina S1 flow cell) using 28 cycles for read 1 and 91 cycles for read 2.

### Arrayed gRNA cloning and lentiviral production

For the competitive cell growth assays, we used a RfxCas13d guide-only vector that also expresses GFP and puromycin resistance, pLentiRNAGuide\_004 (Addgene 223175). For all validation assays, we cloned three individual gRNAs per gene into this construct using *Esp31* sites and produced corresponding lentiviruses. All gRNA sequences for the arrayed validation are given in [Table S3A](#). In brief, we seeded one million HEK293FT cells per 6-well and transfected them with 7.5  $\mu$ l polyethylenimine linear MW 25000 (Polysciences), 1.5  $\mu$ g gRNA cloned pLentiRNAGuide\_004, 1.25  $\mu$ g psPAX2 and 0.5  $\mu$ g pMD2.G. Two days post-transfection, the viral supernatant was collected, filtered through a 0.45- $\mu$ m filter, and monoclonal Cas13 cell lines were transduced at a low MOI (~0.5).

### Competitive cell growth assays

We performed two independent transductions for each gRNA and selected transduced cells with 1  $\mu\text{g/ml}$  puromycin for 3 days. Selected GFP-positive cells were then co-cultured with parental cells for 24 hours and the ratio of GFP-positive cells was determined using a live cell imaging system (Incucyte S3) at 20 $\times$  magnification for HAP1, MDA-MB-231 and HEK293FT cells. After that, 1  $\mu\text{g/ml}$  doxycycline was added to induce Cas13 expression. Over the course of 4 - 6 days, the ratio of GFP-positive to GFP-negative cells was observed by taking nine images per transduction. We then determined relative survival by normalizing each ratios to 1) the initial time point prior to Cas13 induction and 2) the median of cell mixtures containing cells transduced with three different non-targeting (negative control) gRNAs. Representative endpoint images show confluence masks of GFP-positive and GFP-negative cells (Incucyte Live Cell Analysis software).

For competition assays in THP1, GFP quantification was performed using flow cytometry (Sony SH800S) six days after mixing with parental cells and Cas13 induction (1  $\mu\text{g/ml}$  doxycycline). THP1 cells were gated by forward and side scatter and signal intensity to remove potential multiplets and additionally gated for living cells using Fixable Violet Dead Cell Stain exclusion (Thermo L34963). For each sample, we analyzed the distribution of GFP-negative and GFP-positive cells from 9,000 gated (singlets and live) cells. We then determined relative survival by normalizing each ratio to the median of cell mixtures containing cells transduced with three different non-targeting (negative control) gRNAs.

### Cell cycle analyses

We used a fluorescence ubiquitin cell cycle indicator (FUCCI)-based reporter system to determine cell cycle changes using live-cell imaging. For that, we cloned the FUCCI cassette (AzaleaB5-hCdt1(1/100)-P2A-h2-3-hGem(1/110)) from tFUCCI(CA)5 (Addgene 153521) into a lentiviral plasmid driven by a short EF-1 $\alpha$  promoter (EFS). We modified the backbone from pLentiRNAguide\_001 (Addgene 138150) by replacing the U6-gRNA and EFS-puromycin cassettes with an EFS promoter and a downstream multiple cloning site (MCS). We digested pLentiRNAguide\_001 with *PacI* and *Apal* restriction enzymes and amplified EFS-MCS and WPRE-LTR cassettes with Gibson overhangs using Q5 High-Fidelity DNA Polymerase (NEB M0491L) using 0.5  $\mu\text{l}$  of enzyme and 10 ng pLentiRNAguide\_001 plasmid in 50  $\mu\text{l}$  reactions: 98  $^{\circ}\text{C}$  for 30 s, 25 $\times$  (98  $^{\circ}\text{C}$  for 10 s, 60  $^{\circ}\text{C}$  for 15 s, 72  $^{\circ}\text{C}$  for 30 s), 72  $^{\circ}\text{C}$  for 1 min. For the PCRs 2.5  $\mu\text{l}$  of the following primers (10  $\mu\text{M}$ ) were used:

#### EFS-MCS

5'-ACAGCAGAGATCCAGTTTGGTTAATTAATCTTGAAAGGAGTGGAATTGACTCCG-3'

5'-CGTGAATTCTCGGATCCGCTAGCCGTCTCCTCTAGTTAGCCAGCCGGTCCTGTGTTCTGGCGCAAACC-3'

#### WPRE-LTR

5'-AGCGGATCCGAGAATTCACGGTACCCGTCTCTAAGGACTCTCGCGTTAAGTCGACAATCAACCT-3'

5'-CTGATCAGCGGGTTAAACGGGCCCTGCTAGAGATTTCCACACT-3'

We assembled the final plasmid using the digested pLentiRNAguide\_001 plasmid and both PCR products by Gibson cloning. Then, we cloned the FUCCI cassette into this lentiviral plasmid using *BamHI* (Thermo FD0055) and *KpnI* (Thermo FD0524) restriction sites and termed the plasmid pLentiFUCCI(CA)5 (Addgene 223176). We produced a corresponding lentivirus, as described above, and transduced monoclonal Cas13-expressing MDA-MB-231 cells. For all cell cycle assays, we cloned individual gRNAs targeting lncRNAs into pLentiRNAguide\_001 (Addgene 138150) as described in the [arrayed gRNA cloning and lentiviral production](#) section.

MDA-MB-231 Cas13 cells expressing the FUCCI reporter were transduced at a low MOI ( $\sim 0.5$ ) with these lentiviruses. We performed two independent transductions for each gRNA and selected transduced cells with 1  $\mu\text{g/ml}$  puromycin for three days. Then we seeded 2,000 into three wells of a 96-well plate (Corning 3904) per transduction and monitored cell cycle changes for 84 hours using live imaging (Incucyte S3) by taking nine images per well at 20 $\times$  magnification. We induced Cas13 expression by addition of 1  $\mu\text{g/ml}$  doxycycline 12 hours after seeding. For the last 24 hours of the experiment, a subset of cells transduced with non-targeting gRNAs were treated with compounds that inhibit cell cycle progression, the CDK1/2/5/9 inhibitor dinaciclib (0.5  $\mu\text{M}$ , MedChemExpress HY-10492) and the DNA damage-inducing agent doxorubicin (1  $\mu\text{M}$ , MedChemExpress HY-15142), which trigger G1-S and G2-M arrest, respectively.

Images were analyzed using the Incucyte Cell-by-Cell Analysis Software Module (Sartorius 9600-0031). Intensity of the FUCCI signal was measured per cell by masking each cell for the *red* and *green* fluorescence channels using a top-hat masking strategy restricted to the mean cell area. Classification of cells into high-*red* (G1), high-*green* (S phase) and high-*red* / high-*green* (G2-M) was done within the Cell-by-Cell Analysis Software based on the distribution of *red* and *green* intensities across cells. We computed the percentage of cells with high or low levels of either or both *red* and *green* signal intensity and the mean number of cells per well. To test if there were differences in the distribution of the high-*red* (G1), high-*green* (S phase) and high-*red* / high-*green* (G2-M) populations between the cells perturbed with non-targeting gRNAs and with gRNAs targeting specific lncRNAs, we conducted a Mann-Whitney *U* test comparing each lncRNA-targeting gRNA to the control (non-targeting) gRNA. The cell counts per well at 24-, 48- or 72-hour timepoints were normalized to the timepoint right after addition of doxycycline (0 hour). To evaluate changes in cell viability at the endpoint, the cell counts per well for each perturbation were normalized to the median cell count for the cells transduced with control (non-targeting) gRNA.

### Apoptosis assays

RfxCas13d-expressing MDA-MB-231 cells were transduced in two biological replicates with lentiviruses produced from corresponding pLentiRNAguide\_001, as described in *Cell cycle analyses*. We selected the transduced cells for three days using 1  $\mu\text{g/ml}$

puromycin. Then, we seeded 2,000 cells into three wells of a 96-well plate (Corning 3904) per transduction and cultured the cells in media supplemented with Annexin V (Sartorius 4642, final concentration 5  $\mu$ M Annexin V). At 72 hours, we acquired nine images per well at 20 $\times$  magnification (Incucyte S3). We determined the relative area of Annexin V-positive cells by measuring the area of Annexin V-positive cells and the total cell area. Representative endpoint images show the confluence masks of total and Annexin V-positive cells (Incucyte Live Cell Analysis software).

### RNA interference

The small interfering RNAs (siRNAs) were designed using the IDT Custom Dicer-Substrate siRNA (DsiRNA) tool ([https://www.idtdna.com/site/order/tool/index/DSIRNA\\_CUSTOM](https://www.idtdna.com/site/order/tool/index/DSIRNA_CUSTOM)). A DsiRNA targeting the coding sequence of *Renilla* luciferase was selected as a negative control (CTRL). For the lncRNAs, sequences targeting 1 - 3 different exons were chosen (Table S3D). For each target lncRNA, we pooled three individual DsiRNAs (IDT) at equimolar ratios to ensure robust knockdown and reduce off-target effects. We seeded 250,000 HEK293FT cells in 12-well plates and transfected each well with 25 nM DsiRNA pools using 4.5  $\mu$ l Lipofectamine RNAiMAX (Thermo 13778075). Twenty-four hours later, 2,000 cells were seeded in 96-well plates and monitored for 60 hours in media supplemented with Annexin V (Sartorius 4642, final concentration 5  $\mu$ M Annexin V). At 72 hours, we acquired nine images per well at 20 $\times$  magnification (Incucyte S3). We determined the proliferation of cells transfected with lncRNA-targeting siRNA pools by normalizing the cell area to 1) the initial time point (24 hours after transfection) and 2) the median of cells transfected with CTRL DsiRNA (median computed over 54 images with 9 images per biological replicate and 6 biological replicates for CTRL DsiRNA). For apoptosis, we determined the relative area of Annexin V-positive cells by measuring the area of Annexin V-positive cells and the total cell area. Representative endpoint images show the confluence masks of total and Annexin V-positive cells (Incucyte Live Cell Analysis software).

### RNA-sequencing

For cell line expression profiles, total RNA-sequencing libraries were prepared from parental and *RfxCas13d*-expressing HAP1, K562, HEK293FT and THP1 cells using the KAPA Total RNA-seq kit with RiboErase (Roche) seven days after doxycycline induction (1  $\mu$ g/ml). Both parental HAP1, K562, HEK293FT and THP1 cells and *RfxCas13d*-expressing HAP1, K562, HEK293FT and THP1 cells were treated with doxycycline. RNA extraction, library preparation and sequencing (Illumina NovaSeq 2500) were performed by the New York Genome Center's Sequencing Platform. Total RNA-seq files for MDA-MB-231 were downloaded as fastq from the RNA Atlas.<sup>77</sup>

For differential gene expression after lncRNA perturbations (bulk mRNA-seq), *RfxCas13d*-expressing MDA-MB-231 cells were transduced in two biological replicates with lentiviruses produced from corresponding pLentiRNAguide\_004, as described in [arrayed gRNA cloning and lentiviral production](#). We chose the same gRNAs used in the cell cycle (FUCCI) and apoptosis (Annexin V) assays. We selected the transduced cells for three days (1  $\mu$ g/ml puromycin) and induced Cas13 expression by 1  $\mu$ g/ml doxycycline for 48 hours. Total RNA was isolated using the Direct-zol RNA Purification Kit (Zymo R2062) with DNaseI treatment and quantified using the Qubit RNA XR Assay Kit (Thermo Q10210). To generate strand-specific mRNA-seq libraries, we used the Stranded mRNA Prep kit (Illumina 20040532) with RNA UD Indexes Set A (Illumina 20040553) and followed the manufacturer's protocol using 1  $\mu$ g total RNA as input for mRNA capture. Libraries were quantified using the Qubit dsDNA HS Assay Kit (Thermo Q32851) and the High Sensitivity DNA Kit (Agilent 5067-4626) using a Bioanalyzer 2100 (Agilent), as described in *CaRPool-seq experiments*. Pooled libraries (bulk mRNA-seq) were sequenced using a NextSeq500 (Illumina).

### H3K27ac AQuA-HiChIP

We prepared H3K27ac AQuA-HiChIP libraries using a modified protocol with a mouse spike-in control<sup>108</sup> and two biological replicates. Briefly, we fixed ten million HAP1 cells in 1% formaldehyde for 10 minutes and quenched to a final concentration of 125 nM glycine. The cells were lysed in 0.5% SDS, quenched with 10% Triton X-100, and digested with 200 units *Mbol* (NEB R0147M) at 37°C for 2 hours to produce blunt ends. After heat inactivation at 62°C for 20 minutes, the blunt DNA overhangs were biotinylated using DNA Polymerase I Large (Klenow) Fragment (NEB M0210L), 288  $\mu$ M biotin-dATP (Thermo 19524016), dTTP, dGTP, and dCTP at 37°C for 1 hour. Biotinylated products were ligated using T4 DNA ligase (NEB B0202S) at room temperature for 4 hours. Nuclei were spun down, resuspended in nuclear lysis buffer (50 mM Tris-HCl pH 7.5, 10 mM EDTA, 1% SDS) and sonicated using a Covaris LE220 with the following conditions: Fill level 10, PIP 450, Duty factor 30, CPB 200. We incubated the sheared DNA with Dynabeads Protein A (Thermo 10001D) for 2 hours at 4°C. We then placed the tubes on a magnet and the supernatant was kept. We performed immunoprecipitation with a cross-species reactive H3K27ac antibody (Active Motif 39133). The samples were incubated with the antibody overnight at 4°C. Dynabeads Protein A (Thermo 10001D) were added to the samples and incubated for 2 hours at 4°C to bind the DNA with H3K27ac antibodies. The beads with bound DNA were washed, the DNA was eluted, and the DNA was treated with Proteinase K (NEB P8107S). We purified the samples using DNA Clean & Concentrator (Zymo D4014). Biotin capture was performed with Dynabeads M-280 Streptavidin (Thermo 11205D), followed by library preparation.<sup>108</sup> We purified the amplified libraries with Sample Purification Beads (Illumina). Libraries were sequenced to generate 100–200 million read pairs per replicate (Illumina NextSeq 500).

### Quantitative reverse-transcription PCR (RT-qPCR)

To measure the target expression after lncRNA perturbations, *RfxCas13d*-expressing cells were transduced in two biological replicates with lentiviruses produced from corresponding pLentiRNAguide\_004, as described in *Arrayed gRNA cloning and lentiviral*

*production*. We selected the transduced cells for three days (1  $\mu$ g/ml puromycin) and then induced Cas13 expression by 1  $\mu$ g/ml doxycycline. At 24 hours after Cas13 induction, total RNA was isolated using the Direct-zol RNA Purification Kit (Zymo R2062) with DNaseI treatment. For cDNA synthesis, 1  $\mu$ g total RNA served as a template using RevertAid Reverse Transcriptase (Thermo EP0442) and random hexamer primers. RT-qPCR was performed using a QuantStudio 5 (Applied Biosystems) with Luna Universal qPCR Master Mix (NEB M3003E) and 2.5  $\mu$ l 1/20-diluted cDNA as template in 5  $\mu$ l reactions: 95  $^{\circ}$ C for 60 s, 45  $\times$  (95  $^{\circ}$ C for 15 s, 60  $^{\circ}$ C for 30 s). The relative transcript abundance was normalized to *ACTB* and control (non-targeting) gRNAs ( $\Delta\Delta$ Ct method). Primer sequences can be found in Table S3B.

## QUANTIFICATION AND STATISTICAL ANALYSIS

### Pooled screen analysis

Quality of the raw fastq files was assessed using MultiQC.<sup>109</sup> We processed reads from pooled Cas13d screens following established pipelines.<sup>23,50</sup> In brief, reads were de-multiplexed based on Illumina i7 barcodes and custom i5 barcodes. We trimmed reads to the expected gRNA length by identifying known anchor sequences relative to the guide sequence. We did this using Cutadapt (v.1.13)<sup>80</sup> with the following parameters: -g CTGGTCGGGGTTTGAAAC -e 0.2 -O 5 -discard-untrimmed and -a TTTTGAATTCGCTAGCT -e 0.1 -O 5 -minimum-length 15 -discard-untrimmed.

We aligned processed reads to the designed crRNA reference using bowtie (v.1.1.2)<sup>81</sup> allowing for up to three mismatches (parameters: -v 1 -m 3 -best -q). The raw gRNA counts were normalized using median-of-ratios (geometric mean), similar to DESeq2,<sup>87</sup> and batch correction was applied using combat from the SVA R package (v.3.34.0).<sup>82</sup> We removed nonreproducible technical outliers by pair-wise linear regression for each sample, collecting residuals, and taking the median value for each gRNA across biological replicates.

To calculate the correlation between biological replicates, we log-transformed the count ratios between time points (Day 14 or Day 7) after Cas13-induction and the corresponding early time point (Day 0). To identify essential genes, the mean  $\log_2$  fold-change was determined using the five most depleted gRNAs per target gene and robust rank aggregation (RRA, v1.2.1).<sup>83</sup> As a negative control, RRA analysis of randomized gRNAs and genes, repeated ten times, yielded no significant hits. For downstream screen analyses, we only considered expressed genes (TPM > 0) based on total RNA-seq in each cell line. RNA-seq expression data for lncRNAs and PCGs are summarized for each cell line in Tables S1C and S1D. For essential lncRNAs, we determined enrichment for genomic class and evolutionary age using Fisher's exact test over all lncRNAs in the Cas13 library.

### Total RNA-sequencing analyses

We aligned total RNA-seq fastq reads from five cell lines (HAP1, HEK293FT, K562, MDA-MB-231 and THP1). Gene expression for protein-coding genes (PCGs) was determined by aligning to the GENCODE GRCh38 reference genome (GRCh38.d1.vd1.fa.tar) with the GENCODE v36 reference gene annotation (gencode.v36.annotation.gtf.gz) using the STAR aligner.<sup>84</sup> Gene expression for long noncoding RNAs (lncRNAs) was determined by aligning to the GENCODE GRCh38 reference genome (GRCh38.d1.vd1.fa.tar) with the Sarpopoulos et al. lncRNA developmental atlas annotation (human.lncRNA.gtf) using the STAR aligner. For that, we first converted the lncRNA atlas from hg19 to hg38 using UCSC Lift Genome Annotations (<https://genome.ucsc.edu/cgi-bin/hgLiftOver>).

For both alignments, quantification was conducted using RSEM.<sup>85</sup> To identify differentially-expressed genes (DEGs) between parental and Cas13-engineered cell lines for HAP1, HEK293FT, K562, the RSEM files were imported and summarized into matrices for gene-level analysis using the tximport R package.<sup>86</sup> We applied the Wald test within the DESeq2 (v.3.19) R package,<sup>87</sup> utilizing an experimental design formula of  $\sim 0 + \text{cell\_line} + \text{cas13\_engineered}$  to zero-center the data. The inclusion criteria for the analysis mandated that genes possess a minimum of 10 reads across all samples. We then categorized genes as differentially expressed if they had an adjusted *P* value < 0.05.

### H3K27ac AQuA-HiChIP and Hi-C analysis

HiChIP paired end reads were mapped to hg38 genome using HiC-Pro<sup>99</sup> with default settings, which included removing duplicate reads, identifying valid interactions, and generating contact maps. Valid pairs supported by at least three reads and spanning distances greater than 5 kb were preserved and binned into 5 kb bins. We used pybedtools (v.0.10.0)<sup>100,101</sup> to intersect valid pairs with the promoter regions of expressed lncRNAs in HAP1 cells and protein-coding genes (PCGs). Promoter regions were defined as  $\pm 2$  kb of the transcription start site from the most abundant transcript. To focus our analyses on PCGs beyond the closest genes in 2D, we removed any contacts between lncRNAs and their closest (2D) PCG. To identify protein-coding genes localized in the same topologically associating domain (TAD) as essential lncRNAs, we intersected the promoter regions of expressed essential lncRNAs with bed files containing TAD boundaries from the Hi-C data Browser<sup>78</sup> (<http://3dgenome.fsm.northwestern.edu/view.php>) using pybedtools (v.0.10.0).<sup>100,101</sup> For TADs in HAP1 cells, we used its parental cell line, KBM7. Essential PCGs were identified as those with a median DepMap score of less than -0.5 across all cell lines (DepMap release 23Q2).

### CaRPool-seq analysis: Pooled screen

For the CaRPool-seq pooled screen readout, we first identified all reads containing the end of the U6 promoter (last 24 nucleotides) and the first direct repeat, allowing up to three mismatches for each sequence. For these reads, we then searched for the barcode

gRNA, allowing for up to one mismatch. The processed reads were aligned to the barcode/library reference (Table S4A) using bowtie (v.1.1.2)<sup>81</sup> with the following parameters: `-v 1 -m 1 -best -strata`. Raw counts were normalized using a median of ratios methods as in DESeq2.<sup>87</sup> For each barcode guide RNA (bcgRNA), we calculated the mean fold-change for the three gRNA arrays for each gene across the two replicates (Day 0 vs Day 12) (Table S4B).

### CaRPool-seq analysis: Single-cell

Sequencing reads from the cDNA library were mapped to a pre-built reference (refdata-gex-GRCh38-2024-A, downloaded from <https://www.10xgenomics.com/support/software/cell-ranger/downloads>) using 10x Genomics Cell Ranger (v.6.0.0).<sup>92</sup> Barcode guide RNA (bcgRNA) library reads were concurrently mapped to a barcode reference (Table S4A) using Cellranger count function with the following parameter: `-expect-cells=13000 -nosecondary -chemistry=SC3Pv`. The resulting count matrices were then used as input into the Seurat R package (v.4.1.1)<sup>93</sup> to perform all downstream analyses.

We performed an initial quality control step to preserve only those cells of sufficiently high quality: Cells with high mitochondrial gene content (> 20%) and low or high number of genes detected (< 1000 and > 8000) were removed from the analysis. The median number of detected genes per cell was 5,457 for HAP1 and 4,974 for MDA-MB-231, with a median of unique molecular identifiers (UMIs) of 23,817 and 22,654 per cell, respectively. RNA counts were log normalized using the `NormalizeData` function. We used the `FindVariableFeatures` function to identify the top 2,000 most variable features for scaling the data using the `ScaleData` function with the following parameters: `vars.to.regress = c("nCount_RNA")`. Guide array identity for cells in the CaRPool-seq pool was assigned based on bcgRNA UMI counts, which were normalized using the centered log-ratio transformation approach, with `margin = 2` (normalizing across cells). A gRNA array was considered detected if it had  $\geq 3$  UMI counts. The median UMI counts per bcgRNA was 134.5, and 95% of cells had  $\geq 1$  bcgRNA.

We observed that 46% of the cells had more than one detected bcgRNA (49% had one bcgRNA, 30% had two bcgRNAs, and 11% had three bcgRNAs). To maximize cell recovery, we retained cells with multiple bcgRNA detected by comparing UMI counts for the bcgRNA with the highest UMI count (g1) to the second detected bcgRNA (g2). We assigned g1, as previously described,<sup>50</sup> if: (1) g1 had between 5 and 9 UMI counts and g2 had 0 or 1 UMI count, or (2) g1 had more than 9 UMI counts,  $g1/(g1 + g2)$  was greater than 0.8, and g2 had fewer than 11 UMI counts. After this step, we obtained 6,606 HAP1 and 5,933 MDA-MB-231 single cells. Cells with  $g1 < 3$  were considered negative and all other cells were considered bcgRNA multiplets and were discarded.

To identify target gene perturbations that lead to transcriptomic changes, we used `FindMarkers` to find differentially-expressed genes between non-targeting cells and cells that belonged to a targeted gene class with the following parameters: `pseudocount.use=0.01, logfc.threshold=0.01, test.use="wilcox"`. The mean expression of each gene was calculated using `AverageExpression`. The number of differentially-expressed genes per perturbation was calculated using Bonferroni-adjusted  $P < 0.05$ . For the heatmaps in Figures 5C, S8C, and S8E, we selected the nine lncRNA perturbations that resulted in the highest number of differentially expressed genes for display and re-normalized data including only these perturbations and the non-targeting control. Using this re-normalized data, for each perturbation, we identified up to 25 of the most significantly differentially expressed protein-coding genes (Bonferroni-adjusted  $P < 0.05$ ). Among the downregulated genes, those with the lowest DepMap scores (release 23Q2) were highlighted. For the upregulated genes, we highlighted those with the lowest fold-change in an overexpression screen for the proliferation of human mammary epithelial cells (HMEC).<sup>52</sup>

### Bulk mRNA-seq processing

Quality of the raw fastq files was assessed using MultiQC.<sup>109</sup> Sequencing adapters were clipped off using Cutadapt (v2.10)<sup>80</sup> with the following parameters: `-q 20 -O 7 -m 20 -trim-n`. The processed sequencing reads were aligned to a pre-defined reference (UCSC hg38, downloaded from <https://daehwankimlab.github.io/hisat2/download/>) using HiSat2 (v2.1.0)<sup>95</sup> with the following parameters: `-q -dta -k 5`. Alignments in the obtained bam files were sorted and indexed using samtools (v1.9).<sup>104</sup> FeatureCounts (v2.0.4)<sup>94</sup> was used for summarizing gene-mapped reads with the following parameters: `-p -s 0`. GENCODE v36 (gencode.v36.annotation.gtf.gz) served as annotation basis. Differential gene expression between lncRNA perturbations and cells transduced with non-targeting gRNAs was determined using DESeq2 (v.3.19)<sup>87</sup> with the two biological replicates as condition in the design formula.

### Developmental gene expression analyses

To analyze gene expression during human development, we used data from two recently published studies.<sup>19,55</sup> For each organ, we compared the expression (in RPKM) of lncRNAs or PCGs in prenatal and postnatal tissues and calculated median expression values for each time point across samples and for all genes in the respective groups based on essentiality in our Cas13 screens. Tissue- and time-specificity indices were previously determined for each corresponding gene in these studies<sup>19,55</sup>: They range between 0 for broad expression and 1 for restricted expression. We also compared the dynamics in expression (significant temporal alterations during development) across four tissues (brain, heart, kidney, and liver) for different sets of lncRNAs, as classified by essentiality (shared, partially shared and cell-type-specific essential, as well as non-essential lncRNAs). For co-expression studies, we computed the correlation between the expression of each lncRNA and that of each PCG at matched time points and donors. This was done using the  $\log_2$ -transformed expression data ( $\log_2(\text{RPKM}+1)$ ).

### Tumor gene expression and survival analyses

Fastq files of TCGA RNA-seq samples across 29 cancer types were accessed from database of Genotypes and Phenotypes (dbGaP) via accession number phs000178.v11.p8, and downloaded from NIH Genomic Data Commons Data Portal (<https://portal.gdc.cancer.gov/>). These 29 cancer types included in this study are adrenocortical carcinoma (ACC), bladder urothelial carcinoma (BLCA), brain lower grade glioma (LGG), breast invasive carcinoma (BRCA), cervical squamous cell carcinoma and endocervical adenocarcinoma (CESC), cholangiocarcinoma (CHOL), colon adenocarcinoma (COAD), glioblastoma multiforme (GBM), head and neck squamous cell carcinoma (HNSC), kidney chromophobe (KICH), kidney renal clear cell carcinoma (KIRC), kidney renal papillary cell carcinoma (KIRP), liver hepatocellular carcinoma (LIHC), lung adenocarcinoma (LUAD), lung squamous cell carcinoma (LUSC), lymphoid neoplasm diffuse large B cell lymphoma (DLBC), mesothelioma (MESO), pancreatic adenocarcinoma (PAAD), pheochromocytoma and paraganglioma (PCPG), prostate adenocarcinoma (PRAD), rectum adenocarcinoma (READ), sarcoma (SARC), skin cutaneous melanoma (SKCM), testicular germ cell tumors (TGCT), thymoma (THYM), thyroid carcinoma (THCA), uterine carcinosarcoma (UCS), uterine corpus endometrial carcinoma (UCEC), and uveal melanoma (UVM). The sample set consists of 9,564 total TCGA samples, including 8,878 primary tumor samples and 686 normal tissue samples.

Fastq reads were aligned to the GENCODE GRCh38 reference genome (GRCh38.d1.vd1.fa.tar) with the GENCODE v36 reference gene annotation (gencode.v36.annotation.gtf.gz) using the STAR aligner.<sup>84</sup> Gene expression for long noncoding RNAs (lncRNAs) was determined by aligning to the GENCODE GRCh38 reference genome (GRCh38.d1.vd1.fa.tar) with the Sarropoulos et al. lncRNA developmental atlas annotation (human.lncRNA.gtf) using the STAR aligner. For that, we first converted the lncRNA atlas from hg19 to hg38 using UCSC Lift Genome Annotations (<https://genome.ucsc.edu/cgi-bin/hgLiftOver>). For both alignments, quantification was conducted using RSEM.<sup>85</sup> The GRCh38 reference genome and the GENCODE v36 annotation file were downloaded from <https://gdc.cancer.gov/about-data/gdc-data-processing/gdc-reference-files>. Subsequently, RSEM files were imported and summarized into matrices in R for gene-level analysis, utilizing the tximport R package.<sup>86</sup> For the identification of differentially expressed genes (DEGs), we applied the standardized Wald test within the DESeq2 (v.3.19) function,<sup>87</sup> utilizing an experimental design formula of  $\sim 0 + \text{sample\_type}$  to zero-center the data. The inclusion criteria for the analysis mandated that genes possess a minimum of 10 reads across all samples. We then categorized genes as differentially expressed if had an adjusted  $P$  value  $< 0.2$ . DEG analysis was only conducted for 22 cancer types where normal tissue samples were available.

For survival analysis, primary tumor samples were stratified based on the expression levels of the corresponding lncRNAs: samples with TPM values exceeding the median were assigned to the high group, while those with TPM values less than or equal to the median were assigned to the low group. The survival probability for both progression-free survival and overall survival was subsequently computed for each group using the survival (v.3.2.7) and survminer (v.0.4.9) R packages.<sup>88–90</sup> We assessed the association of the respective lncRNAs with changes in overall or progression-free survival using the logrank test, and the results were adjusted for the large number of comparisons using Benjamini-Hochberg correction ( $P_{\text{adj}} < 0.05$ ). After identifying these, we assessed the significance of the proportion in each category of essential lncRNAs relative to non-essential lncRNAs using a Fisher's exact test. For co-expression studies, we matched our annotated lncRNA and existing PCG expression data (<https://portal.gdc.cancer.gov/>) for each individual sample based on the provided TCGA identifier. We determined the Pearson correlation for each lncRNA with every PCG on  $\log_2$ -transformed data.

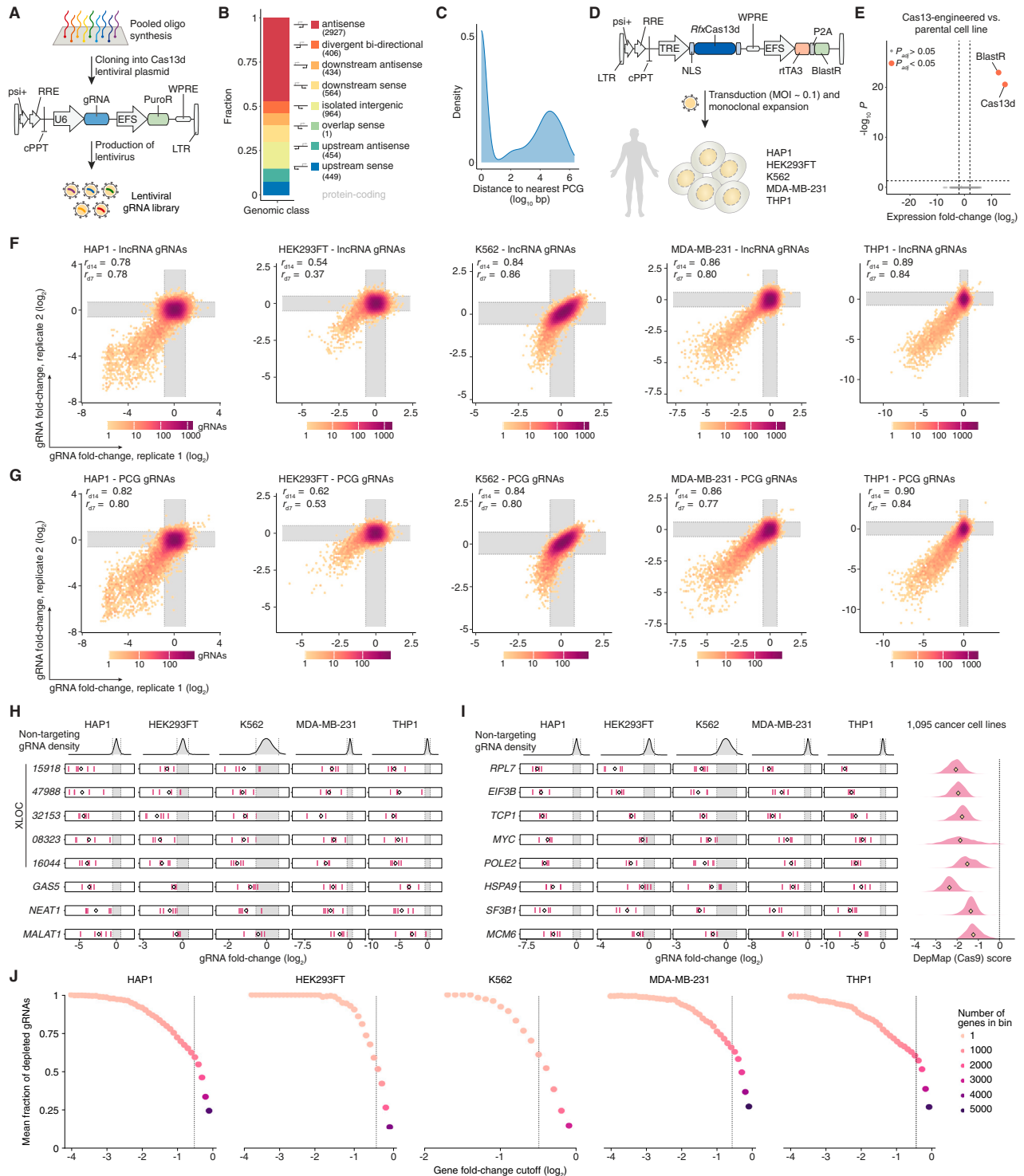
### Matched expression lncRNA analyses

To control for the effect of maximum expression of essential and non-essential lncRNAs in developmental tissues or tumor samples, we generated sets of expression-matched lncRNAs. For direct matching, we paired essential lncRNAs with their closest non-essential counterparts by sampling without replacement. For the 778 essential lncRNAs, we matched 683 unique non-essential lncRNAs based on their closest expression levels in developmental tissues and 690 unique non-essential lncRNAs based on their closest expression levels in tumor samples.

### Gene set enrichment analyses

Gene set enrichment analyses (GSEA) were conducted on pre-ranked lists using the R package clusterProfiler (v4.10.0)<sup>91</sup> using MSigDB (v2023.2)<sup>110,111</sup> gene sets for 50 Hallmarks pathways (geneSetFile = h.all.v2023.1.Hs.symbols.gmt) using the GSEA function with the following parameters: geneList = geneList, TERM2GENE = geneSetFile, exponent = 0, pAdjustMethod = "FDR", pvalueCutoff = 1, by = "fgsea". For the geneList, protein-coding genes (PCGs) were ranked based on either their fold-change ( $\log_2$ ) following lncRNA perturbations in single-cell or bulk mRNA-seqs or their co-expression (pearson correlation coefficient) with the specified lncRNAs across human organ development or in primary human tumors.  $P$  values were adjusted for multiple comparisons using Benjamini-Hochberg correction. To categorize the 50 Hallmark pathways, we annotated the following hallmarks as proliferation pathways, as described recently<sup>51</sup>: *G2M checkpoint*, *E2F targets*, *Mitotic spindle organization*, *MYC targets (v1 and v2)*, and the *p53 pathway*.

# Supplemental figures



(legend on next page)

---

**Figure S1. Cas13 lncRNA library design and gRNA depletion, related to Figure 1**

- (A) Pooled cloning for the lentiviral Cas13 guide RNA (gRNA) library.
- (B) Distribution of long noncoding RNAs (lncRNAs) in the Cas13 library by their genomic classification (position relative to neighboring PCGs, in gray in the legend).
- (C) Distances between lncRNAs in the Cas13 library and their closest PCGs in the Cas13 library.
- (D) Generation of monoclonal Cas13 cell lines via lentiviral transduction and clonal isolation.
- (E) Differential gene expression of HAP1, HEK293FT, K562, and THP1 cells engineered with Cas13 (and induced with doxycycline for 7 days) compared with respective parental cell lines ( $n = 8$  expression libraries with 4 cell lines with and without Cas13). Each point represents the average value of one transcript over eight experiments, with significance determined by a  $\log_2(\text{FC}) \geq 1$  and  $p_{\text{adj}} < 0.05$  (Wald test with Benjamini-Hochberg correction).
- (F and G) Fold-change (FC) of gRNAs targeting lncRNAs (F) and PCGs (G) in two independent replicates for HAP1, HEK293FT, K562, MDA-MB-231, and THP1 cells at 14 days after Cas13 induction (compared with day 0, prior to Cas13 induction). Dots are colored by the number of gRNAs with the indicated FC. Pearson correlation between biological replicates was calculated for day 7 ( $r_{d7}$ ) and day 14 ( $r_{d14}$ ).
- (H) FC (day 14 vs. day 0) of five individual gRNAs (pink lines) targeting the indicated lncRNAs with the density of non-targeting (NT) gRNAs (gray). The diamond denotes the mean FC of the five gRNAs.
- (I) FC (day 14 vs. day 0) of five individual gRNAs (pink) targeting the indicated PCGs with the density of NT gRNAs. The diamond denotes the mean FC of the five gRNAs (left). The DepMap essentiality scores for the indicated PCG (right); the diamond indicates the median DepMap score ( $n = 1,095$  cell lines).
- (J) Consistency among gRNAs as a function of gene (lncRNA and PCG) depletion. For each gene, the gene FC (day 14 vs. day 0) is defined as the mean of the five most depleted gRNAs. Each point in the plot denotes all genes with the same or less gene FC than the indicated cutoff (x axis). The mean fraction of depleted gRNAs (y axis) is the mean fraction of gRNAs that are more depleted than the 97.5th percentile (dashed line) of the NT guide RNAs. This mean is taken over all genes with the same or less gene FC. The number of genes used for each point is denoted by the color scale.
- In (F)–(I), the gray areas indicate the 95% confidence interval using the distribution of NT gRNAs.

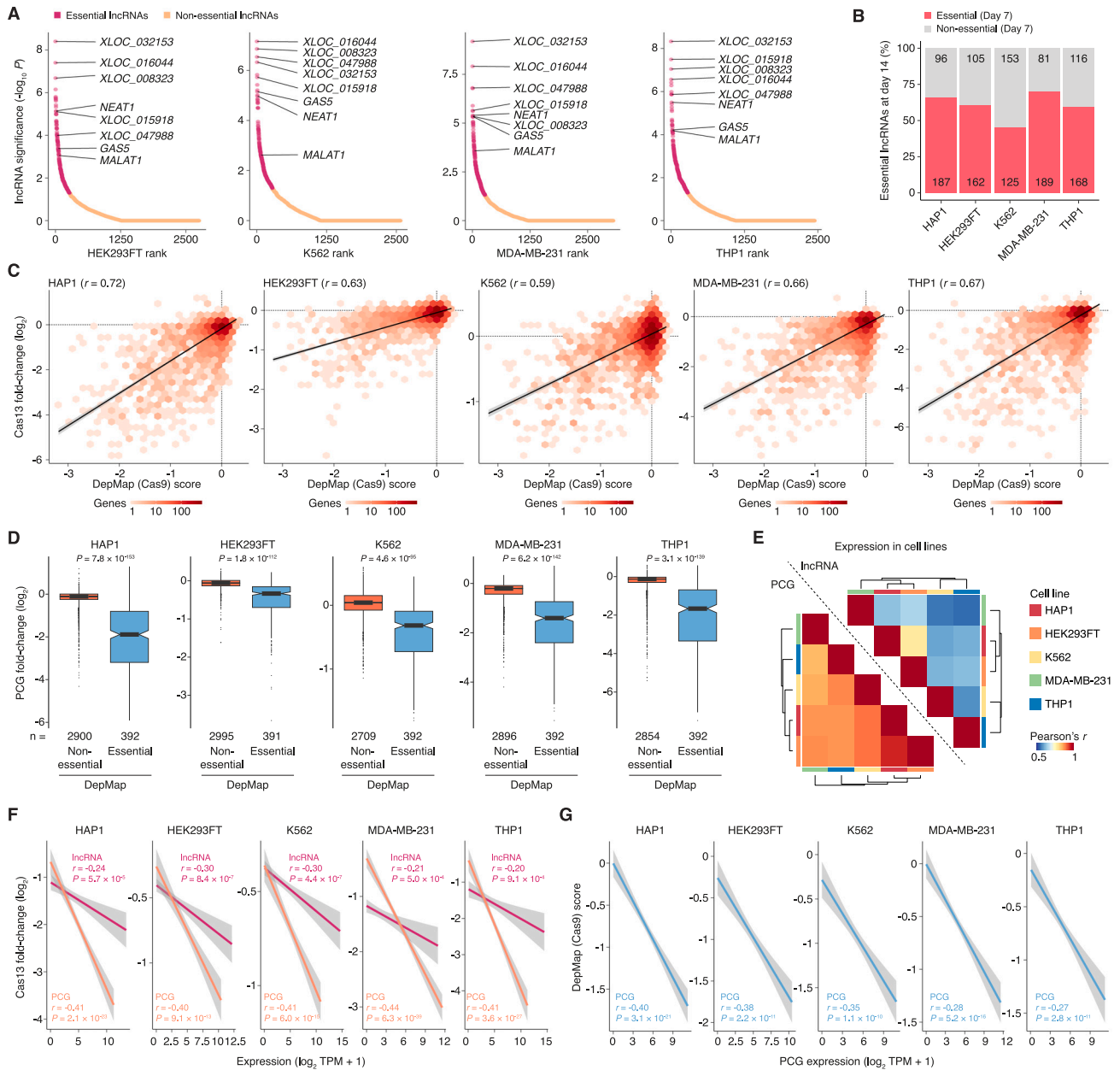


**Figure S2. Identification of essential lncRNAs and correlation analysis of Cas13 screens compared with DepMap scores, related to Figure 1** (A) Robust-rank aggregation (RRA) of lncRNAs in the HEK293FT, K562, MDA-MB-231, and THP1 screens, based on consistent depletion of five gRNAs at 14 days after Cas13 induction.

(B) Essential lncRNAs (RRA  $p < 0.05$ , day 14) at 7 days after Cas13 induction.

(C) Correlation between FC (day 14 vs. day 0) of 4,390 protein-coding genes (PCGs) from the Cas13 screens (this study) and DepMap scores from Cas9 perturbation studies.<sup>30</sup> Dot colors represent gene counts.

(D) Fold-change (FC) of PCGs from the Cas13 screens (this study), grouped by their essentiality status defined by DepMap. Statistical significance was determined by a Mann-Whitney U test.

(E) Correlation coefficients for expression of PCGs or lncRNAs across five cell lines.

(F) Correlation of Cas13 screen FC (day 14 vs. day 0) with the expression of essential lncRNAs (pink) and PCGs (orange) in the five cell lines.

(G) Correlation of DepMap scores from Cas9-based knockout screens with the expression of essential PCGs identified in Cas13 screens in the five cell lines. In (F) and (G), gray areas indicate the 95% confidence interval for regression fit to the respective gene FCs.

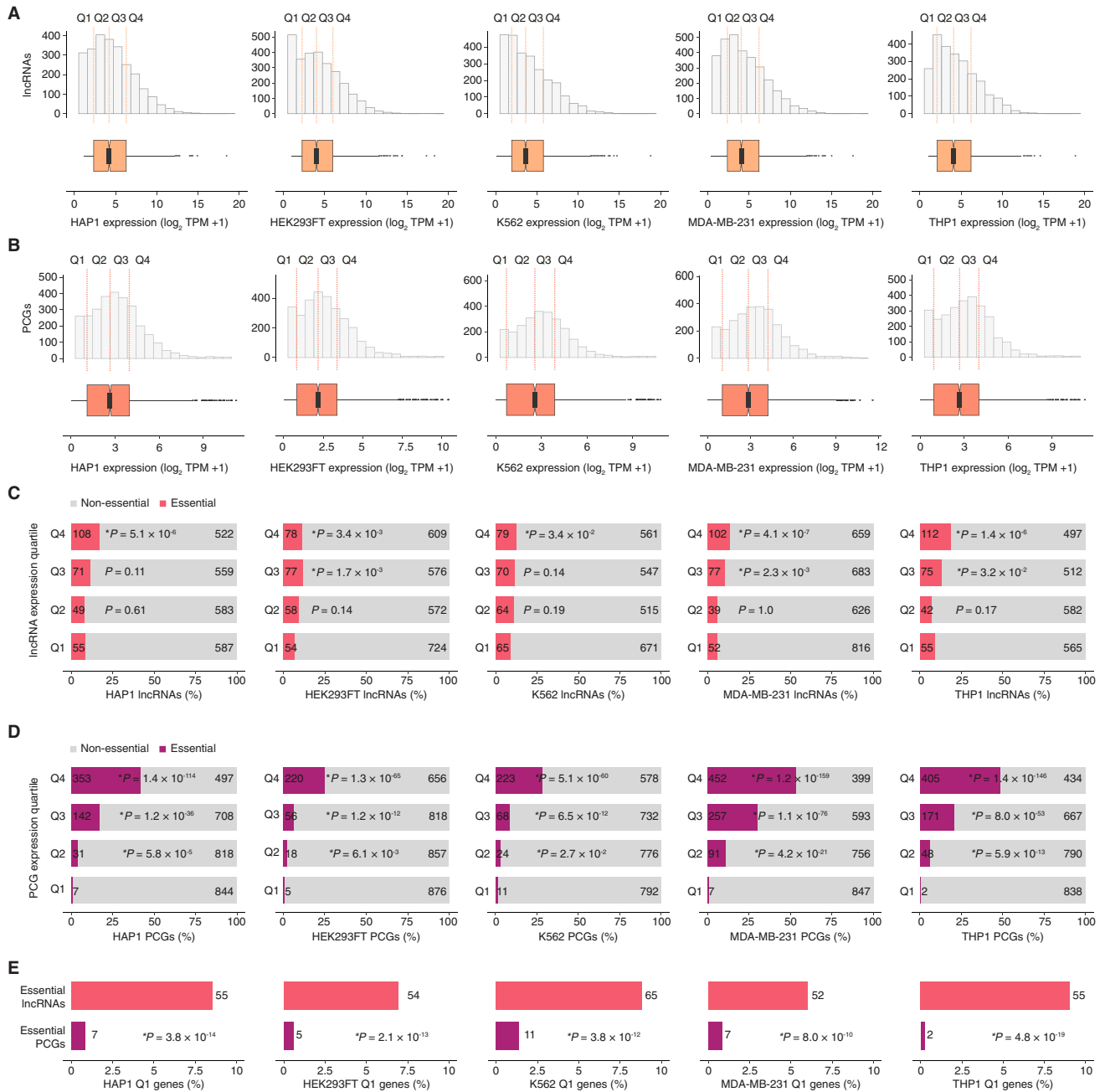
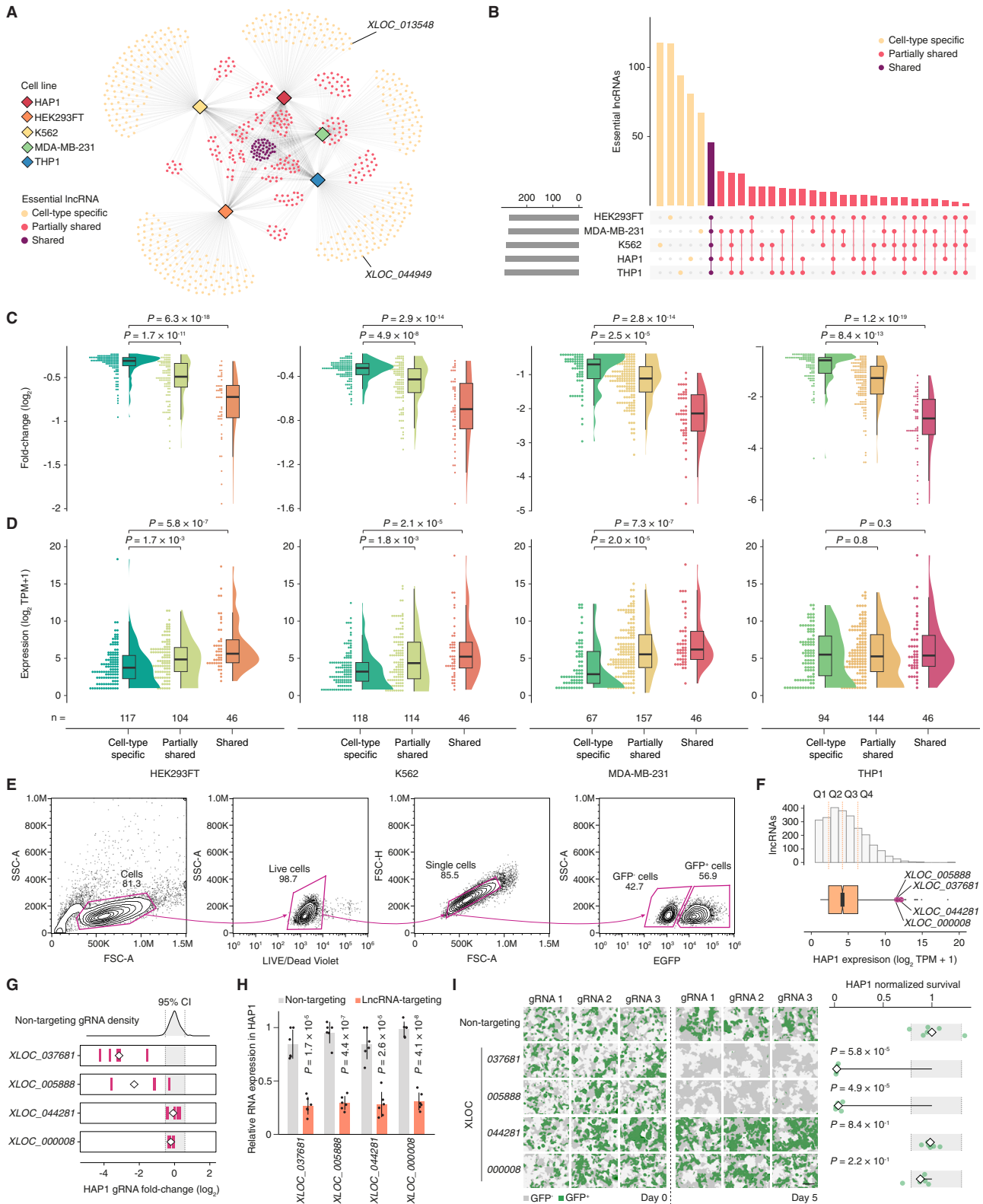


**Figure S3. Expression of essential lncRNAs and protein-coding genes (PCGs) across five cell lines, related to Figure 1**

(A and B) Expression distribution of expressed lncRNAs (A) and expressed PCGs (B) from Cas13 screens across the five cell lines used in this study.

(C and D) The proportion of for essential and non-essential genes binned by quartile of expression (Q1: lowest expression; Q4: highest expression) for lncRNAs (C) and PCGs (D) (Fisher's exact test with non-essential lncRNAs, C, and non-essential PCGs, D).

(E) The proportion of lowest-expressed genes (Q1) for essential lncRNAs and essential PCGs in five cell lines (Fisher's exact test).



(legend on next page)

---

**Figure S4. Distinct and shared essential lncRNAs across five cell lines, related to Figure 2**

(A) Essential lncRNAs labeled by essentiality (shared, partially shared, and cell-type specific) and cell lines.

(B) Overlap of essential lncRNAs between cell lines.

(C) Fold-change (FC, day 14 vs. day 0) of cell-type-specific, partially shared, and shared essential lncRNAs in HEK293FT, K562, MDA-MB-231, and THP1 cells.

(D) Expression of cell-type-specific, partially shared, and shared essential lncRNAs in HEK293FT, K562, MDA-MB-231, and THP1 cells.

(E) Gating strategy for competitive growth assay in THP1 cells. Cells are gated for singlets and live cells prior to GFP quantification.

(F) Expression distribution of lncRNAs expressed in HAP1 and targeted in the Cas13 screen. The four indicated lncRNAs are highly expressed (highest expression quartile, Q4) and used in (G)–(I).

(G) FC (day 14 vs. day 0) of five individual gRNAs (pink lines) targeting the highly expressed lncRNAs in HAP1 cells (expression shown in F). The diamond denotes the mean fold-change of the five gRNAs.

(H) RNA knockdown for the indicated highly expressed lncRNAs. RNA knockdown is measured using RT-qPCR relative to cells transduced with a non-targeting (NT) gRNA as a control (gRNA 1) and was normalized to *ACTB* (two-tailed Student's t test; mean  $\pm$  SD,  $n = 3$  different gRNAs for each target lncRNA with two biological replicates per gRNA).

(I) Representative images of HAP1 cells transduced with individual gRNAs targeting the indicated highly expressed lncRNAs on the day of (left) and 5 days after Cas13 induction (middle). Survival of GFP<sup>+</sup> cells transduced with three non-overlapping gRNAs per gene normalized to the NT gRNAs (right). Each green circle denotes a single gRNA and single transduction replicate. The diamonds denote the mean survival ( $n = 6$  experiments with three gRNAs from two independent transductions). Statistical significance was determined by a Student's t test. Scale bar: 200  $\mu$ m.

In (C) and (D), the statistical significance was determined by a Mann-Whitney U test. In (G) and (I), the gray areas indicate the 95% confidence interval computed using the distribution of NT gRNAs.



---

**Figure S5. Shared essential lncRNAs in proliferation, cell cycle, and apoptosis using Cas13 knockdown and RNA interference, related to Figure 3**

(A) Distribution of genomic location (relative to nearby protein-coding genes, in gray in the legend) for non-essential, cell-type-specific, partially shared, and shared essential lncRNAs.

(B) Fraction of divergent bi-directional transcripts (left) or isolated intergenic transcripts (right) for non-essential, cell-type-specific, partially shared, and shared essential lncRNAs. Statistical significance was assessed using Fisher's exact test relative to non-essential lncRNAs.

(C) RNA knockdown for the indicated shared essential lncRNAs at 24 h after Cas13 induction. RNA knockdown is measured using RT-qPCR relative to cells transduced with a non-targeting (NT) gRNA as a control (gRNA 1) and was normalized to *ACTB* (two-tailed Student's t test; mean  $\pm$  SD,  $n = 3$  different gRNAs for each target lncRNA with two biological replicates per gRNA).

(D) Representative images of MDA-MB-231 (left) and HEK293FT (right) cells transduced with individual gRNAs targeting shared essential lncRNAs 5 days after Cas13 induction. Scale bar: 200  $\mu$ m.

(E) Schematic of the lentiviral fluorescence ubiquitination cell cycle indicator (FUCCI) to measure changes in cell cycle.

(F) Distribution of MDA-MB-231 cells in cell-cycle phases G1 (red), S (green), and G2-M (yellow) transduced with NT gRNAs and exposed to dinaciclib (0.5  $\mu$ M), doxorubicin (1  $\mu$ M) for 24 h ( $n = 54$  images per perturbation and time point with 9 images per biological replicate and 6 biological replicates per perturbation).  $p$  values from the predominantly enriched cell-cycle phase (determined for each condition individually) were computed by a Mann-Whitney U test to test for differences from cells transduced with NT gRNAs.

(G) Representative images of MDA-MB-231 cells transduced with NT gRNAs and treated with dinaciclib and doxorubicin for 24 h. Scale bar: 50  $\mu$ m.

(H) Representative images of perturbed MDA-MB-231 cells at 48 h after Cas13 induction. In (G) and (H), red, cells undergoing G1 phase; green, S phase; yellow, G2-M phase. Scale bar: 50  $\mu$ m.

(I) Fold-change (FC) in cell number (indicated time point vs. 0 h) of MDA-MB-231 cells perturbed with targeting guides compared with NT gRNAs at 0, 24, 48, and 72 h after Cas13 induction (left). Normalized cell count (to cells transduced with NT gRNAs) at 72 h after Cas13 induction ( $n = 6$  biological replicates per perturbation) (right).

(J) Schematic of RNA interference-mediated transcript knockdown using small interfering RNA (siRNA) pools with 3 siRNAs per lncRNA target followed by proliferation and apoptosis assays.

(K) RNA knockdown of the indicated shared essential lncRNAs by siRNA pools is measured using RT-qPCR at 48 h, relative to cells transfected with a control siRNA (targeting luciferase, CTRL) and normalized to *ACTB* (one-way ANOVA with Tukey's HSD post hoc test  $F(7, 20) = 88.5$ ,  $p = 1.2 \times 10^{-13}$ ; mean  $\pm$  SD,  $n = 2$  biological replicates per siRNA pool).

(L) Representative images of HEK293FT cells transfected with siRNA pools targeting indicated genes at 24 and at 84 h after transfection (left). Proliferation of cells transfected with siRNA pools normalized to the median of CTRL siRNA transfections (middle). Annexin V<sup>+</sup> cells were quantified and normalized to the total cell area (right). Each green or pink circle denotes a single transfection replicate. The diamonds denote the mean survival ( $n = 54$  images per siRNA pool with 9 images per biological replicate and 6 biological replicates per siRNA pool). The dashed lines indicate the 95% confidence interval for CTRL siRNA transfections. Scale bar: 200  $\mu$ m.

In (I) and (L), statistical significance was determined by a two-sided Student's t test.

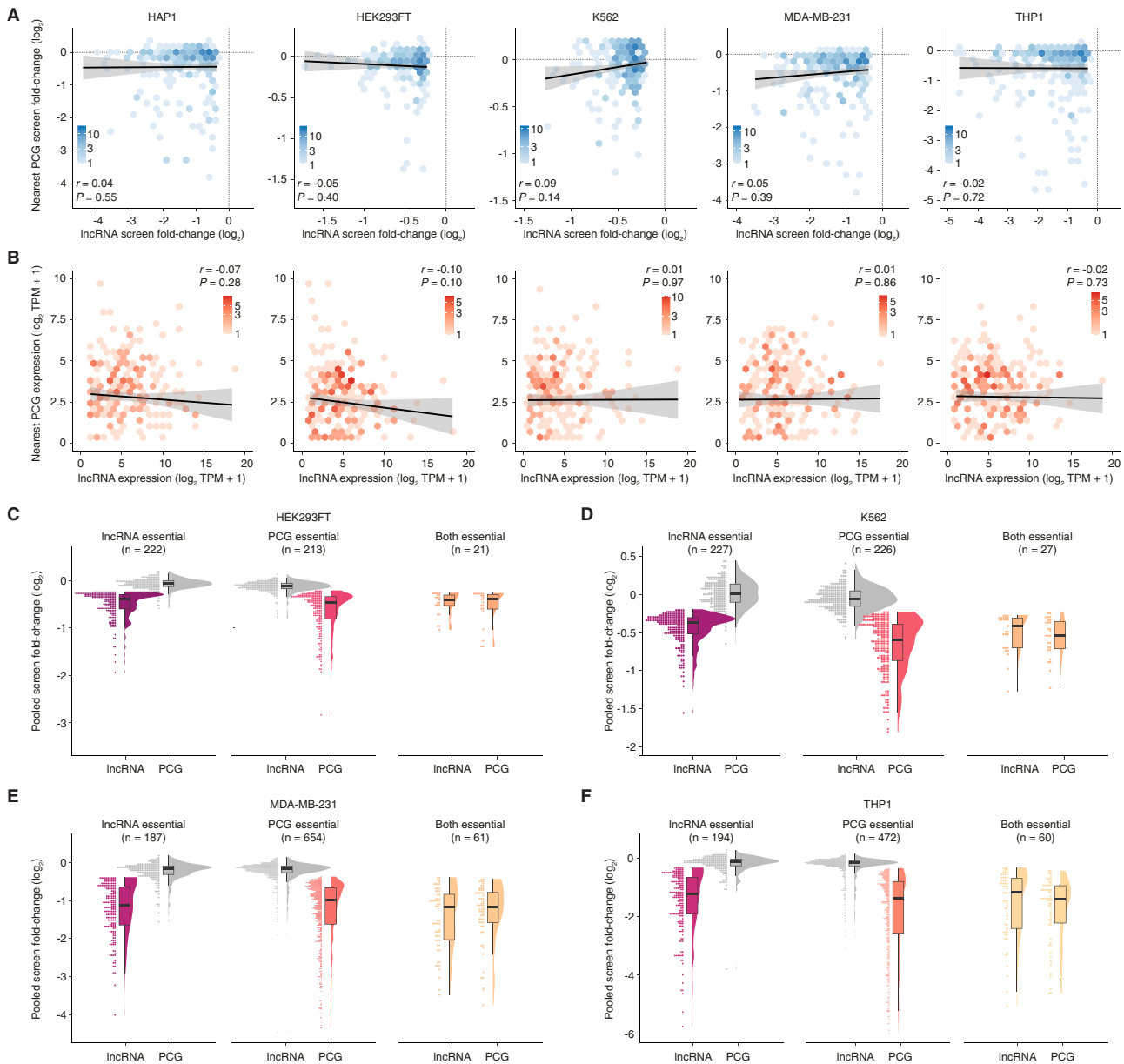


**Figure S6. Essential lncRNAs act independently of nearest protein-coding genes (PCGs), related to Figure 4**

(A) Minimal correlation between the fold-changes (FC, day 14 vs. day 0) of lncRNAs and their closest PCGs in the Cas13 screens for the indicated cell lines. Color scale indicates the number of lncRNA-PCG pairs ( $n = 264$  [HAP1], 278 [HEK293FT], 213 [K562], 250 [MDA-MB-231], 262 [THP1] lncRNA-PCG pairs).

(B) Minimal correlation between the transcript expression of lncRNAs and their closest PCGs in the indicated cell lines. In (A) and (B), gray areas indicate the 95% confidence interval for regression line fit. Color scale indicates the number of lncRNA-PCG pairs.

(C–F) FC (day 14 vs. day 0) of lncRNAs and PCGs in the Cas13 screens for HEK293FT (C), K562 (D), MDA-MB-231 (E), and THP1 (F) cells. In each cell line, we have separated the pairs by those where only the lncRNA is essential (left), only the PCG is essential (middle), and where both the lncRNA and PCG are essential (right).

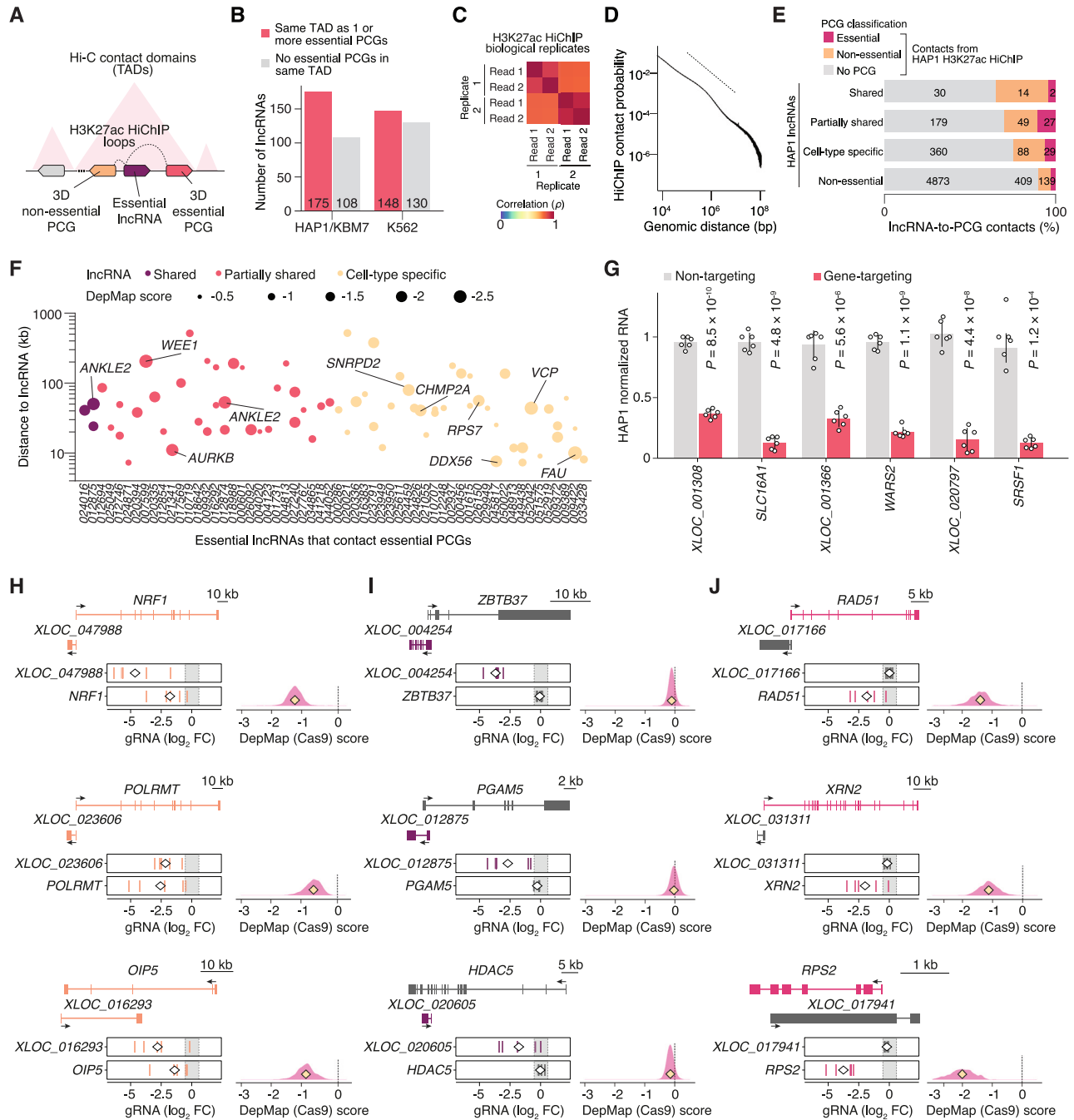


**Figure S7. Essentiality of nearby genes using linear distance and three-dimensional looping from Hi-C and H3K27ac HiChIP, related to Figure 4**

(A) Hi-C to identify topologically associating domains (TADs) containing lncRNAs and H3K27ac HiChIP to identify distal protein-coding genes (PCGs) that contact with lncRNAs.

(B) Number of lncRNAs that are either located in the same TADs as one or more essential PCGs (red) or in a TAD without any essential PCGs (gray) in HAP1/KBM7 and K562 cells.

(C) H3K27ac HiChIP read correlation in HAP1 cells ( $n = 2$  biological replicates).

(D) Average genome-wide contact probabilities at different genomic distances between H3K27ac HiChIP anchors in HAP1 cells. Dashed line denotes the slope.

(E) Percent of lncRNAs with contact to PCGs in the HAP1 H3K27ac HiChIP. The lncRNAs are categorized by essentiality (shared, partially shared, cell-type specific, or non-essential). The HiChIP contacts for each lncRNA are colored by the type of PCG contacted: no PCG contact detected (no essential PCG contact present), or essential PCG contact detected.

(legend continued on next page)

---

(F) Distance between the transcription start sites of essential lncRNAs and their essential PCGs as given by H3K27ac HiChIP contact (y axis). Only essential lncRNAs contacting essential PCGs from HAP1 H3K27ac HiChIP are shown (x axis). Dot size indicates the DepMap score of the contacting essential PCGs. The ten most essential PCGs (lowest DepMap scores) are labeled.

(G) RNA knockdown for the indicated genes (lncRNAs and their closest PCGs) at 24 h after Cas13 induction. RNA knockdown is measured using RT-qPCR relative to cells transduced with a non-targeting (NT) gRNA as a control (gRNA 1) and was normalized to *ACTB* (two-tailed Student's t test; mean  $\pm$  SD,  $n = 3$  different gRNAs for each target lncRNA with two biological replicates per gRNA).

(H–J) Examples of lncRNA-PCG pairs (left) where both genes (H) are essential, only the lncRNA is essential (I), or only the PCG is essential (J) in HAP1 Cas13 screens. Fold-change (FC, day 14 vs. day 0) of five individual gRNAs (lines) targeting the indicated genes is shown with the 95% confidence interval of NT gRNAs (gray) from the HAP1 Cas13 screens. The diamond denotes the mean FC of the five gRNAs (left). The DepMap essentiality scores for each PCG in the lncRNA-PCG pair (diamond indicates the median DepMap score,  $n = 1,095$  cell lines) (right).

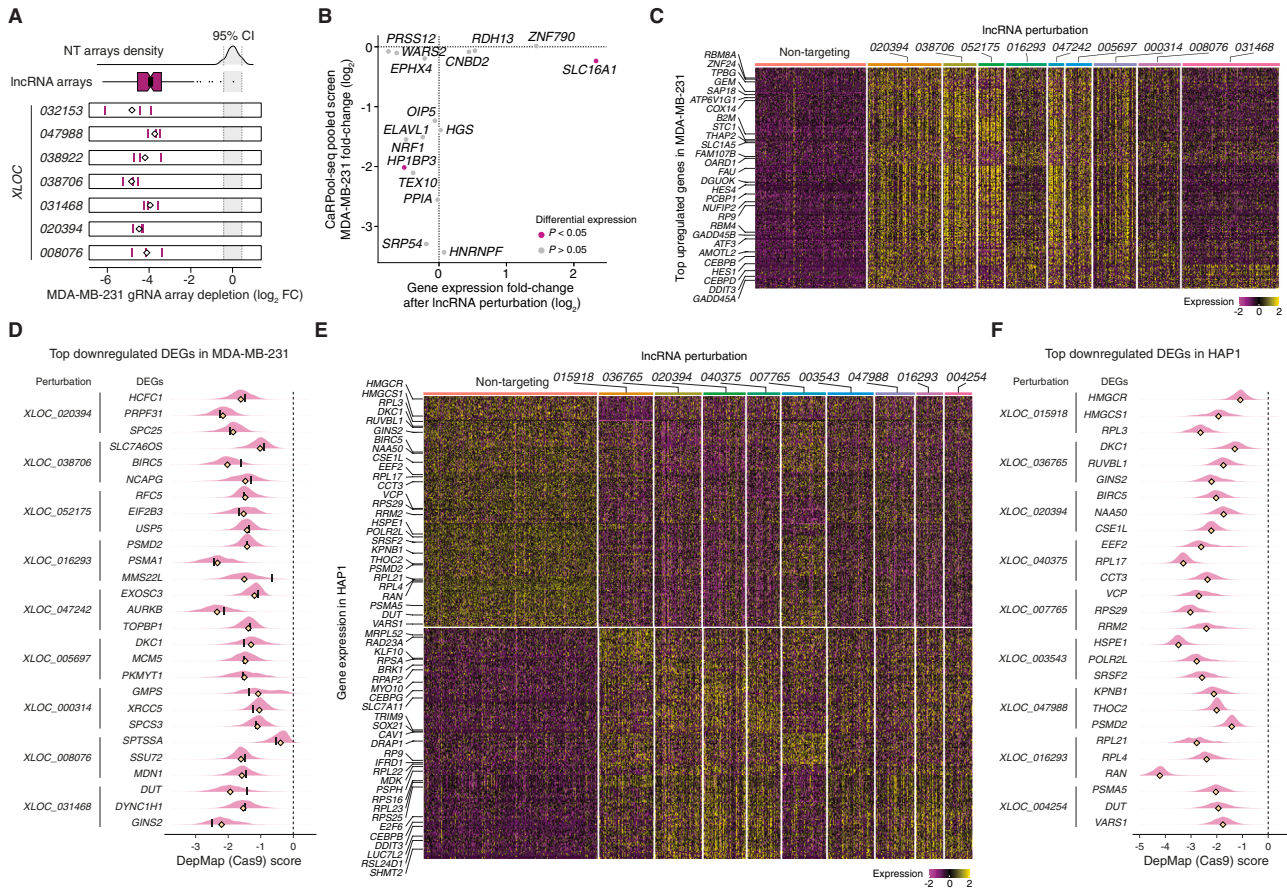


**Figure S8. Additional analysis of single-cell transcriptomics after Cas13 perturbation (CaRPool-seq) in MDA-MB-231 and CaRPool-seq in a second cell line, HAP1, related to Figure 5**

(A) Fold-change (FC, day 12 vs. day 0, CaRPool-seq pooled screen) of three individual guide RNA (gRNA) arrays (purple lines) targeting the indicated essential lncRNAs. The shaded region indicates the 95% confidence interval computed using the distribution of non-targeting (NT) gRNA arrays. The diamond denotes the mean FC of the three gRNA arrays in MDA-MB-231 cells. The boxplot indicates the median and interquartile range (IQR) with whiskers indicating 1.5x IQR.

(B) Depletion of the PCGs from the CaRPool-seq pooled screen (pooled screen FC, y axis) and single-cell mRNA expression of the closest PCGs after lncRNA perturbation in MDA-MB-231 cells (PCG FC, x axis). The PCG FC (single-cell mRNA expression) was calculated by comparing the PCG expression in cells with lncRNA perturbations to the PCG expression from cells with NT perturbations. Differentially expressed PCGs ( $p < 0.05$ ) are labeled in pink.

(C) Single-cell mRNA expression heatmap with the 25 most differentially upregulated genes for each lncRNA perturbation in MDA-MB-231 cells ( $p_{adj} < 0.05$ ). Most depleted PCGs from a prior genome-scale overexpression screen<sup>52</sup> are labeled ( $n = 3$  most depleted PCGs per lncRNA).

(D) The DepMap essentiality scores for the indicated downregulated PCGs labeled in Figure 5C (diamond indicates the median DepMap score,  $n = 1,095$  cell lines). The solid line indicates the DepMap score in MDA-MB-231 cells.

(E) Single-cell mRNA expression heatmap with the 25 most differentially downregulated (upper) and upregulated (lower) genes for each lncRNA perturbation in HAP1 cells ( $p_{adj} < 0.05$ ). The genes labeled were chosen based on median DepMap scores for the downregulated PCGs ( $n = 3$  most essential transcripts per lncRNA and median over 1,095 DepMap cell lines) or a prior genome-scale overexpression screen<sup>52</sup> for the upregulated PCGs ( $n = 3$  most depleted PCGs per lncRNA).

(F) The DepMap essentiality scores for the indicated downregulated PCGs labeled in (E) (diamond indicates the median DepMap score,  $n = 1,095$  cell lines).

In (B), (C), and (E), the statistical significance was determined by a two-sided Mann-Whitney U test with Bonferroni correction.

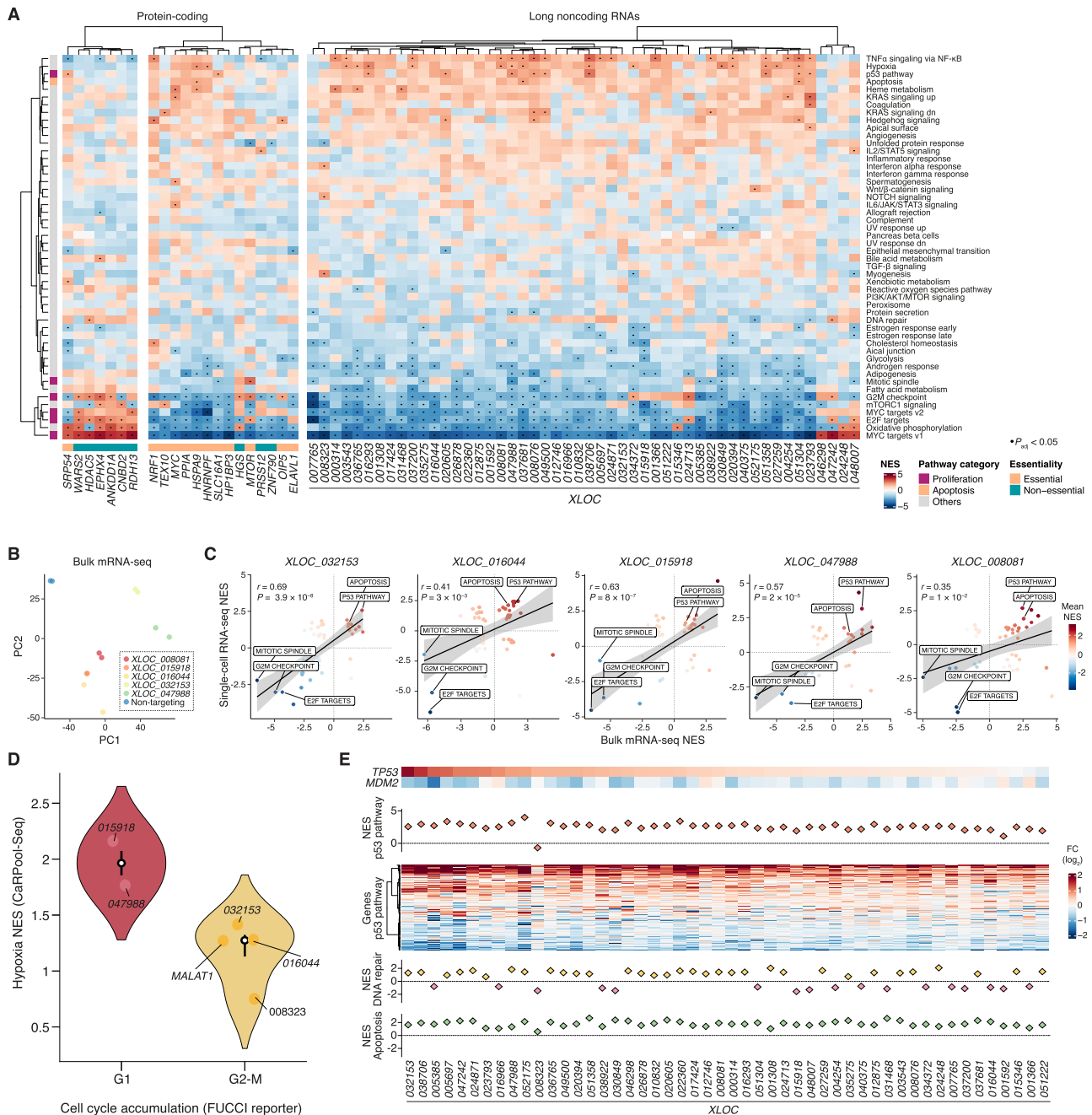


**Figure S9. Transcriptional profiling after Cas13 perturbation of essential lncRNAs identifies differential expression of hypoxia-related and DNA repair-related genes, related to Figure 5**

(A) Normalized enrichment scores (NESs) from gene set enrichment analysis (GSEA)<sup>110</sup> for 21 perturbed protein-coding genes (PCGs) (left) and 50 perturbed essential lncRNAs (middle) in HAP1 cells. Pathways are from MSigDB Hallmark pathways<sup>51</sup> (right). Pathways categorized as proliferation or apoptosis are labeled (far left column).

(B) Principal-component analysis of bulk mRNA-seq data from MDA-MB-231 cells transduced with guide RNAs targeting the indicated essential lncRNAs ( $n = 2$  biological replicates).

(C) Correlation of GSEA NES from bulk mRNA-seq and single-cell CaRPool-seq after perturbation of the indicated lncRNAs.

(D) Hypoxia gene set (MSigDB Hallmark pathways<sup>51</sup>) NES for essential lncRNA perturbations in MDA-MB-231 cells. The essential lncRNAs are categorized by the fluorescence ubiquitination cell cycle indicator (FUCCI) assay after lncRNA knockdown (also in MDA-MB-231 cells, see Figure 3D). Using FUCCI, we categorized cells after knockdown of these essential lncRNAs as inducing either G1 or G2-M cell-cycle phase accumulation.

(E) Gene expression fold-change (FC) of genes involved in the p53 pathway and NES of the specified pathways for the 50 perturbed lncRNAs from CaRPool-seq in MDA-MB-231 cells. Gene expression fold-changes are calculated using lncRNA-perturbed cells vs. cells that received a non-targeting (NT) gRNA array.

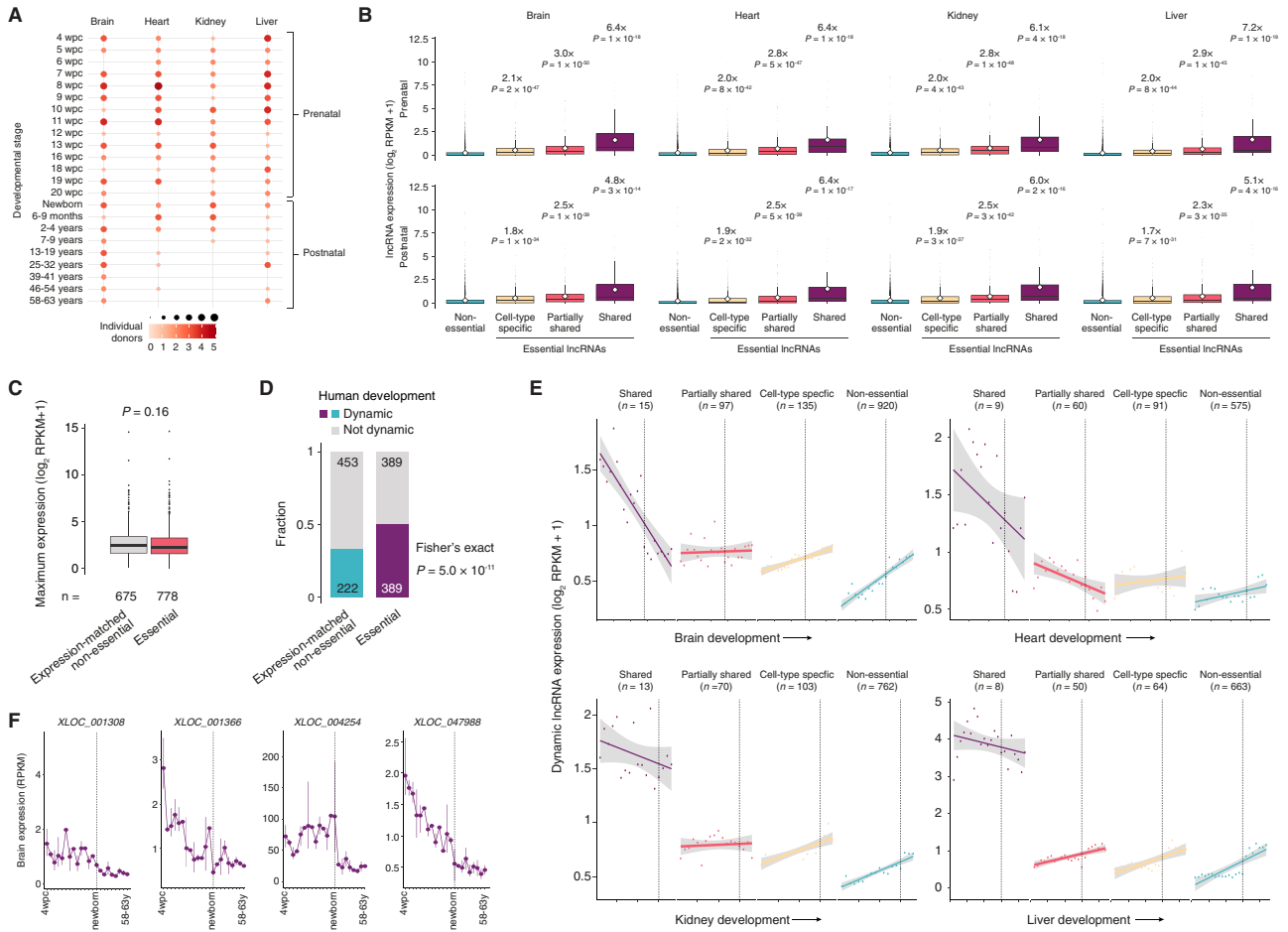


**Figure S10. Expression of essential lncRNAs in human primary tissues across development, related to Figure 6**

(A) Number of donors for each RNA-seq library categorized by tissue and time point from recent developmental atlases of lncRNA and protein-coding gene (PCG) expression ( $n = 182$  tissue samples).<sup>19,55</sup>

(B) Median expression of non-essential and essential (cell-type specific, partially shared, shared) lncRNAs in prenatal and postnatal brain, heart, kidney, and liver tissues. The diamond denotes the mean expression of each group. The fold-change (FC) was derived by comparing the mean expression of essential lncRNA groups compared with non-essential lncRNAs.

(C) Maximum expression (across brain, heart, kidney, and liver) of essential lncRNAs and expression-matched non-essential lncRNAs in human developmental samples.

(D) The fraction of dynamic lncRNAs for essential and expression-matched non-essential lncRNAs (Fisher's exact test).

(E) Expression of dynamic shared (purple), partially shared (pink), cell-type-specific (light pink), and essential and non-essential (turquoise) lncRNAs at different developmental time points in each tissue. Each dot indicates the median across lncRNAs of the indicated essentiality and tissue. Shaded regions denote 95% confidence interval.

(F) Mean expression of indicated dynamic shared essential lncRNAs in brain development ( $n = 1-4$  brain tissue samples per time point). Error bars denote minimum and maximum values.

In (B) and (C), boxplots indicate the median 25th and 75th percentiles, while whiskers are 1.5 times the interquartile range, and statistical significance was determined by a two-sided Mann-Whitney U test. In (E) and (F), the dashed line indicates birth/newborn time point.

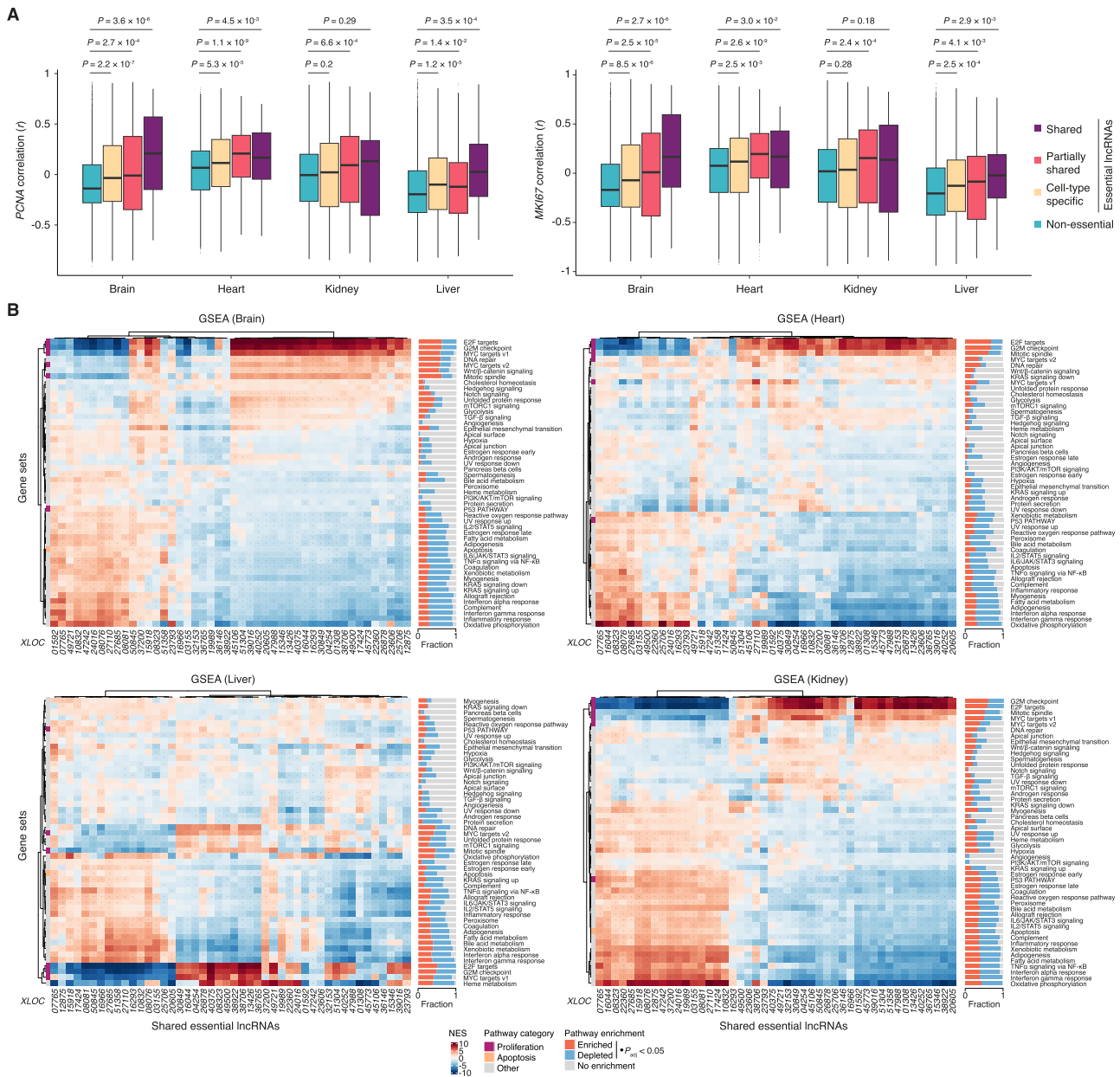
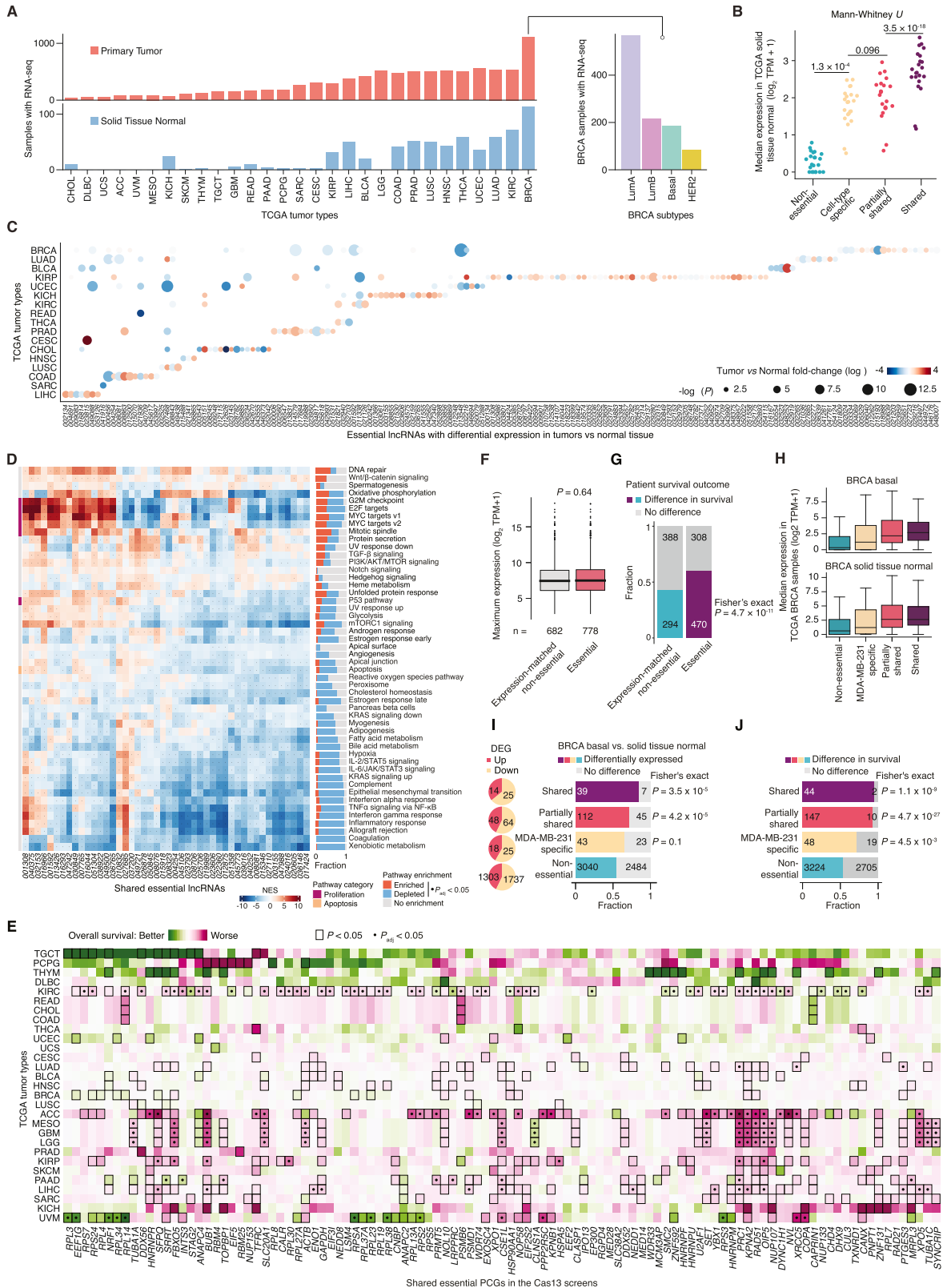


**Figure S11. Identifying co-expressed protein-coding genes (PCGs) and pathways with essential lncRNAs in human primary tissues across development, related to Figure 6**

(A) Correlation of shared (purple), partially shared (pink), cell-type-specific (light pink), and essential and non-essential (turquoise) lncRNAs with proliferation markers *PCNA* and *MKI67* in brain, heart, kidney, and liver development. Boxplots indicate the median 25th and 75th percentiles, while whiskers are 1.5 times the interquartile range, and statistical significance was determined by a two-sided Mann-Whitney U test.

(B) Normalized enrichment scores (NESs) from gene set enrichment analysis (GSEA)<sup>110</sup> for co-expressed protein-coding genes of shared essential lncRNAs in brain, heart, kidney, and liver developmental tissues (left). The fraction of shared essential lncRNAs with the indicated pathway (MSigDB Hallmark pathways<sup>51</sup>) enriched or depleted is shown on the right.



(legend on next page)

**Figure S12. Expression of essential lncRNAs in TCGA tumor and normal tissues, related to Figure 7**

(A) TCGA primary tumor (upper) and normal tissue (lower) samples with RNA-seq across the 29 cancer types analyzed in this study.<sup>112</sup> Breast invasive carcinoma (BRCA) primary tumor samples by subtype (right).

(B) Median expression of essential and non-essential lncRNAs ( $n = 1-113$  samples per tissue type, 22 normal solid tissue types in TCGA). Statistical significance was determined by a Mann-Whitney U test in comparison to non-essential lncRNAs.

(C) Median fold-change (FC) of differentially expressed lncRNAs in primary tumors compared with matched normal tissues in different cancers (Wald test).

(D) Normalized enrichment scores (NESs) from gene set enrichment analysis (GSEA)<sup>110</sup> for MSigDB Hallmark pathways<sup>51</sup> using the co-expressed (in primary tumors) protein-coding genes (PCGs) of shared essential lncRNAs ( $n = 8,878$  tumors).

(E) Survival analysis (Cox regression coefficients) of PCGs identified in the Cas13 screens as essential across all cell lines. PCGs with negative coefficients (pink) are associated with decreased survival. Conversely, PCGs with positive coefficients (green) are associated with better survival. Significance was given by a Benjamini-Hochberg-adjusted log rank test.

(F) Maximum expression of essential lncRNAs and expression-matched non-essential lncRNAs across TCGA primary tumor samples ( $n = 8,878$  tumors, two-sided Mann-Whitney U test).

(G) The proportion of essential and expression-matched non-essential lncRNAs associated with better or worse overall survival or progression-free survival.

(H) Median expression of essential and non-essential lncRNAs in BRCA basal samples (upper,  $n = 186$  tumors) and normal breast tissue samples (lower,  $n = 113$  normal breast tissues).

(I) The fraction of differentially expressed lncRNAs in BRCA basal samples compared with normal breast tissue samples (right). The pie charts (left) separate differentially expressed lncRNAs: up (increased expression in BRCA basal) and down (decreased expression in BRCA basal).

(J) The proportion of lncRNAs associated with better or worse overall survival or progression-free survival in BRCA basal.

In (G), (I), and (J), the statistical significance is determined by Fisher's exact test relative to non-essential lncRNAs. In (F) and (H), boxplots indicate the median 25th and 75th percentiles, while whiskers are 1.5 times the interquartile range.